

The Electrodeposition of Composite Materials using Deep Eutectic Solvents

Thesis submitted for the degree of
Doctor of Philosophy
At the University of Leicester

By

Khalid El ttaib
Department of Chemistry
University of Leicester
December 2010



The Electrodeposition of Composite Materials using Deep Eutectic Solvents

Khalid El ttaib
PhD Thesis
University of Leicester 2011

Abstract

Composite materials are important for their improved strength and wear resistance compared to pure materials. Metal composites have been electrodeposited from aqueous solutions although the instability of colloidal dispersions makes it difficult to obtain reproducible composite compositions. In this thesis metal composites are prepared using Deep Eutectic Solvents, DESs, which are a type of ionic liquid.

The electro-deposition of copper and copper composites from DESs based on ethylene glycol and urea were investigated. The mass transport in both electrolytes was found to be diffusion controlled. The mechanism of copper nucleation is studied using chronoamperometry and it is shown that 3D progressive nucleation leads to bright nanostructure deposits. It was found that dispersed colloidal particles are stable over a prolonged period of time in DESs.

This work uses an electrochemical quartz crystal microbalance (EQCM) to monitor both the current efficiency and the inclusion of inert particles into the copper co-deposits. The technique showed the majority of second phase was dragged onto the surface instead of sedimented. The effect of the addition of surfactants was also studied.

DESs were also used in the electro-deposition of silver composites with alumina and silicon carbide. It was found that improved mechanical properties such as hardness and wear resistance could be obtained. The addition of LiF to the Type 3 deep eutectic solvents was also found to further improve the quality of the mechanical properties and led to smoother surfaces with lower friction coefficients.

The final part of this study involved the deposition of nickel composites with the aim of producing coatings with hardness similar to chromium. The addition of organic additives as brighteners (ethylene diamine) leads to smooth and bright finishes. Two types of composites were added to the nickel electrolytes; SiC 1-3 μm and Teflon μm . The surface morphology was found to change with particle size and type. The mechanical properties were studied and found to be affected by the type and the concentration of particulate incorporated in the nickel deposits.

Acknowledgements

Firstly, I would like to express my tremendous gratitude and appreciation to my supervisor Professor Andrew Abbott for his continuous invaluable support in guiding and bringing new ideas. Also a big thanks to my co-supervisor Dr. Karl Ryder for helping and providing assistance and always welcoming me at his office, even when he is busy. I would like to thank Dr. E. Smith, G. Frisch, Dr. Katy McKenzie. Again my thanks goes to everybody in the Scionix group. I would also like to thank Dr. Simon and Mr G. Clark from the engineering department for their assistance with SEM and the wear analysis machine. Many thanks go to the people in the workshop Keith, John, Roy and Karl who have provided the facilities to run the experiments. I would like to thank Phil for his assistance whenever I needed help. I dedicate this work to my parents, my wife, my son and my two little daughters.

Section	Chapter 1: Introduction	Page
1.1	Electroplating in non-aqueous solution	2
1.2	Ionic Liquids	3
1.3	Deep Eutectic Solvents	7
1.4	Applications of Deep Eutectic Solvents	10
1.4.1	Electrochemical Applications	10
1.4.2	Electrodeposition of Metals	11
1.4.3	Electropolishing	13
1.4.4	Processing of metals and Metal Oxides	14
1.4.5	Immersion Silver	15
1.4.6	Other Applications	16
1.5	Project Aims	16
1.6.	References	17
	Chapter 2: Experimental	22
2.1	Materials	23
2.2	Speciation	23
2.2.1	Fast atom bombardment mass spectrometry (FAB MS)	23
2.2.2	Uv visible spectrophotometer	23
2.3	Electrochemical Methods	24
2.4	Quartz Crystal microbalance (QCM)	24
2.5	Surface microstructure analysis	26
2.5.1	Atomic force microscope (AFM)	26
2.5.2	Scanning electron microscope (SEM)	26

2.5.3	Cross-section microstructure	26
2.6	Surface profile analysis	27
2.6.1	Profilometry	27
2.6.2	Digital holographic microscope	27
2.7	Mechanical properties	27
2.7.1	Hardness	27
2.7.2	Wear test	27
2.8	Viscosity	27
2.9	References	27
	Chapter 3: The Electrodeposition of Copper Composites using Deep Eutectic Solvents	28
3.1	Introduction	29
3.2	Electrodeposition of Copper	31
3.2.1	Cyclic voltammetry	31
3.2.2	Diffusion coefficients	33
3.2.3	Chronocoulometry	37
3.2.4	Chronoamperometry	38
3.2.5	Gravimetric investigation	40
3.3	Electrodeposition of Composites Materials	42
3.3.1	Cyclic voltammetry	43
3.3.2	Gravimetric analysis of the Cu composites	45
3.3.3	Addition of a hard dispersed phase (SiC 1-3 μm)	48
3.3.4	Addition of a soft dispersed phase (polytetrafluoroethylene, PTFE 1 μm)	50
3.3.5	Use of Surfactants	51

3.4	Conclusions	57
3.5	References	58
	Chapter 4: The Electrodeposition of Silver Composites using Deep Eutectic Solvents	61
4.1	Introduction	62
4.1.1	Silver composites	62
4.1.2	Silver deposition from ionic liquids	63
4.2	Electrodeposition of Silver	65
4.2.1	Electrodeposition of Ag / SiC (45-55 nm) composites	66
4.2.2	Electrodeposition of Ag / SiC (1-3 μm) composites	67
4.2.3	Electrodeposition of Ag / Al ₂ O ₃ (50 nm) composites	69
4.2.4	Hardness of composite films	69
4.2.5	Wear analysis	72
4.2.6	Effect of LiF on hardness and friction coefficient of Ag / SiC films	80
4.3	Conclusion	82
4.4	References	83
	Chapter 5: The Electrodeposition of Nickel and Nickel Composites using Deep Eutectic Solvents	86
5.1	Introduction	87
5.2	Nickel electrochemistry	88
5.2.1	Cyclic voltammetry	88
5.2.2	Chronocoulometry	90
5.2.3	Under-potential deposition (UPD) of nickel	92
5.2.4	Bulk electrolysis and morphology	92
5.3	Addition of brighteners: ethylene diamine	93

5.3.1	Speciation	94
5.3.2	Cyclic voltammetry	96
5.3.3	Chronocoulometry	98
5.3.4	Under-potential deposition (UPD) of nickel	98
5.3.5	Bulk electrolysis and morphology	100
5.3.6	Effect of addition of LiF	103
5.4	Addition of brighteners: sodium acetylacetonate	104
5.4.1	Cyclic voltammetry	105
5.4.2	Chronocoulometry	106
5.4.3	Under-potential deposition (UPD) of nickel	107
5.4.4	Bulk electrolysis and morphology	108
5.5	Composites	110
5.5.1	Nickel/ SiC composites	110
5.5.1	Nickel/ PTFE composites	118
5.6	Anodic behaviour of nickel in Ethaline and Reline	121
5.7	Conclusions	123
5.8	References	125
	Chapter 6: Conclusions and Suggestions for Further Work	126
6.1	Summary	127
6.1.1	Cu and Cu composites	127
6.1.2	Ag and Ag composites	127
6.1.3	Ni and Ni composites	128
6.2	Future work	129
	Appendix	130

Chapter 1: Introduction

1.1. Electroplating and non-aqueous solution

1.2. Ionic Liquids

1.3. Deep Eutectic Solvents

1.4. Applications of Deep Eutectic Solvents

1.4.1 Electrochemical Applications

1.4.2 Electrodeposition of Metals

1.4.3 Electropolishing

1.4.4 Processing of metals and Metal Oxides

1.4.5 Immersion Silver

1.4.6 Other Applications

1.5. Project Aims

1.6. References

1.1 Electroplating in non-aqueous solution

The first experiment to electroplate metals was carried out in 1805 by Luigi Brugnatelli who used a Voltaic Pile to deposit gold.¹ Later improvements by John Wright using KCN led to electrolytes for silver and gold plating which are relatively similar to those used today. While initially limited to the deposition of decorative metals, more functional metals such as nickel and chromium were deposited by Bird in 1837² and Junot de Bussey in 1848.³ In depth reviews on the history of metal electroplating can be found in several reviews.^{4,5,6}

The electroplating industry is dominated by the deposition of Cr, Ni, Cu, Au, Ag, Zn and Cd and some copper and zinc-based alloys from aqueous solutions.¹ Other metals are usually deposited using plasma or chemical vapour deposition techniques (PVD and CVD). While these are versatile in being able to coat any substrate (metal, plastic, glass, ceramic etc.) they are difficult to apply to large and complex surfaces. Aqueous techniques have dominated due to low cost, high solubility of electrolytes, high conductivities and good throwing power, high solubility of metal salts, and high mass transfer rates. There are, however limitations of using water based electrolytes including limited potential windows (c.a. 1.4 V), hydrogen embrittlement, passivation of the anode or cathode, the use of complexants such as cyanide and the environmental issues associated with treating large volumes of water to remove metals and electrolytes before returning to the water course.

Of the metals listed above, nickel, cadmium and chromium have significant toxicity issues and in an ideal scenario metals such as Ti, Al and W would be ideal replacements. These metals are abundant and excellent for corrosion resistance. It is however the stability of their oxides that makes these metals difficult to extract from minerals and apply as surface coatings.

There are clearly a range of other solvents that could be used, both ionic and molecular; polar and non-polar. Ideally, to dissolve electrolytes polar solvents are the most desirable and small solvent molecules will generally provide a high fluidity. Unfortunately all polar molecules have electronegative elements which by their nature make them good electron donors. These will strongly coordinate to metal ions making them difficult to reduce. Some of the more electropositive metals have been plated from polar organic solvents but these offer few technological advantages. Non-polar organic solvents, mainly aromatic hydrocarbons have been used for metal deposition. These have the advantage of wide potential windows but the obvious

disadvantage of poor conductivity. The Alumiplate process was developed in the late 1980s to plate aluminium from a toluene.^{7,8} Triethyl aluminium was used as the source of aluminium but it is pyrophoric and this in combination with a highly flammable solvent made the process difficult to run. A review of electrochemistry in non-aqueous solutions is given by Izutsu.⁹

1.2 Ionic Liquids

High temperature molten salts have long been used for metal extraction and metals such as Li, Na, Ti and Al have been electrowin for molten salts.^{10,11,12} The main limitation with high temperature molten salts is clearly the operation temperature which makes operation difficult and limits the range of substrates that can be used. In an endeavour to reduce the melting temperature of salts numerous studies focussed on $\text{Li}^+ / \text{K}^+ / \text{AlCl}_3$ eutectics which have freezing points close to 100°C .¹³ The use of quaternary ammonium salts particularly pyridinium and imidazolium salts has pushed the freezing point down to ambient conditions. The term “ionic liquids” has been used to distinguish between high temperature and low temperature systems.

One of the key breakthroughs in the development of ionic liquids came with the synthesis of a 1 mol. eq. N-ethylpyridinium bromide : 2 AlCl_3 by Hurley and Wier in 1951¹⁴ which was a eutectic liquid at 20°C . This was used for the electrodeposition of aluminium¹⁵ and therefore sparked a large amount of research for metal deposition. Using molecular orbital theory, Wilkes and co-workers¹⁶ developed an ionic liquid, AlCl_3 : 1-ethyl-3-methyl-imidazolium, which had a room-temperature liquid range between 33 and 67 mol% AlCl_3 . In addition these “first generation” ionic liquids had a significantly lower viscosity than the corresponding pyridinium liquids and it is the imidazolium cation that still dominates the ionic liquid literature.

Discrete anion or “second generation” ionic liquids are composed of simple anions, as opposed to a mixture of anions in equilibrium. Their discovery is ascribed to Wilkes and Zaworotko who produced 1-ethyl-3-methylimidazolium tetrafluoroborate and acetate for the first time.¹⁷ It is this class of ionic liquid which has dominated the literature ever since. Anions such as BF_4^- and PF_6^- were initially used because of their wide potential window,^{18,19} however, they were found to slowly hydrolyse yielding HF,²⁰ and liquids with more hydrophobic anions such as trifluoromethanesulphonate (CF_3SO_3^-) and bis-(trifluoromethanesulphonyl)imide $[(\text{CF}_3\text{SO}_2)_2\text{N}^-]$ have subsequently become popular.²¹ The potential window of these liquids can be extremely

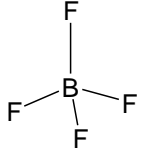
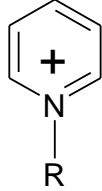
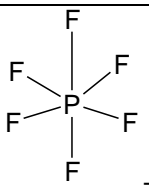
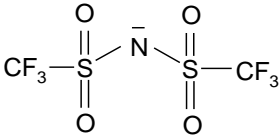
large making it possible to electroplate reactive metals.²² The properties of these liquids are covered in a series of reviews.^{23,24,25,26}

Ionic liquids are salts that have a melting temperature below 100 °C. Generally one of the ionic components is organic, most commonly the cation. The ions have a low degree of symmetry. By careful choice of the components it is possible to tune the properties of the liquid. In general ionic liquids;

- Are good solvents for organic and inorganic materials.
- Are generally considered to be polar yet non-coordinating solvents.
- Immiscible with many organic solvents providing a polar alternative for two-phase systems.
- Have low vapour pressures.

It is generally accepted that the first ionic liquid was [EtNH₃][NO₃], and had a melting point of 12 °C. Ionic liquids as a low temperature alternative are currently a popular area of research. Ionic liquids are systems with an anionic and a cationic component which are liquid below 100°C.²⁷ The definition is used to distance these fluids with high temperature molten salts but is completely arbitrary. Ionic liquids have been of great interest, due to them having many advantageous properties from molten salts, yet negating the difficulties of high temperature. A variety of cations and anions are described in the literature but for the application of metal deposition only a relatively small pallet of ionic liquids has been used. These are shown in Table 1.1. The possibility to choose a possible ligand as the anionic component allows control over speciation and thus redox properties of metal solutes to a much greater extent than in aqueous media since extremely high activities of the ligands can be achieved.

Table 1.1: A selection of cations and anions used to make ionic liquids for metal deposition.

Common Cations	Discrete Anions
 $R_1 = \text{CH}_3$ $R_2 = \text{Et}$ emim $R_2 = \text{Bu}$ bmim $R_2 = \text{Hex}$ hmim	
 $R = \text{CH}_3$ BPY	
$R_1 R_2 R_3 R_4 N^+$ $R_1 = R_2 = R_3 = \text{CH}_3$ $R_4 = \text{C}_2\text{H}_4\text{OH}$ Choline	 Tf_2N^-

Ionic Liquids have clearly been reported to be green solvents most notably for their low vapour pressure compared to molecular alternatives. In the application of ionic liquids to metal deposition the green credentials of this methodology could also come from a significant reduction in the volume of low level aqueous streams that would need to be processed. Today, it is generally recognised that this is only part of the picture since many ionic liquids do have significant toxicity. Some ionic liquids have been designed to contain ions which are known to have lower toxicity and these include functionalised imidazoles,²⁸ lactams,²⁹ amino acids³⁰ and

choline³¹ although it is only the last of these which have been extensively applied to metal deposition.

Ionic liquids in electrodeposition

Initially the main drive to use ionic liquids was the ability to obtain high concentrations of aluminium in a highly conducting aprotic medium. As ionic liquids have developed the key advantages of the liquids have become;

- the wide potential windows,
- high solubility of metal salts,
- avoidance of water and metal/water chemistry and
- high conductivity compared to non-aqueous solvents.

The use of ionic liquids heralds not only the ability to electrodeposit metals that have hitherto been impossible to reduce in aqueous solutions but also the capability to engineer the redox chemistry and control metal nucleation characteristics. It is the latter area that is only now being addressed and will no doubt be the focus of research over the forthcoming decade.

The main driver for using ionic liquids for metal plating has been the ability to obtain wide potential windows which is the potential range of which the electrolyte is neither oxidised nor reduced at the electrode surface. Some ionic liquids have a very large potential window of up to 4.15 V for [Bmim (PF₆)] at a Pt electrode,³² 5.5 V for [BMP(TF₂N)] at a glassy carbon electrode.³³ The importance of potential windows is well known from aqueous processes where hydrogen evolution can be hazardous and lead to brittle electrodeposits (hydrogen embrittlement). Ionic liquids may even be chemically altered and hence destroyed if potential limits are not considered. The wide potential window of ionic liquids makes it possible to electrodeposit elements with low redox potentials that cannot be reduced in other media such as Al,³⁴ Mg,³⁵ Ge,³⁶ and Si³⁷.

The relevant aspects of metal deposition using ionic liquids with discrete anions are reviewed in each of the following results chapters but for more general summaries on the subject a number of reviews have recently been published.^{22,38,39}

1.3 Deep Eutectic Solvents

The requirements for ionic liquids to be used on a bulk scale for metal deposition are that they need to be;

- Low cost
- Non-toxic
- Pre-registered for REACH
- Water insensitive.

The majority of discrete anions do not achieve all of these criteria and so it is more likely that eutectic based ionic liquids will be more applicable for bulk-scale electrodeposition.

The systems studied so far described can be expressed in terms of the general formula



where Cat^+ is in principle any ammonium or phosphonium cation, X is generally a halide anion (usually Cl^-). They are based on equilibria set up between X^- and a Lewis or Brønsted acid Y, z refers to the number of Y molecules which complex X^- .

The melting point of two component mixtures is dependent upon the size of the interaction between the components. For ideal mixtures (non-interacting components) the freezing point will vary linearly with mole fraction whereas large negative deviations can occur when the components interact strongly with each other. This is shown schematically in Figure 1.1. The composition at which the minimum freezing point occurs is known as the Eutectic point and this is also the temperature where the phases simultaneously crystallise from molten solution.

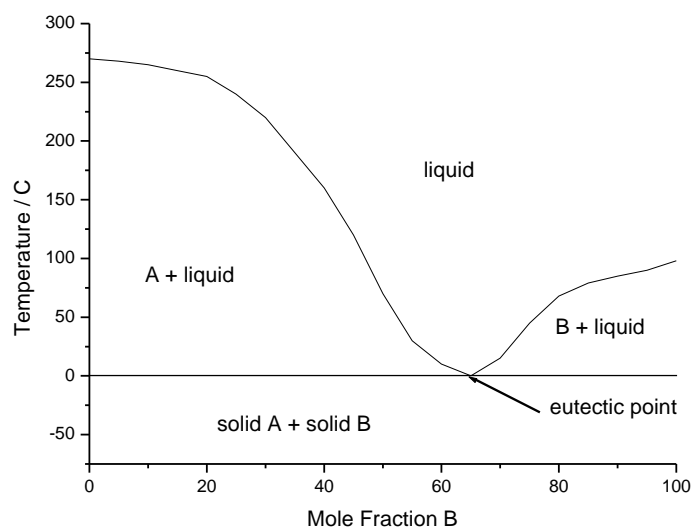


Figure 1.1: Schematic representation of a eutectic point on a two component phase diagram.

One of the key advantages of these types of ionic liquids is the ease of manufacture. The liquid formation is generally mildly endothermic and requires simply mixing the two components with gentle heating. Another key advantage is that they are water insensitive which is very important for practical electroplating systems. The final key advantage of eutectic based systems is that because they are simple mixtures of known chemicals they do not have to be registered as new entities as they revert to their constituent components upon excessive dilution in water.

The ionic liquids described can be subdivided into three types depending on the nature of the complexing agent used.

Eutectic Type 1 $Y = MCl_x$, $M = Zn$,^{40,41,42} Sn ,⁴³ Fe ,⁴⁴ Al ,⁴⁵ Ga , In ⁴⁶

Eutectic Type 2 $Y = MCl_x \cdot yH_2O$, $M = Cr$,⁴⁷ Co , Cu , Ni , Fe

Eutectic Type 3 $Y = RZ$, $Z = CONH_2$,⁴⁸ $COOH$ ⁴⁹, OH

To date the only Cat^+ species studied have been based on pyridinium, imidazolium and quaternary ammonium moieties. In general, as with the chloroaluminate and discrete anion systems, the imidazolium based liquids have the lowest freezing points and viscosities and higher

conductivities. The depression of freezing point is related to the strength of interaction between the anion and complexing agent although this has not really been quantified as yet due primarily to a lack of thermodynamic data about the individual components.

A fourth type of eutectic has been described involving just a metal salt and a hydrogen bond donor.⁵⁰ It was shown that ZnCl_2 when mixed with acetamide or urea could also form eutectics which had all the properties of ionic liquids.

The novelty of Type 3 eutectics is that they use a simple hydrogen bond donor to complex the simple anion (usually chloride). The majority of the work to date has focussed on simple amides, alcohols and carboxylic acids. The first reported eutectics were those formed between choline chloride and amides such as urea and acetamide.⁴⁹ These materials have been called Deep Eutectic Solvents to differentiate them from ionic liquids with discrete anions. A eutectic forms when there is a large interaction between the two species in the mixture. An example of this is the choline chloride: urea mixture. By themselves they have freezing points of $303\text{ }^\circ\text{C}$ and $135\text{ }^\circ\text{C}$ respectively. By combining these two compounds in a ratio of 1:2 (choline chloride: urea), the product formed has a freezing point of $12\text{ }^\circ\text{C}$ which is a depression of freezing point of $178\text{ }^\circ\text{C}$. For comparison the freezing point depression for the choline chloride-zinc chloride system was much larger ($272\text{ }^\circ\text{C}$)⁵¹ due to the covalent bonds formed in the metal chloride case. The main reason behind choline chloride being such a useful quaternary ammonium salt is to do with the fact it is an asymmetric quaternary ammonium salt with a polar functional group, but is also small. The asymmetric nature of this molecule reduces the freezing point of the ionic-molecular liquid, as does the polar functional group. The group of Abbott has published extensively on the subject of choline chloride $\text{HOC}_2\text{H}_4\text{N}^+(\text{CH}_3)_3\text{Cl}^-$ (ChCl) because it is non-toxic and readily available as a bulk commodity chemical. Its common use stems in part from its simple manufacture; an efficient gas phase reaction between trimethylamine, ethylene oxide and HCl. This means that the Sheldon E factor⁵² for this salt is close to zero because almost no waste products are formed during this reaction.

For monofunctional HBDs e.g. urea, phenylpropionic acid, the eutectic point occurs at 67 mol% HBD, for difunctional HBDs e.g. oxalic acid and malonic acid the eutectic point occurs at 50 mol% HBD and for citric acid the eutectic occurs at 33 mol% HBD. The tris-carboxylic acids exhibit the properties of gels due to extensive bridging of the acids between neighbouring

chloride ions. The existence of hydrogen bonding in ChCl/urea eutectic mixtures can be observed using NMR spectroscopy. HOESY spectra of $\text{HOCH}_2\text{CH}_2\text{N}^+(\text{CH}_3)_3\text{F}\cdot 2(\text{NH}_2)_2\text{CO}$ show intense cross-correlation between the fluoride ion and the NH_2 protons on the urea molecule.³¹ Some anion complexes have been identified using FAB-MS and it is evident that the HBD is sufficiently strongly coordinated to the chloride anion to be detected by this technique. In a 1 choline chloride: 2 urea mixture the presence of Cl^- with both one and two ureas were observed.

The freezing point of the HBD- salt mixtures will be dependent upon the lattice energies of the salt and HBD and how these are counteracted by the anion-HBD interaction and the entropy changes arising from forming a liquid. For a given quaternary ammonium salt, the lattice energy of the HBD will be related to the anion-HBD interaction and hence to a first approximation the depression of freezing point will be a measure of the entropy change. It has been shown that the depression of freezing point correlates well with the mass fraction of HBD in the mixture.⁴⁹

The lowest viscosities and highest conductivities are obtained with diol based HBDs. It is thought that the comparatively weak interactions between the alcohol and the chloride mean that some 'free' glycol is able to move decreasing the viscosity of the liquid. The glycol based liquids tend also to have comparatively large potential windows.⁵³

1.4 Applications of Deep Eutectic Solvents

Deep eutectic solvents are easy to synthesise, economically viable to produce on a large scale, relatively insensitive to water, exhibit high metal solubility, pre-registered for reach and can be recycled make them useful in wide range of application, such as metal plating, electro-polishing and metal recycling. Type III eutectics have the ability to dissolve high concentrations of metal oxides which allows them to be used for metallurgy. As a consequence they can be applied to large-scale processes.

1.4.1 Electrochemical Applications

Deep eutectic solvents have been used for electrochemical application and these have focussed mainly on electrodeposition of metals and electropolishing of steel. Choline chloride based liquids using ethylene glycol as the hydrogen bond donor has been the most commonly used liquid. The main advantage over aqueous media has been the increased current efficiency

(typically > 80 %). Despite the short development time good reproducible surface finishes have already been achieved.

1.4.2 Electrodeposition of Metals

The electrochemical potential window of most DESs is typically in the range of 3V. This precludes applications such as lithium batteries and the deposition of electropositive metals such as titanium and aluminium. The applications of deep eutectic ionic liquids have focussed on the deposition of metals and metal alloys such as Zn, Cu, Ni, Ag, Cr, and Sn, zinc -tin, zinc-nickel, and nickel-tin alloys. While these can be deposited from aqueous solutions, the studies to date have focused on the advantages that DES present *i.e.* deposition on water sensitive substrates such as aluminium and the deposition of specialized alloys.

Zinc is one of the most important metals in the metal plating industry due to its low cost, environmental compatibility and corrosion resistance. Abbott *et al.* investigated the deposition of Zn from type II deep eutectic solvents (ChCl/ZnCl₂) at 60°C and reported that the deposition morphology obtained is not different from obtained by Sun.⁵⁴ The current efficiency was found to be 100 % and a variety of Zn alloys could be deposited. Modified type I and III are subjected to investigation by Iwagishi⁵⁵ for deposition of Zn from a number of glycol and urea bases eutectic and report that Zn deposition considerable affected by the nature of hydrogen bond donor used.

Electrodeposition using eutectic based ionic liquids has almost exclusively used quaternary ammonium halides with metal halides primarily in the chloride form. Aqueous plating solutions rarely use chlorides as they tend to yield black powdery deposits and the inclusion of halides into metallic coatings is seen as undesirable due to the possibility that it can lead to the breakdown of passivating layers and exacerbate corrosion. The morphology issue is thought to be due to the ease of nucleation from halide salts which leads to large numbers of small nuclei forming at the electrode surface. Lewis basic anions cannot be circumvented for eutectic based ionic liquids as they need to be good ligands to interact strongly with the Lewis acid. The question that needs to be posed is whether chloride ions actually cause a problem when their activity is negligible due to the presence of a strong Lewis acid. The issue that needs to be addressed is that Type I and II eutectic based ionic liquids necessarily have high concentrations of metal chlorides and will tend to promote nucleus formation. In many cases the working

concentration equates to 5 to 10 mol dm⁻³ which although seemingly high is not overly different to many aqueous plating solutions. Further ionic liquid formulation needs to address how nucleation can be suppressed while growth is supported.

Zinc alloys deposition

The deposition of Zn alloys from aqueous media can be affected by the potential window of water and the difference in redox potentials between zinc and the alloying element. In ionic liquids, and in particular Deep Eutectic Solvents many metals have similar coordination geometries and the redox potentials of metals are changed from the standard aqueous potentials. The area of Zn alloy deposition has been covered in depth by Sun *et al.* who published a number of reports on the deposition of Zn alloys with Cu,^{56,42} Cd,⁵⁷ Mg,⁵⁸ Sn,⁵⁹ Co,⁴² Fe,⁶⁰ The majority of these are from Type I ZnCl₂ eutectics. The deposition of a Zn-Sn alloy was successfully obtained from deep eutectic solvent electrolytes based on mixtures of choline chloride and ethylene glycol and urea. It was shown that the morphology and the composition may vary depending upon the selection of the type of ionic liquid. Barron⁶¹ has extended these ideas to Zn-Cu and Zn-Co alloys deposits from ClCl:2EG and ClCl:2urea eutectics. The area of zinc and zinc alloy deposition has been reviewed by Sun.**Error! Bookmark not defined.**

Chromium deposition

The deposition of chromium from aqueous electrolytes suffers from low current efficiency and the use of toxic CrO₃. Choline chloride forms eutectic mixtures with CrCl₃.6H₂O, CaCl₂.6H₂O, LaCl₃.6H₂O CoCl₂.6H₂O, LiNO₃.4H₂O and Zn(NO₃)₂.4H₂O⁴⁷ and these liquids are highly conducting. Studies have shown that chromium and cobalt can be efficiently deposited from these liquids. The high ionic strength prevents the water molecules acting as bulk water as they are strongly coordinated to the ions and therefore they are not easily reduced at the electrode surface. Accordingly the deposition of metals such as chromium can be carried out with high current efficiencies.⁴⁷ It was found that the addition of up to 10 wt % LiCl, could lead to the deposition of black chromium which is amorphous in morphology but is free of surface cracks. Analysis of the film produced using an ionic liquid showed that it was homogeneous with no structural characteristics even under the highest magnification. Deposition rates in the region of 60 μm hr⁻¹ could be obtained.⁶² This is close to current aqueous Cr(VI) plating rates.

Subsequent improvements have been made to the technology and brighteners have been incorporated in these eutectic mixtures. The process has been operated at pilot plant scale although no details about the improvement have been given in the open literature.⁶³

1.4.3. Electropolishing using ionic liquids

Electropolishing is the controlled corrosion of a metal surface to bring about a reduction in surface roughness. The current stainless steel electropolishing process is performed worldwide on a commercial scale and is based on concentrated phosphoric acid and sulfuric acid mixtures. The polishing process is thought to involve formation of a viscous layer at the metal surface and many processes employ viscosity improvers such as glycerol. The practical aspects of electropolishing have been reviewed by Mohan *et al.*⁶⁴ whereas the more fundamental aspects are covered by a review of Landolt.⁶⁵ While electropolishing is an extremely successful process there are major issues associated with the technology most notably that the solution used is highly corrosive and extensive gassing occurs during the process, which results in very poor current efficiency.

It has previously been shown^{66,67} that ethylene glycol can also be used as the hydrogen bond donor and eutectic mixtures with choline chloride can be used for the electropolishing of stainless steel. This process has the advantage that high current efficiencies are obtained with negligible gassing at the anode/ solution interface. The liquid used is also relatively benign and non-corrosive compared to the current aqueous acid solutions. It was shown that a different mechanism occurred for the electropolishing in an ionic liquid and instead of forming a dense passivating layer polishing was controlled by the availability of the chloride ion at the electrode surface.

This technology was scaled up to pilot plant scale (50 litres) and then to commercial scale (1300 litres). In extended trials it was found that the cost of electropolishing using DESs was the same as that using aqueous acid based systems due largely to the increased current efficiency of the ionic liquid (approximately 4 times better than the aqueous system). A review of the commercial application of electropolishing has recently been published.⁶³

1.4.4 Processing of metals and metal oxides

Hydrometallurgy is central to many industrial processes and produces large volume of aqueous waste. Neutralising dilute streams of acidic and basic by products is both energy and chemical intensive and causes possibly the largest source of metal-based emissions into the environment. Over the past decade several groups have studied the use of ionic liquids for metal dissolution, extraction and recovery but most work has been carried out in the field of extraction. This is clearly due to the practicality of using ionic liquids on a large scale. Assuming metal solubilities could reach 10 wt % then a 10 times excess of solvent (and more typically 100 times) is required even for relatively soluble salts. Loss of the ionic liquid will limit the choice of ionic liquids which can be used. Physical losses from adsorption on the matrix will be significant. It is therefore likely that only valuable metals will be extracted in this way. The high cost and viscosity of these liquids means that they are more suitable for small volume applications and the prospect of concentrating metals from dilute aqueous solution into small volumes of ionic liquids.

Dai *et al.*⁶⁸ the first to study metal oxide solubility in ionic liquids. They investigated the dissolution of UO_3 in imidazolium chloroaluminate melts. The main solute species was found to be $[\text{UO}_2\text{Cl}_4]^{2-}$. The solvation of U and Eu ions in the same liquid was also studied by Chaumont and Wipff.⁶⁹ These may not seem suitable liquids due to their water sensitivity but the principle that the study raised is very important. Huang *et al.* studied the dissolution of nano-scale zinc particles from an ash using an imidazolium PF_6 salt and this was the first study of digestion from a complex matrix using ionic liquids with discrete anions.⁷⁰

The dissolution and solubility of metal oxides is poorly understood due largely to a lack of data in comparable systems. Abbott *et al.* have carried out in depth studies on the solubility of metal oxides in a variety of Deep Eutectic Solvents. The mixtures have been shown to have similar solvent properties to ionic liquids with discrete anions⁷¹ but clearly have the advantage that they are easier to produce on a large scale which has obvious implications for metal recovery processes. Ligands such as urea, thiourea or oxalate are well known complexants for a variety of metals and can be made part of the ionic liquid. It has been shown that these types of ionic liquids can dissolve a range of metal oxides and they can be used to separate metals from a complex mixture using electrochemistry.⁷² These liquids are however all totally miscible with

water and cannot be used for biphasic extraction. The solubility of 17 metal oxides in the elemental mass series Ti through Zn was reported in 3 ionic liquids based on choline chloride.⁷³ Judicious choice of the hydrogen bond donor can lead to selectivity for extracting certain metals from complex matrices.⁴⁹

The only large scale extraction process carried out to date was that by Abbott *et al.* who used a DES of choline chloride and 2 urea to extract zinc and lead oxides from a waste material produced by the electric arc furnace (EAF).⁷² The liquid was designed and optimised such that iron and aluminium oxides were insoluble. Because the liquid was very viscous (~800cP at 298K) a hybrid liquid using a second hydrogen bond donor was used. A ratio of 1 choline chloride: 1.5 ethylene glycol: 0.5 urea showed the same solubility of zinc or lead oxides and insolubility of iron oxides but it led to a greatly reduced viscosity (56 cP at 298K). Scale up to pilot plant led to an increase in extraction efficiency due to improved mass transport in the tank. Particles also appeared to decrease the viscosity of the ionic liquid as the particles act as micro stirrers.⁷⁴ The area of ionic liquid application in metal oxide processing has recently been reviewed by Abbott *et al.*⁷⁵

1.4.5. Immersion Silver

Electroless deposition can be classified in two divisions; catalyst activated deposition and immersion coatings, the former is used in the electroless deposition of Ni and Cu and is employed extensively in the PCB industry. The addition of reducing agents creates a galvanic potential difference between the ions in solution and the substrate, whereas the latter is primarily used for electroless Ag.

Smith *et al.* showed that a sustained galvanic coating of silver could be deposited onto copper from an ionic liquid based on a choline chloride and ethylene glycol.^{76,77,78} The silver deposit was porous and this allowed thick deposits to be obtained. This is in contrast to the commercial aqueous process of dip-coating silver where deposition does not continue once surface coverage has been achieved, unless a catalyst is added. The process was commercialised and a full production scale plant was constructed using over 1 tonne of ionic liquid.

1.4.6. Other Applications

Deep Eutectic Solvents have been used by a variety of groups in a range of applications which are summarised briefly here. The largest number of applications has been in the field of synthesis. In the same way that ionic liquids have been used as bulk solvents for synthesis, the same is true for DESs. There are a limited number of applications in organic synthesis,^{79, 80} although the applications to inorganic synthesis and particularly in the area of template growth of solids is more extensive.^{81,82,83,84,85,86} DESs have also been used as media for biocatalysis as several enzymes have been found to be stable in these liquids.^{87,88,89,90,91} There are two reports of DESs based on choline chloride and glycerol being used for the purification of biodiesel through the extraction of excess glycerol.⁹² There are also reports of DESs being used as electrolytes in dye sensitised solar cells.^{93, 94}

1.5. Project Aims

The overall aim of the project was to investigate the inclusion of particles into metal coatings deposited onto an electrode surface using an ionic liquid. Three metals were chosen; copper, silver and nickel and three types of particles were used; aluminum oxide, silicon carbide and Teflon. In the first results chapter copper is used as a model system to investigate the rate of particle inclusion. In the second chapter silver was investigated for the practical application of producing hard wearing silver coatings for electrical interconnects. The final results chapter investigates the use of nickel as the metal matrix in an attempt to produce a surface with hardness values approximating those of chromium which is the industry standard for hard coatings. In each section the size of the particulate particles and the particulate loading in solution were investigated together with the morphology of the metal.

The main advantage of using ionic liquids for the electrodeposition of composite materials is that the liquids are viscous and this decreases the rate of settling of particles in solution. It is also expected that the high ionic strength may help to shield the particles from each other in solution and thus stabilize the colloidal dispersion.

The project to date has produced two publications^{95,96} and these have already been cited.^{97,98} Copies of the papers are included in the appendix for reference.

1.5 References

- ¹ Modern Electroplating (4th edition), M. Schlesinger and M. Paunovic (editors), Wiley, New York, **2000**
- ² G. Bird, *Phil. Trans.* **1837**, 127, 37
- ³ Junot de Bussey, *Fr. Pat.* 3564, **1848**
- ⁴ J. K. Dennis and T. E. Such, Nickel and chromium plating, 3rd Ed. Woodhead Publishing, Cambridge **1993**
- ⁵ W. Burkhardt, *Galvanotechnik* **1989**, 80, 3385
- ⁶ W. Burkhardt, *Galvanotechnik* **1989**, 80, 2622
- ⁷ E. Peled, E. Gileadi, *J. Electrochem. Soc.* **1976**, 123, 15.
- ⁸ L. Simanavicius, *Chemija*, **1990**, 3, 3
- ⁹ K. Izutsu, *Electrochemistry in Non-aqueous Solutions*, Wiley VCH, Weinheim, **2002**
- ¹⁰ W.H. Kruesi and D.J. Fray, *Met. Trans. B.*, **1993**, 24B, 605.
- ¹¹ D. J. Fray and G. Z. Chen, *Materials Science and Technology* **2004**, 20, 295
- ¹² G. Grjotheim, C. Krohn, M. Malinovsky, K. Matiasovsky, and J. Thonstad, *Aluminum Electrolysis* (2nd Edition), Aluminium-Verlag, Dusseldorf, **1982**
- ¹³ F. Lantelme, H. Alexopoulos, M. Chemla and O. Haas, *Electrochim. Acta* **1988**, 33, 761.
- ¹⁴ F. H. Hurley and T. P. Wier, *J. Electrochem. Soc.*, **1951**, 98, 203.
- ¹⁵ F. H. Hurley and T. P. Wier, *J. Electrochem. Soc.*, **1951**, 98, 207.
- ¹⁶ J. S. Wilkes, J. A. Lewinsky, R. A. Wilson and C. L. Hussey, *Inorg. Chem.*, **1982**, 21, 1263.
- ¹⁷ J. S. Wilkes and M. J. Zaworotko, *Chem. Commun*, **1992**, 965.
- ¹⁸ J. Fuller, R. T. Carlin and R. A. Osteryoung, *J. Electrochem. Soc.*, **1997**, 144, 3881.
- ¹⁹ B. M. Quinn, Z. Ding, R. Moulton and A. J. Bard, *Langmuir*, **2002**, 18, 1734.
- ²⁰ R. P. Swatloski, J. D. Holbrey and R. D. Rogers, *Green Chem.*, **2003**, 5, 361.
- ²¹ P. Bonhôte, A.-P. Dias, N. Papageorgiou, K. Kalyanasundaram and M. Grätzel, *Inorg. Chem.*, **1996**, **35**, 1168.
- ²² F. Endres, A. P. Abbott and D. MacFarlane, Eds., *Electrodeposition of Metals from Ionic Liquids*, Wiley VCH, Weinheim, **2007**.

-
- 23 P. Wasserscheid, T. Welton, *Ionic Liquids in Synthesis* Wiley-VCH Verlag, Weinheim,
Germany 2003.
- 24 T. Welton, *Chem. Rev.*, **1999**, 99, 2071.
- 25 P. Wasserscheid and W. Keim, *Angew. Chem. Int. Ed.* **2000**, 39, 3772
- 26 M. J. Earle and K. R. Seddon, *Pure Appl. Chem.* **2000**, 72, 1391
- 27 K. Seddon, *Nat. Mater.*, **2003**, 2, 363.
- 28 N. Gathergood, P. J. Scammells and M. T. Garcia, *Green Chem.*, **2006**, 8, 156.
- 29 Z. Du, Z. Li, S. Guo, J. Zhang, L. Zhu and Y. Deng, *J. Phys. Chem. B*, **2005**, 109, 19542.
- 30 K. Fukumoto, M. Yoshizawa and H. Ohno, *J. Am. Chem. Soc.*, **2005**, 127, 2398.
- 31 A. P. Abbott, G. Capper, D. L. Davies, R. Rasheed and V. Tambyrajah *Chem. Commun*,
2003, 70.
- 32 Schroder, U.; Wadhawan, J. D.; Compton, R. G.; Marken, F.; Suarez, P. A. Z.; Consorti,
C. S.; de Souza, R. F.; Dupont, J., *New J. Chem.* **2000**, 24, 1009.
- 33 D. R. MacFarlane, P. Meakin, J. Sun, N. Amini and M. Forsyth, *J. Phys. Chem. B* **1999**,
103, 4164.
- 34 J. Robinson, and R. A. Osteryoung, *J. Electrochem. Soc.* **1980**, 127, 122.
- 35 Y. NuLi, J. Yang, J. Wang, J. Xu and P. Wang, *Electrochem. Solid-State Let.* **2005**, 8,
C166.
- 36 W. Freyland, C. A. Zell, S. Z. El Abedin, and F. Endres, *Electrochim. Acta* **2003**, 48,
3053.
- 37 N. Borisenko, S. Z. El Abedin, and F. Endres, *J. Phys. Chem. B* **2006**, 110, 6250.
- 38 A. P. Abbott and K. J. McKenzie, *Phys. Chem. Chem. Phys.*, **2006**, 8, 4265.
- 39 F. Endres, *Chem. Phys. Chem* **2002**, 3, 144.
- 40 N. Koura, T. Endo and Y. Idemoto, *J. Non-Cryst. Solids*, **1996**, 205, 650. b) L.
Simanavicius, A. Stakenas, A. Starkis, *Electrochim. Acta*, 1997, **42**, 1581.
- 41 P. Chen, M. Lin and I. Sun, *J. Electrochem. Soc.*, **2000**, 147, 3350
- 42 P. Chen, and I. Sun, *Electrochim. Acta*, **2001**, 46, 1169.
- 43 A. P. Abbott, G. Capper, D. L. Davies, H. Munro, R. Rasheed and V. Tambyrajah *Chem.*
Commun., **2001**, 2010

-
- 44 M. S. Sitze, E. R. Schreiter, E. V. Patterson and R. G. Freeman, *Inorg. Chem.*, **2001**, 40,
2298.
- 45 Y. Zhao and T. J. VanderNoot. *Electrochimica Acta*, **1997**, 42, 3.
- 46 J-Z. Yang, Y. Jin, W. G. Xu, Q-G. Zhang, S. L. Zang, *Fluid Phase Equil.* **2005**, 227, 41.
- 47 A. P. Abbott, G. Capper, D. L. Davies and R. Rasheed *Chem. Eur. J.* **2004**, 10, 3769
- 48 A. P. Abbott, G. Capper, D. L. Davies, R. Rasheed and V. Tambyrajah *Chem. Commun*,
2003, 70.
- 49 A. P. Abbott, D. Boothby, G. Capper, D. L. Davies and R. Rasheed *J. Am. Chem. Soc.*
2004, **126**, 9142
- 50 A. P. Abbott, J. C. Barron, K. S. Ryder and D. Wilson, *Chem. Eur. J.* 2007, 13, 6495
- 51 A. P. Abbott, G. Capper, D. L. Davies, H. Munro and R. Rasheed, *Inorg. Chem.* **2004**, 43,
3447.
- 52 R. A. Sheldon, *Chem. Ind. (London)*, **1992**, 903
- 53 R. C. Harris PhD Thesis, University of Leicester, **2009**.
- 54 Y.-F. Lin, I. W. Sun, *Electrochim. Acta* **1999**, 44, 2771
- 55 T. Iwagishi, H. Yamamoto, K. Koyama, H. Shirai, H. Kobayashi, *Electrochem.* **2002**, 70,
671.
- 56 P.-Y. Chen, M.-C. Lin, I. W. Sun, *J. Electrochem. Soc.* **2000**, 147, 3350.
- 57 T. Iwagishi, K. Sawada, H. Yamamoto, K. Koyama, H. Shirai, *Electrochem.* **2003**, 71,
318.
- 58 J.-F. Huang, I. W. Sun, *Electrochim. Acta* **2004**, 49, 3251.
- 59 J.-F. Huang, I. W. Sun, *J. Electrochem. Soc.* **2003**, 150, E299.
- 60 J.-F. Huang, I. W. Sun, *J. Electrochem. Soc.* **2004**, 151, C8.
- 61 J. C. Barron, PhD Thesis, University of Leicester, **2009**
- 62 A. P. Abbott, G. Capper, D. L. Davies, R. K. Rasheed, J. Archer and C. John *Trans. Inst.*
Metal Finish, **2004**, 82, 14
- 63 A. P. Abbott, K. S. Ryder and U. Koenig, *Trans. Inst. Metal Finish*, **2008**, 196
- 64 S. Mohan, D. Kanagaraj, R. Sindhuja, S. Vijayalakshmi and N. G. Renganathan, *Trans.*
Inst. Metal Finish., **2001**, 79, 140.
- 65 D. Landolt, *Electrochim. Acta*, **1987**, 32 1

-
- 66 A. P. Abbott, G. Capper, B. Swain and D. Wheeler, *Trans. Inst. Metal Finish*, **2005**, 82,
51
- 67 A. P. Abbott, G. Capper, K. J. McKenzie and K. S. Ryder *Electrochim. Acta* **2006**, 51,
4420.
- 68 S. Dai Y. S. Shin, L. M. Toth, and C. E. Barnes *Inorg. Chem.* **1997**, 36, 4900.
- 69 A. Chaumont and G. Wipff, *Chem. Eur. J.*, **2004**, 10, 3919.
- 70 H-L. Huang, H. P. Wang, E. M. Eyring and J. E. Chang, *Env. Chem.*, **2009**, 6, 268.
- 71 A. P. Abbott, R. C. Harris and K. S. Ryder *J. Phys. Chem. B*, **2007**, 111, 4910.
- 72 A. P. Abbott, G. Capper and P. Shikotra, *Trans. Inst. Min. Metall. C*, **2006**, 115, 15.
- 73 A. P. Abbott, G. Capper, D. L. Davies, K. J. McKenzie and S. U. Obi, *J. Chem. & Eng.
Data* **2006**, 51, 1280.
- 74 A. P. Abbott, J. Collins, I. Dalrymple, R. C. Harris, R. Mistry, F. Qiu, J. Scheirer, and W.
R. Wise, *Aust. J. Chem.* **2009**, 62, 341–347.
- 75 A. P. Abbott, G. Frisch, J. Hartley and K. S. Ryder, *Green Chem.*, in press
- 76 E. L. Smith, J. C. Barron, A. P. Abbott and K. S. Ryder, *Anal. Chem.* **2009**, 81, 8466
- 77 A. P. Abbott, S. Nandhra, K. S. Ryder and E. Smith, *Phys. Chem. Chem. Phys.* **2007**, 9,
3735
- 78 A. P. Abbott, J. Griffith S. Nandhra, C. O'Connor, S. Postlethwaite, K. S. Ryder and E.
Smith, *Surf. Coat. Tech.* **2008**, 202, 2033
- 79 S. B. Phadtare, G. S. Shankarling, *Green Chem.*, **2010**, 12, 458
- 80 Z. Chen, W. Zhu, Z. Zheng, and X. Zou, *J. Fluor. Chem.* **2010**, 131, 340.
- 81 F. Himeur, I. Stein, D. S. Wragg, A. M. Z. Slawin, P. Lightfoot, R. E. Morris, *Solid State
Sci.* **2010**, 12, 418.
- 82 S. M. Wang, Y. W. Li, X. J. Feng, Y. G. Li, E. B. Wang, *Inorgan. Chim. Acta* **2010**,
363, 1556.
- 83 J. Y. Dong, Y-J. Hsu, D. S. H. Wong, S. Y. Lu, *J. Phys. Chem. C* **2010**, 114, 8867
- 84 P. C. Jhang, N. T. Chuang, S. L. Wang, *Angew. Chem., Int. Ed.* **2010**, 49, 4200
- 85 S. Chen, J. Zhang, T. Wu, P. Feng, X. Bu, *Dalton Trans.* **2010**, 39, 697.
- 86 E. A. Drulie, D. S. Wragg, E. R. Parnham, P. S. Wheatley, A. M. Z. Slawin. J. E. Warren,
R. E. Morris *Angew. Chem., Int. Ed.* **2007**, 46, 7839.

-
- 87 J. T. Gorke, F. Srienc, R. J. Kazlauskas, ACS Symp. Ser. **2010**, 1038 (Ionic Liquid Applications), 169.
- 88 D. Lindberg, M. de la Fuente Revenga, M. Widersten, *J. Biotech.* **2010**, 147, 169.
- 89 J. T. Gorke; F. Srienc, R. J. Kazlauskas *Biotech. Bioproc. Eng.* **2010**, 15, 40.
- 90 Y. A. Sonawane, S. B. Phadtare, B. Borse, A. R. Jagtap, G. S. Shankarling, *Org. Lett.* **2010**, 12, 1456.
- 91 M. C. Gutierrez, M. L. Ferrer,; C. R. Mateo, F. del Monte, *Langmuir* **2009**, 25, 5509.
- 92 M. Hayyan, F. S. Mjalli, M. A. Hashim, I. M. AlNashef, *Fuel Proc. Tech.* **2010**, 91, 116
- 93 A. P. Abbott, P. M. Cullis, M. J. Gibson, R. C. Harris and E. Raven *Green Chem.*, **2007**, 9, 868
- 94 H. R. Jhong, D. S. H. Wong, C. C. Wan, Y. Y. Wang, T. C. Wei, *Electrochem. Commun.* **2009**, 11, 209.
- 95 A. P. Abbott, K. El Ttaib, K. S. Ryder and E. L. Smith, *Trans. I. M. F.* **2008**, 86, 234
- 96 A. P. Abbott, K. El Ttaib, G. Frisch, K. J. McKenzie and K. S. Ryder *Phys. Chem. Chem. Phys.* **2009**, 11, 4269
- 97 C. D. Gu, X. Xu, J. P. Tu, *J. Phys. Chem. C* **2010**, 114, 13614
- 98 P. Martis, V. S. Dilimon, J. Delhalle, Z. Mekhalif, *Electrochim. Acta* **2010**, 55, 5407.

Chapter 2: Experimental

2.1 Materials

2.2 Speciation

2.2.1 Fast atom bombardment mass spectrometry (FAB MS)

2.2.2 Uv visible spectrophotometer

2.3 Electrochemical Methods

2.4 Quartz Crystal microbalance (QCM)

2.5 Surface microstructure analysis

2.5.1 Atomic force microscope (AFM)

2.5.2 Scanning electron microscope (SEM)

2.5.3 Cross-section microstructure

2.6 Surface profile analysis

2.6.1 Profilometry

2.6.2 Digital holographic microscope

2.7 Mechanical properties

2.7.1 Hardness

2.7.2 Wear test

2.8 Viscosity

2.10 Bulk Deposition

2.11 References

2.1 Materials

Choline chloride [$\text{HOC}_2\text{H}_4\text{N}(\text{CH}_3)_3\text{Cl}$] (ChCl) (Aldrich 99 %) was, when necessary, recrystallised from absolute ethanol, filtered and dried under vacuum. Urea (Aldrich > 99%) was dried under vacuum prior to use. Ethylene glycol (EG) (Aldrich + 99 %), was used as received. The mixtures were formed by stirring the two components together (in a 1: 2 molar ratio of ChCl: hydrogen bond donor) at 60 °C until a homogeneous, colourless liquid formed.

The metal halide salts; $\text{CuCl}_2 \cdot 2\text{H}_2\text{O}$ (Aldrich ≥ 98 %), $\text{NiCl}_2 \cdot 6\text{H}_2\text{O}$ (Aldrich ≥ 98 %), AgCl (Aldrich), were used as obtained. The concentrations of metal salts were 0.02 mol dm^{-3} of $\text{CuCl}_2 \cdot 2\text{H}_2\text{O}$, 0.2 mol dm^{-3} $\text{NiCl}_2 \cdot 6\text{H}_2\text{O}$ and 0.1 mol dm^{-3} AgCl unless otherwise stated. Lithium fluoride (BDH) was used as received.

The additives ethylene diamine (en) (Aldrich) sodium acetyl acetoacetate (Na acac) (Aldrich) and the surfactants hexacetylammoniumbromide (CTAB), (Aldrich) and sodium dodecyl sulphate, (SDS) (Aldrich) were all used as received.

The composite materials used in this study were alumina (Al_2O_3) with two particle sizes; 50 nm and 1 μm (Buehler, deagglomerated gamma alumina), silicon carbide in two sizes 45-55 nm (Alfa Aesar β -phase) and 1-3 μm (SKOA grade from ESK) and polytetrafluoroethylene 1 μm (Aldrich).

2.2 Speciation

2.2.1 Fast atom bombardment mass spectrometry (FAB MS)

FAB MS was carried out using a KRATOS CONCEPT IIIH Mass spectrometer using Xe gas at about 7-8 KV.

2.2.2 Uv visible spectrophotometer

A Shimadzu model uv-1601 spectrophotometer was used with the cell path length equal to 10mm. Values for λ_{max} were determined using the spectrophotometer's built-in peak-pick feature, using uv- probe software.

2.3 Electrochemical methods

All voltammetry and chronocoulometry investigations were carried out using an Autolab PGSTAT 20 potentiostat (Ecochemie, Holland) controlled with GPES software. Two systems each consists three electrodes, platinum microelectrode (0.12cm² area) (made in-house) a platinum flag counter electrode and a silver wire reference electrode. The working electrode was polished with 0.3 μm alumina paste, sonicated for 10 minutes in deionized water and washed with acetone and dried with N₂ prior to each experiment. All voltammograms were performed at room temperature at different scan rates.

The bulk copper and silver deposition was performed on nickel substrates and the bulk nickel depositions were conducted on copper substrates which were first manually polished with progressively finer grades of silicon carbide polishing paper, rinsed with water, sonicated 15 minutes in acetone and dried with N₂. The anode for the bulk copper deposition was copper plate, for the bulk nickel deposition was nickel plate and for bulk silver depositions was a dimensionally stable iridium oxide coated Ti mesh.

2.4 Quartz crystal microbalance (QCM)

In 1880, Jacques and Pierre Curie¹ discovered that a mechanical stress applied to the surfaces of various crystals such as quartz, afforded a corresponding electrical potential across the crystal whose magnitude was proportional to the applied stress. The converse piezoelectric effect also exists in which application of a voltage across these crystals afforded a corresponding mechanical strain and this is the basis of the QCM.

Consider that a reduction process takes place which results in a mass load on the crystal. This will lead to a fractional change in thickness and a resultant fractional change in the oscillating frequency of the crystal. The relationship between the change in mass (Δm) and change in frequency (Δf) is given by Sauerbrey equation, **Equation 2.1**²

$$\Delta f = -\frac{2f_o^2}{\rho v} \Delta m \quad \mathbf{2.1}$$

where ρ is the density of quartz and v is the wave velocity. The Sauerbrey equation assumes that the shift in frequency at the centre of the crystal is the same as that at the

edges of the crystal, furthermore the deposited mass acts as a rigid resonator³ this will lead to any shift in frequency is due to mass loaded.

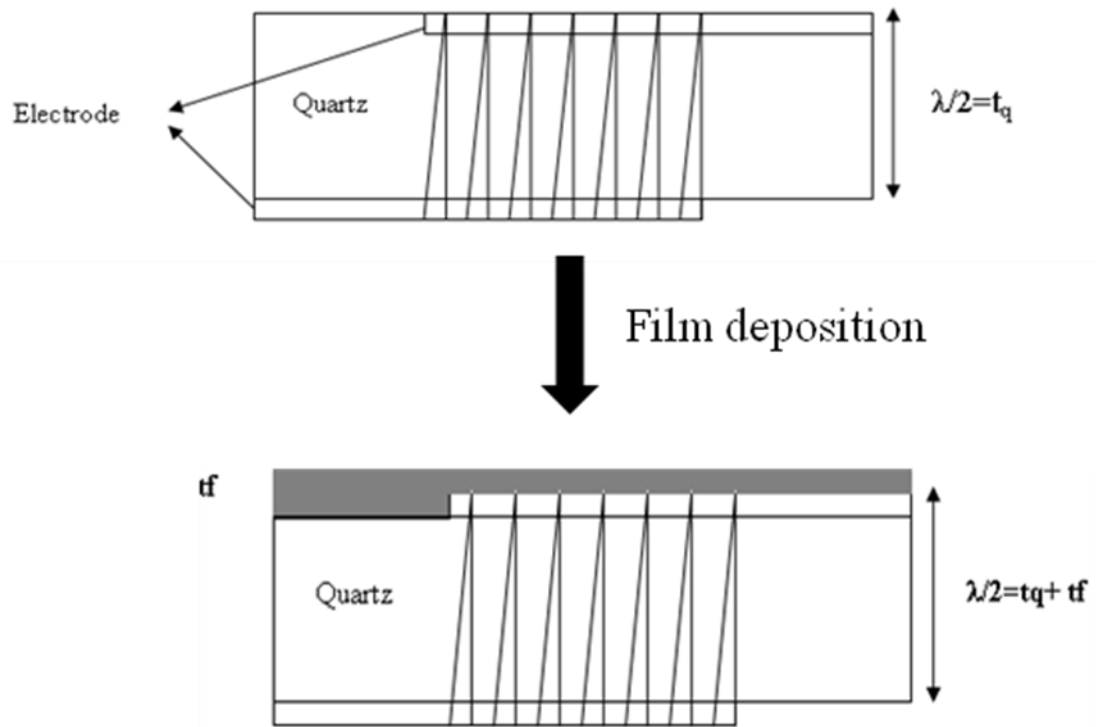


Figure 1 Schematic representation of the transverse shear wave in a quartz crystal and a composite resonator comprising the quartz crystal and a layer of a foreign material. The acoustic wavelength is longer in the composite resonator due to the greater thickness, resulting in a low resonant frequency compared to the quartz crystal

Crystal impedance spectra were recorded using a Hewlett Packard HP8751A network analyzer, connected to a HP87512A transmission/reflection unit via 50 ohm coaxial cable as detailed elsewhere. The working electrode was a thin gold film evaporated onto a 10MHz quartz crystal with a unpolished "frosted" finish (purchased from the International Crystal Manufacturing Co. Oklahoma City, USA) . The piezoelectric active electrode area was 0.23cm^2 .

The measured data were fitted to a Lorentzian equivalent circuit model, **Equation 2.2**, incorporating the in-phase impedance, inductance and centre frequency, with an iterative difference method using Microsoft Excel. The fitting procedures used are described in depth in the literature. In order to improve the temporal resolution, network analyzer data

acquisition was controlled by a computer running HP VEE. This program was capable of recording admittance spectra every 2-3 s. The crystal was placed into a cell such that one face of the crystal was exposed to the solution and one face was exposed to air. The electrodes used to complete the electrochemical cell were platinum flag and silver wire as reference electrode. EQCM experiments were performed at room temperature (typically 20-23 °C) except otherwise stated.

$$U(f) = a + ((R)/(R^2 + 16\pi^2 L^2 (f - f_o))) \quad 2.2$$

Here $U(f)/\Omega^{-1}$ is the measured admittance curve as a function of applied frequency f/Hz (and $U(f) = 1/Z(f)$), R/Ω is the real component of the impedance (Z), $L/Henry$ is the inductance, f_o/Hz is the centre frequency and a/Ω^{-1} is the base line offset. The latter was used during fitting to compensate for variations in the static calibration of the network analyser.

2.5 Surface microstructure analysis

2.5.1 Atomic force microscope (AFM)

Digital Instruments Nanoscope IV Dimension 300 (Veeco) atomic force microscope with a 100 mm scanning head was used in both contact and tapping (resonant) modes. Images were acquired in air.

2.5.2 Scanning electron microscope (SEM)

SEM and EDX elemental analysis was carried out under vacuum using a Philips XL30 ESEM instrument.

2.5.3 Cross-section microstructure

The samples were mounted in a resin using a Struers Labo Press 3. The samples were then polished first with 240 grit silicon carbide paper to make them flat, then with diamond abrasives of successively 9 μm and 3 μm size and finally with 0.5 μm colloidal silicon carbide paste.

2.6 Surface profile analysis

2.6.1 Profilometry

The depth and the area of worn surface (scar) of the nickel and silver deposits were determined by Taylor Hobson Surtronic 3+ and data obtained analyzed by Taly profile software.

2.6.2 Digital holographic microscope (DHM)

The surface roughness of silver deposits and worn surfaces with and without composites were determined using a Lancee tec DHM with sensor Baumer model TXF14, and the data obtained were analyzed by Koala software.

2.7 Mechanical properties

2.7.1 Hardness

The hardness test for copper, nickel and silver deposits with and without composites was performed by Mitutoyo model MVK-G100.

2.7.2 Wear test

Wear volumes using a Teer Coatings Ltd. model ST200 instrument using virtual instrument Lab View, and the friction was determined by MATLAM R2010a.

2.8 Viscosity

Viscosity measurements were obtained using a Brookfield DV-E Viscometer fitted with a thermostatted jacket.

2.9 Methodology of bulk deposition

2.10 Bulk Deposition

The substrates made of copper and nickel were used in the deposition of copper, silver and nickel, all the substrates polished by sand paper, washed with deionised water acetone, sonicated and dried. The electrodepositing was carried out using Thrlby Thander PL320 AC power supply.

2.11 References

- ¹ D. Buttry and M. Ward, *Chem. Rev.* **1992**, 92, 1355.
- ² G. Z. Z. Sauerbrey, *Physics* **1959**, 155,206.
- ³ A. Glidle, A. R. Hillman, S. J. Bruckenstein, *J. Electroanal. Chem.* **1991**, 318, 411.

Chapter 3: The Electrodeposition of Copper Composites using Deep Eutectic Solvents

3.1 Introduction

3.2 Electrodeposition of Copper

3.2.1. Cyclic voltammetry

3.2.2 Diffusion coefficients

3.2.3 Chronocoulometry

3.2.4 Chronoamperometry

3.2.5 Gravimetric investigation

3.3 Electrodeposition of Composites Materials

3.3.1. Cyclic voltammetry

3.3.2. Gravimetric analysis of the Cu composites

3.3.3 Addition of a hard dispersed phase (SiC 1-3 μm)

3.3.4. Addition of a soft dispersed phase (polytetrafluoroethylene, PTFE 1 μm)

3.3.5. Use of Surfactants

3.4 Conclusions

3.5 References

3.1 Introduction

The electrodeposition of copper is essential for a variety of industrial and decorative purposes including large scale use in the electronics industry for production of printed circuit boards, selective case hardening of steel for engineering components, and production of electrotypes in the printing industry.^{1,2} Copper may be easily deposited and electroplated with other metals and it is therefore particularly useful as a pre-coating for soft soldered work or for zinc alloy die-castings used by the automotive industry. In these cases the copper deposit provides a protective layer to the metal to allow further coatings to be applied.³ Also the incorporation of particulate material into metal coatings has become an area of technological interest; for example incorporation of poly(ethylene) can act as a corrosion barrier, incorporation of PTFE or mica can reduce surface friction whereas incorporation of alumina, silicon carbide, boron nitride or diamond can greatly increase hardness of the metal coating^{4,5,6,7}.

Commercial copper electroplating is based on aqueous solutions which have high solubility for electrolytes and metal salts resulting in highly conducting solutions. They have high throwing power and components with complex shapes and internal surfaces can be plated with ease. However, the cyanide and acid based copper plating solutions that are most generally employed are highly corrosive and suffer from several drawbacks including, toxic effluent, high energy consumption and air pollution. Recently, ionic liquids have been proposed as alternative plating solutions, and these could offer a less environmentally hazardous option. Copper has been electrodeposited from many ionic liquids and in the 1960s and 1970s the study of these systems was dominated by chloroaluminate ionic liquids.^{8,9,10,11} With the introduction of discrete anions such as $[\text{BF}_4]^-$, and $[\text{F}_3\text{CSO}_2)_2\text{N}]^-$ ($[\text{Tf}_2\text{N}]^-$) in the 1990s copper could be more easily electrodeposited and the air and moisture stability of these system.^{12,13} Endres and co-workers have shown that copper may be deposited from $[\text{BMP}][\text{Tf}_2\text{N}]$ at various temperatures (BMP = butylmethyl pyrrolidinium). However, this particular ionic liquid has limited solubility for copper compounds and copper cations had to be introduced into the liquid *via* anodic dissolution of a copper electrode.¹⁴ This work highlights that a key issue with the design of ionic plating systems is the coordination chemistry and concentration of the metal complex. While ionic liquids with discrete anions show significant potential for the electrodeposition of electronegative metals such as

aluminium,¹⁵ issues such as toxicity, availability and cost may limit their practical use.

It has recently been shown that simple eutectic-based ionic liquids can be produced using quaternary ammonium salts $R_1R_2R_3R_4N^+X^-$ complexed with hydrogen bond donors such as acids, amides and alcohols. These liquids, also known as deep eutectic solvents (DES) have been used for electropolishing,^{16,17,18} polymer synthesis,¹⁹ electroless (immersion) deposition^{20,21} and metal oxide processing.^{22,23} Most of our previous studies have concentrated on choline chloride as the quaternary ammonium salt as it is non-toxic, biodegradable and is used already as a common constituent of various household and industrial products. Hence it can be applied economically to large-scale processes. DESs formed with choline chloride and either urea or ethylene glycol have successfully been employed for the electrodeposition of zinc, tin, and zinc–tin alloys.²⁴ It was shown that the choice of hydrogen bond donor affects the type of alloy and the electrochemistry of the components in solution, as well as the morphology of the coatings. The area of metal deposition using ionic liquids has been thoroughly reviewed in a series of recent articles^{25,26,27,28} and a book.²⁹

In this section it is shown that ionic liquids based on eutectic mixtures of choline chloride and hydrogen bond donors such as urea or ethylene glycol can be used as electrochemical solvents for the electrodeposition of copper. A combination of electrochemical techniques including EQCM, cyclic voltammetry and chronocoulometry together with scanning electron microscopy have been used to characterise these systems. It is shown that in both liquids the current efficiency for copper deposition is close to 100%. Composites of copper with Al_2O_3 and SiC have also been produced and it is shown that the proportion of these species incorporated into the resulting electroplated films is determined by the mass loading in the solution. The main mechanism for particulate inclusion is drag onto the electrode surface. The inclusion of suspended particles in the liquid is found to have negligible effect upon the fluid viscosity of the suspension; it is proposed that this is a consequence of the increased free volume in the fluid component caused by the motion of the suspended particles *i.e.* the particles act as micro stirrers in the liquid.

3.2 Electrodeposition of Copper

3.2.1. Cyclic voltammetry

The potential windows of both urea and ethylene glycol based DESs have been reported previously and are outside the electrochemical regions discussed in this work.^{30,29}

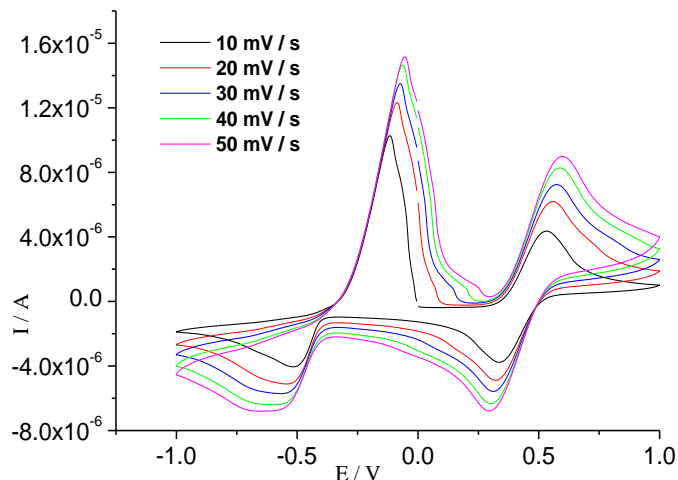


Figure 3.1a Cyclic voltammogram for a Pt disc (1.0 mm diam.) electrode immersed in 0.1 M $[\text{CuCl}_2 \cdot 2\text{H}_2\text{O}]$ in 1 ChCl: 2 urea based liquids as a function of sweep rate. (Potential versus Ag wire quasi-reference electrode).

Cyclic voltammograms (CVs) were recorded at a polished 1.0 mm Pt disc electrode immersed in a solution of 0.1 M $[\text{CuCl}_2 \cdot 2\text{H}_2\text{O}]$ in a 1 ChCl: 2 urea based liquid as a function of sweep rate, **Figure 3.1a**. These voltammograms show that there are two distinct reduction processes corresponding to the reversible $\text{Cu(II)}/\text{Cu(I)}$ couple at +0.43 V followed by the reduction from Cu(I) to Cu(0) at -0.45 V. The latter process results in metallic copper deposition with a characteristic stripping response on the anodic scan. **Figure 3.1b** shows the corresponding CVs for the solution of 0.1 M $[\text{CuCl}_2 \cdot 2\text{H}_2\text{O}]$ in 1 ChCl: 2 EG based liquid. It is interesting to note that the redox potentials of these two processes, $\text{Cu}^{2+}/\text{Cu}^+$ and Cu^+/Cu^0 with respect to the Ag quasi-reference electrode, are essentially the same in both liquids.

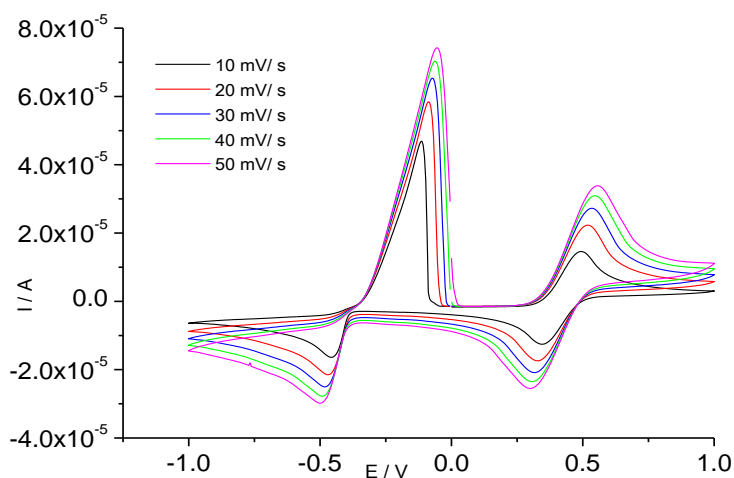


Figure 3.1b Cyclic voltammogram for a Pt disc (1.0 mm diam.) electrode immersed in 0.1 M $[\text{CuCl}_2 \cdot 2\text{H}_2\text{O}]$ in 1 ChCl: 2 EG based liquids as a function of sweep rate. (Potential versus Ag wire quasi-reference electrode)..

Where the voltammetry of the anodic reversible couple was carried out in the absence of cathodic deposition the curve shapes are more clearly defined and the criteria for thermodynamic reversibility are more readily established. The anodic/cathodic peak current ratios are essentially independent of scan rate although the potential peak separation values of $\Delta E_p = 110$ mV and $\Delta E_p = 101$ mV for the urea and EG based liquids respectively (taken from the data presented in **Figure 3.1a** and **3.1b**) are somewhat larger than might be expected for a one electron Nernstian process. However, departure of the experimental ΔE_p measurements from the theoretical value, 59 mV ($T = 298$ K), are common for resistive organic electrolytes and the voltammograms presented here are not compensated for solution resistance.

Both **Figures 3.1a** and **3.1b** also show that the difference in reduction potential between the $\text{Cu}^{2+} / \text{Cu}^+$ and $\text{Cu}^+ / \text{Cu}^0$ couple is 0.88 V which is significantly different to that found in water where the difference is only 0.37 V.³¹ This is due to the instability of Cu^+ in aqueous solutions *i.e.* through disproportionation. In concentrated $\text{HCl}(\text{aq})$, however, disproportionation does not occur and a similar difference in redox potential is observed as in both ionic liquids.

At slow scan rates (10 mV s^{-1}) the $\text{Cu}^{2+}/\text{Cu}^+$ couple appears reversible in both ionic liquids.

The ratio of anodic and cathodic charges for this redox couple (determined by numerical integration between 0.0 V and +1.0 V) is essentially unity in both cases; this indicates that during reduction of Cu^{2+} to Cu^+ no material is irreversibly adhered to the surface either by adsorption or under potential deposition (upd). At faster scan rates, however, a shoulder is clearly visible at around 0.0 V in the voltammogram for the urea based liquid, **Figure 3.1a**, it is proposed, on the basis of previous observations, that this may be due to upd; the absence of a corresponding peak in the voltammogram of the EG liquid is not entirely surprising since the coordination chemistry of EG and urea with respect to $\text{Cu}^{2+/+}$ ions is known to be very different (at least in water). A correlation between upd and deposit morphology for Zn and Al has been observed in different eutectic based ionic liquids.³² It has been found that for these two metals upd encourages the deposition of large crystallites leading to crystalline, dark deposits. Consequently suppression of upd tends to lead to smooth, bright deposits. In the cathodic portion, Cu^+/Cu^0 , of the voltammograms, **Figure 3.1**, the responses of the two liquids is quite different. Whilst the CV in the EG based liquid shows a classical stripping response at all experimental scan rates, the CV in the urea based liquid shows substantial shoulders on the cathodic side of the reduction wave and on the anodic side of the stripping wave. These are especially noticeable at faster scan rates. In recent studies a similar response has been observed for the deposition of zinc from these ionic liquids.³² Using AFM and SEM Smith *et al.* ascribed these processes to the deposition of two different morphologies³³. The origin of the different morphologies probably lies in the formation and extent of upd material formed prior to bulk electrolytic deposition.

3.2.2 Diffusion coefficients

The peak currents from the reversible $\text{Cu}^{2+}/\text{Cu}^+$ couple were plotted against the square root of potential scan rate and good linear correlations were obtained. From these plots the mean diffusion coefficients for $\text{Cu}^{2+/+}$ species, D_0 , were determined using an abbreviated form of the Randles-Sevcik equation, **Equation 3.1**:

$$I_p = K n^{3/2} A C D^{1/2} \nu^{1/2} \quad 3.1$$

$$\text{Where } K = 0.4463 \sqrt{\frac{F^3}{RT}} = 2.687 \times 10^5$$

I_p is the peak current, n is the number of electrons, A is the area of electrode, C is the bulk concentration, ν is the potential sweep rate, F is the Faraday constant, R is the gas constant

and T , the absolute temperature.³⁴ It was found that D_0 for $\text{Cu}^{2+/+}$ in urea-based the ionic liquid was $1.35 \times 10^{-8} \text{ cm}^2 \text{ s}^{-1}$, whilst the corresponding value of D_0 in the EG-based liquid, from **Figure 3.1b**, was $2.42 \times 10^{-7} \text{ cm}^2 \text{ s}^{-1}$. These compare with a value of $1.2 \times 10^{-6} \text{ cm}^2 \text{ s}^{-1}$ recently determined for Cu(I) in trimethyl-*n*-hexylammonium bis((trifluoromethyl)sulfonyl)amide (TMHA-Tf₂N) and with values of between $1 - 10 \times 10^{-6} \text{ cm}^2 \text{ s}^{-1}$ for Cu(II) in aqueous solution.^{35,36,37} The value of D_0 determined for the EG liquid is significantly larger than that for the urea liquid and both of these are very much smaller than those for TMHA-Tf₂N and water. This is not surprising and all of these values scale with the increasing viscosity of the fluids.

Alternatively, the diffusion coefficient for a mobile species in solution can be determined using the Stokes-Einstein model, **Equation 3.2**:

$$D = k T / 6\pi\eta a \quad 3.2$$

where, k , is the Boltzmann constant, T , temperature, η , viscosity, and, a , is the radius of the mobile species. The difficulty with using **Equation 3.2** is the unknown value of a since the Cu(II) species in solution is unknown. The importance of understanding speciation in ionic liquids together with the difficulty of obtaining unequivocal data has recently been highlighted.³⁸ For example FAB MS data whilst relatively easy to acquire have been ambiguous and difficult to interpret (probably because of fragmentation of the ionic species in the mass spectrometer).

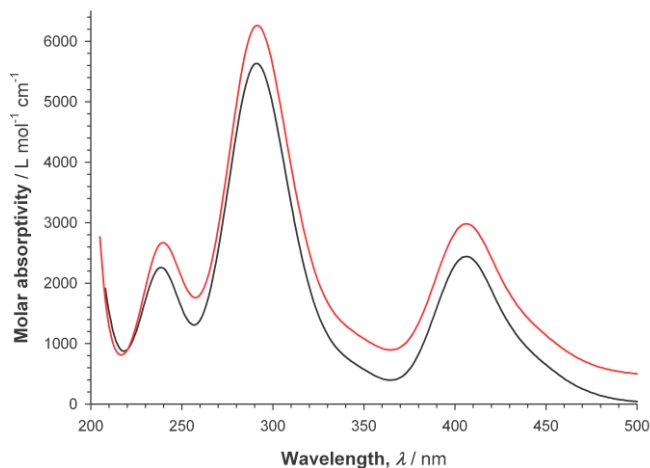


Figure 3.2 UV-Vis spectra of $[\text{CuCl}_2 \cdot 2(\text{H}_2\text{O})]$ (black) and anhydrous $[\text{CuCl}_2]$ (red) (0.2 mM) in 1EG : 2ChCl liquid. The spectra are offset by $500 \text{ L mol}^{-1} \text{ cm}^{-1}$ for clarity.

Notwithstanding this UV-Vis spectroscopy has provided some useful insight. The UV-Vis spectra of 0.2 mM solutions of both $[\text{CuCl}_2 \cdot 2\text{H}_2\text{O}]$ and anhydrous $[\text{CuCl}_2]$ in the 1 ChCl: 2 EG liquid are shown in **Figure 3.2**. The spectra show three charge transfer bands at 239, 291 and 406 nm. The fact that the spectra of both samples from hydrated and anhydrous salts are qualitatively identical in solution is a strong indication that water is displaced from the coordination sphere of the Cu^{2+} ion upon dissolution in the ionic liquid. This is perhaps not surprising given the concentration of chloride ion (4.8 M) in the solution relative to that of the Cu complex. The maximum total molar absorptivity for the $d-d$ transitions of $125 \text{ L M}^{-1} \text{ cm}^{-1}$ at 1119 nm suggests a noncentro-symmetric configuration. The energies of the $d-d$ transitions are between the expected values for tetrahedral (T_d , 1488nm) and square planar (D_{4h} , 615nm) coordination³⁹. Despite small energy shifts, which could be due to solvent effects, the spectra in the ionic liquid are comparable to the known experimental and calculated spectra of $[\text{CuCl}_4]^{2-}$ as Jahn Teller distorted tetrahedra (D_{2d}).⁴⁰

The volume of the sphere that encloses $[\text{CuCl}_4]^{2-}$ can be estimated from the solid state ionic radii of both Cu^{2+} and Cl^- ions.⁴¹ Typical values for Cu^{2+} ($r = 0.57 \text{ \AA}$, CN=4) and Cl^- ($r = 1.81 \text{ \AA}$, CN=6) give a Cu-Cl bond distance of 2.39 \AA and an equivalent ionic radius, based on a simple hard shell model, of $a = 4.19 \text{ \AA}$.

Using the latter value for ionic radius, a , and experimentally determined viscosity data (for the copper ion solutions) the values of D_0 were subsequently calculated using **Equation 2**.

Table 3.1: Comparison of calculated diffusion coefficient (from cyclic voltammogram data) and theoretical diffusion coefficient.

Solution	$D_{\text{calculated}} / \text{cm}^2 \text{s}^{-1}$	$D_{\text{theoretical}} / \text{cm}^2 \text{s}^{-1}$	Viscosity / cP at 20 °C
Cu^{2+} in water	3.29×10^{-6}	6.90×10^{-6}	1.01
CuCl_2 in 1 ChCl: 2 Urea	1.35×10^{-8}	4.27×10^{-8}	120
CuCl_2 in 1 ChCl: 2 EG	2.42×10^{-7}	3.01×10^{-7}	17

The diffusion coefficient for the copper species in 1 ChCl: 2 urea based liquid was found to be $4.27 \times 10^{-8} \text{ cm}^2 \text{ s}^{-1}$ (with $\eta = 120 \text{ cP}$) whilst in the 1 ChCl: 2 EG based liquid the value for diffusion coefficient was found to be $3.01 \times 10^{-7} \text{ cm}^2 \text{ s}^{-1}$ (with $\eta = 17 \text{ cP}$), **Table 3.1**. The experimental value of D_0 in the urea based liquid is somewhat smaller than that predicted by **Equation 3.2**. However, it is also important to note that the ionic radius calculation is based on solid state data and does not take into account any contribution made by the outer ionosphere. Given this limitation and the simplistic nature of the model it is gratifying to note that the experimental and theoretical (Stokes-Einstein) values of D_0 for the glycol based liquid are in good agreement.

Since the UV-Vis data, **Figure 3.2**, suggest that coordinated water molecules from the aqua complex, $[\text{CuCl}_2 \cdot 2(\text{H}_2\text{O})]$, are displaced by chloride, it is important to consider the effect of the liberated water on the physical properties of the bulk liquid, especially viscosity. The viscosity data have been collected as a function of water content for both urea and EG based liquids using a QCM methodology recently described elsewhere. The titration of up to 10% v/v water (equivalent to an H_2O concentration of 5.5 M) to, for example an EG based liquid, causes a decrease in viscosity of no more than 5%.¹⁶ Consequently liberation of coordinated H_2O from $[\text{CuCl}_2 \cdot 2(\text{H}_2\text{O})]$ present in solution at a concentration of 0.1 M results in an H_2O concentration well below the threshold at which significant changes in viscosity would be expected.

3.2.3 Chronocoulometry

Figure 3.3 shows the results of a chronocoulometry experiment for a Pt disc electrode in a 0.01 M [CuCl₂·2H₂O] in both 1 ChCl: 2 EG and 1 ChCl: 2 urea based liquids. The results are for a potential step from +1.00 V (held for 10 s) to -1.00 V for 27 min. The plots of charge versus $t^{1/2}$ are linear suggesting that the processes are diffusion controlled.

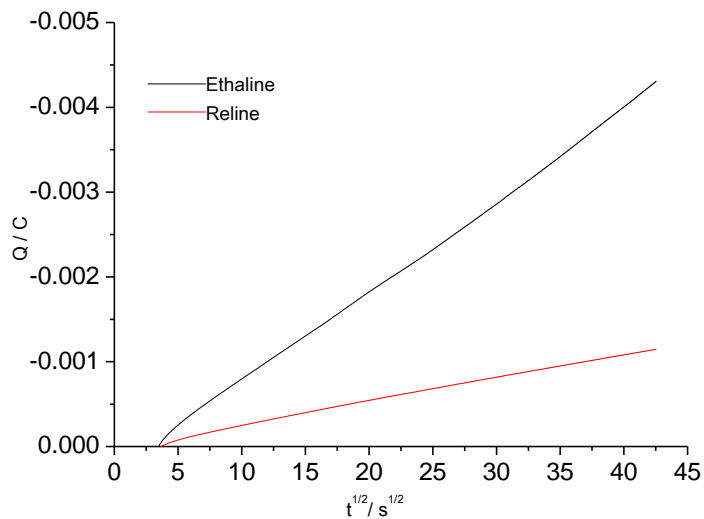


Figure 3.3 Chronocoulometry *e*) based liquids for potential steps from 1.00 V for 10s followed by a step to -1.00V for of 0.01 M [CuCl₂·2H₂O] in both 1 ChCl: 2 EG and 1 ChCl: 2 urea (ca 27 min (1.0 mm diam. Pt wire)).

3.2.4 Chronoamperometry

To elucidate the mechanism of nucleation chronoamperometry was performed on the $[\text{CuCl}_2 \cdot 2\text{H}_2\text{O}]$ solutions in both EG and urea based ionic liquids. It is often the case that nucleation studies are strongly sensitive to experimental conditions including concentration of reactant and applied potential (as well as surface roughness). This is also the case here.

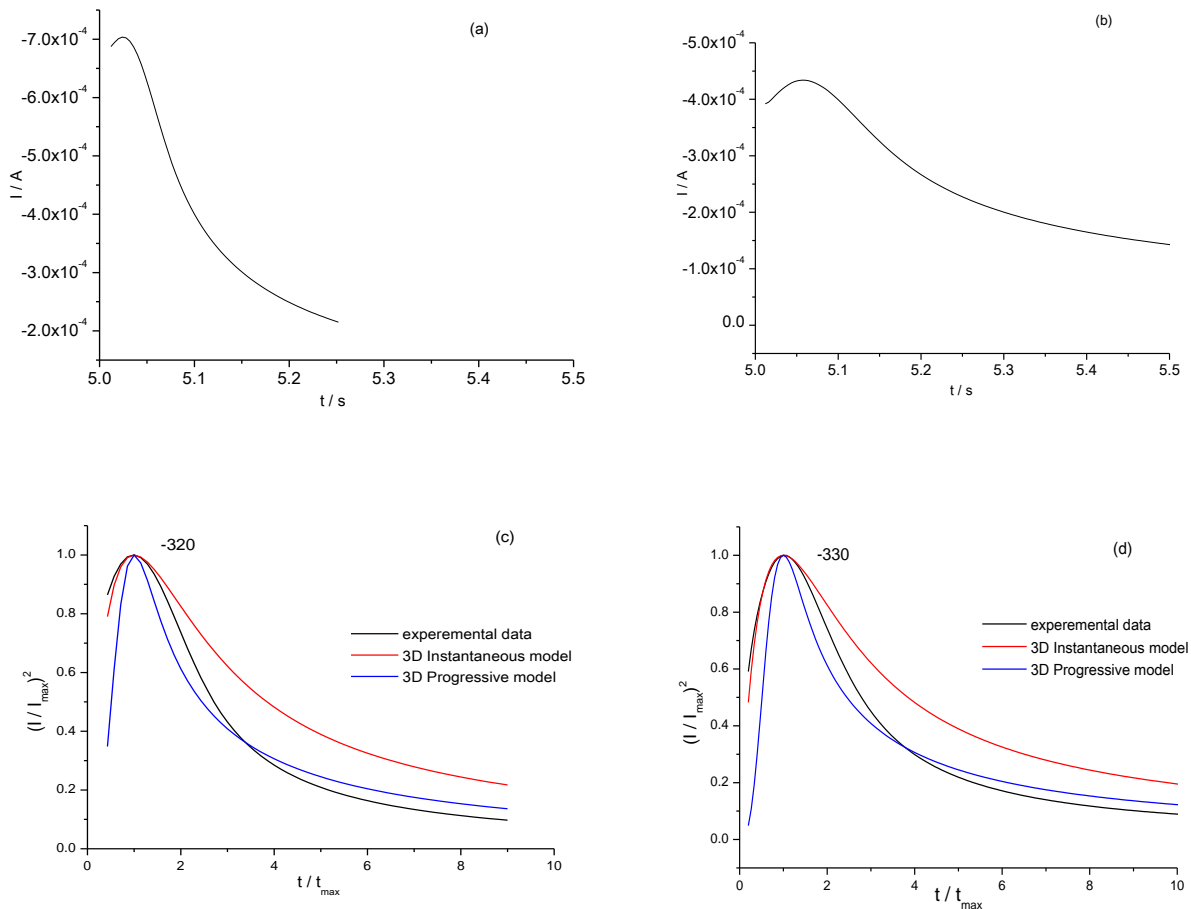


Figure 3.4 The experimental $I-t$ data for the electrodeposition of Cu from 1 ChCl: 2 EG (a) -320 mV (b) -330 mV. Comparison of dimensionless time versus dimensionless current (**Equations 3.3 and 3.4**) for 0.02M $[\text{CuCl}_2 \cdot 2\text{H}_2\text{O}]$ in 1 ChCl: 2 EG following a potential step from 0 to (c) -320 mV (d) -330 mV versus Ag wire quasi-reference electrode.

Consequently choosing the optimum, appropriate and representative values for these key variables can be problematic. In this experiment concentrations of between 0.01 M – 0.02 M were chosen because at higher concentrations nucleation was too fast on the polished Pt disks

to resolve the current maximum. Applied potentials of -0.32 V and -0.33 V were selected for the nucleation studies being the first onset values resulting in a clear and well-defined nucleation peaks. Although this value is at least 100 mV less cathodic than the onset of the deposition wave in the CV, (**Figure 3.1**) it should be noted that the nucleation events are not synchronous with electron-transfer processes observed in the CV, especially at faster scan rates. Additionally, equivalent rates of electron-transfer reactions can often be faster in a potential step experiment than for those observed at the same potential in a CV. This is because surface concentrations of species will be higher (according to equilibration conditions) for the potential step experiment and slow double layer reorganisation (typical in a viscous fluid) may tend to favour closer association of the Cu⁺ ion with the electrode surface established at the equilibration potential. A conventional approach was taken to analyse the chronoamperometric data using dimensionless current and time plots for 3 dimensional instantaneous, **Equation 3.3**, and progressive, **Equation 3.4**, nucleation mechanisms where i_m and t_m represent the current and time coordinate values of the nucleation peak.⁴² This approach has been used extensively to analyse electrodeposition of metals and recently in ionic liquids systems for metals as diverse as Ni and Al.^{43,44} The normalised plot for a typical Cu deposition data set is shown in **Figure 3.4**.

$$\left(\frac{i}{i_m}\right)^2 = 1.9542 \frac{t_m}{t} \left\{ 1 - \exp \left[-1.2564 \left(\frac{t}{t_m} \right) \right] \right\}^2 \quad 3.3$$

$$\left(\frac{i}{i_m}\right)^2 = 1.2254 \frac{t_m}{t} \left\{ 1 - \exp \left[-2.3367 \left(\frac{t}{t_m} \right)^2 \right] \right\}^2 \quad 3.4$$

It can be seen from the data presented in **Figure 3.4** that initially the nucleation conforms to a 3 dimensional instantaneous mechanism, however, at longer time scales, $t > t_m$, the mechanism changes to 3 dimensional progressive nucleation. Bulk electrolysis of an EG based DES containing copper ($0.01 < [\text{Cu}^{2+}] < 0.1 \text{ M}$) results in a bright deposit, however, electrodeposition at a lower copper concentration ($0.01 \text{ M} > [\text{Cu}^{2+}]$) results in a black deposit.

The results above are contrary to those expected from aqueous solutions, i.e. other studies have shown the opposite transition occurs with progressive nucleation giving way to instantaneous upon increasing concentration.³⁶ This shows unequivocally that the rationale for depositing bright metal films onto surfaces with ionic liquid (DES) electrolytes is very

different from that for aqueous solutions. The disparity, highlighted here, in mechanism and experimental conditions, required for control of surface finish, between aqueous systems and ionic liquids also helps to explain the anecdotal experience of many researchers using brighteners and levellers developed for aqueous electrolytes that are ineffective at producing bright coatings using ionic liquids.^{29, 30}

3.2.5 Gravimetric investigation

An electrochemical quartz crystal microbalance, EQCM, was used to determine charge / mass balance for copper deposition and a representative data set is presented in **Figure 3.5**. The current efficiency can be easily obtained from the slope of the mass *versus* charge plot by comparison with the theoretical value calculated from Faraday's law according to **Equation 3.5**.

$$d(\Delta m) / dq = r.a.m / nF \quad 3.5$$

Where, Δm is the change in mass, dq the change in charge *r.a.m* the relative atomic mass, n the number of electrons involved in the process and F the Faraday constant, in this case equivalent to $63.55/2F = 3.29 \times 10^{-4} \text{ g C}^{-1}$). The slope of the graph shown in **Figure 3.5** ($3.27 \times 10^{-4} \text{ g C}^{-1}$) corresponds to a current efficiency of 99.2% at a deposition potential of -0.8 V *versus* Ag wire quasi-reference.

The current efficiency for the deposition process under the conditions presented in **Figure 3.3** was also shown is close to 100%. Under these conditions the rate of deposition was calculated from the chronocoulometric data (**Figure 3.3**) and found to be $8.2 \times 10^{-9} \text{ g cm}^{-2} \text{ s}^{-1}$ in the urea based liquid and $54.9 \times 10^{-9} \text{ g cm}^{-2} \text{ s}^{-1}$ in EG liquid. The ratio of these two growth rates is 6.70; this compares with a value of 7.05 for the ratio of diffusion coefficients calculated from the Stokes-Einstein equation (**Equation 2**). These values are strongly indicative of mass-transport control. The equivalent ratio of experimentally determined diffusion coefficients (from **Figure 3.1**) is 17.9, **Table 3.1**. This discrepancy is accounted for mainly by the value of value of D_0 for the urea liquid. Accurate determination of peak current values from CV data carries a subjective component and commensurate error in the value of D_0 can be quite large. The deposition rates for similar experiments calculated from mass *versus* time data gave comparable values. For example the deposition rate of $14.5 \times 10^{-9} \text{ g cm}^{-2} \text{ s}^{-1}$ was determined for the experimental data shown in **Figure 3.5**.

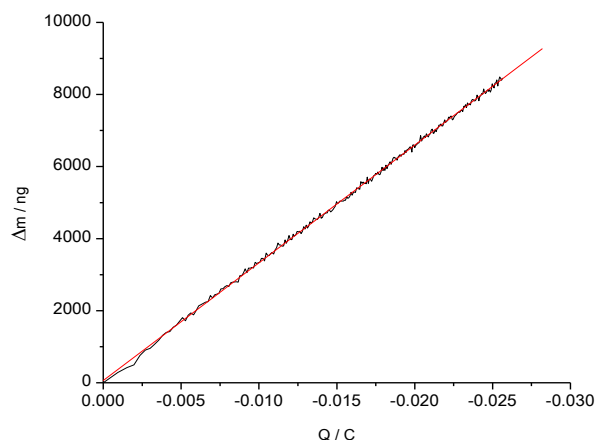


Figure 3.5. Mass-charge plot for the deposition of copper on a gold electrode (0.23 cm^2 QCM crystal) at an applied potential of -0.8 V from $0.02 \text{ M } [\text{CuCl}_2 \cdot 2\text{H}_2\text{O}]$ in $1 \text{ ChCl} : 2 \text{ EG}$. Linear regression gives a slope, $dm/dQ = 3.267 \times 10^{-4} \text{ g C}^{-1}$.

This section clearly shows that copper can be used as a model system to study the incorporation of particulates into electrolytically deposited metal films. The electrodeposition was found to be diffusion limited, effectively 100% current efficient and totally reversible. This means that EQCM can be used to study the electrodeposition of metal composites since the charge passed gives a measure of the total amount of metal deposited whereas the QCM mass response gives information of the amount of metal and composite. Deconvoluting these two signals gives the amount of composite material deposited. This is the first time that this technique has been used to obtain real-time information about composite incorporation.

3.3 Electrodeposition of Composites Materials

Copper composites have been deposited from aqueous solutions and most studies have involved particles which are very small (30-50 nm).^{45,46,47,48} The studies managed to achieve alumina loadings of upto 35 wt % however particulate solution content were as high as 158 g dm⁻³. These particulates were kept in solution using rapid stirring.

Suspensions of various particulate materials including Si₃N₄, SiC, BN, Al₂O₃, and diamond can be formulated simply by stirring the powdered solid with the ionic liquid (DES). A key advantage of DESs for this application is that the particulate suspensions are stable over a prolonged period of time; this is presumably due to a combination of the increased viscosity (of the neat liquid), compared to water and coulombic screening of surface charge by the ionic liquid (high ionic strength). For example, the Al₂O₃ 1 μm particles settle after about 24 hours whereas 0.05 μm particle suspensions are stable for over a week as shown in **Figure 3.6**.



Figure 3.6 Photographs of (from l to r in each photograph) SiCl-3 μm in EG liquid, Al₂O₃ 0.05 μm in EG liquid and Al₂O₃ 0.05 μm in water. Left after 24 hours and right after 7 days.

The velocity of sedimentation, v , for a particle of radius r and density ρ_2 in a liquid of density ρ_1 and viscosity η is given by

$$\frac{2}{9} r^2 \frac{(\rho_2 - \rho_1)g}{\eta} = v \quad 3.6$$

where g is the force due to gravity. The settling rates of the different particles in the different ionic liquids are listed in Table 3.2. It can be seen that there is a significant difference in the settling rate in the three liquids and this shows why the colloidal particles are more stable in the DESs. The high viscosity of the urea based liquid enables the small Al₂O₃ particles to remain

almost static in the liquid. These data are consistent with Figure 3.6 as the SiC particles should settle at a rate of approximately 9 cm/day.

Table 3.2 Sedimentation rate as a function of liquid and particle size.

Liquid	Particle type	$v / \text{m s}^{-1}$
water	0.05 $\mu\text{m Al}_2\text{O}_3$	1.48×10^{-8}
	2 $\mu\text{m SiC}$	1.75×10^{-5}
1 ChCl: 2 EG	0.05 $\mu\text{m Al}_2\text{O}_3$	8.65×10^{-10}
	2 $\mu\text{m SiC}$	9.79×10^{-7}
1 ChCl: 2 urea	0.05 $\mu\text{m Al}_2\text{O}_3$	1.22×10^{-10}
	2 $\mu\text{m SiC}$	1.30×10^{-7}

3.3.1. Cyclic Voltammetry

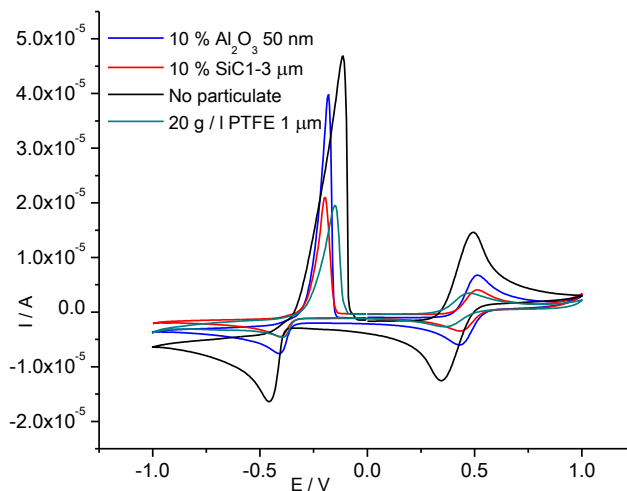


Figure 3.7. Voltammetry of $[\text{CuCl}_2 \cdot 2\text{H}_2\text{O}]$ in 1 ChCl: 2 EG (2 mm diam. Pt disk) with either 10 wt. % alumina or silicon carbide and PTFE at a potential scan rate of 10 mV s^{-1} . $[\text{CuCl}_2 \cdot 2\text{H}_2\text{O}] = 0.1 \text{ M}$ (with no particulate). (Potential versus Ag wire quasi-reference electrode).

Cyclic voltammograms for the deposition of copper from IL solutions containing 10 wt % Al_2O_3 , SiC or PTFE are shown in **Figure 3.7**. It can be seen that the current is significantly attenuated when particulates are added to the solution. One possible cause of this effect could clearly be an

increase in fluid viscosity. The viscosity of the EG based liquid was measured as a function of particulate loading and the results are shown in **Table 3.3**.

Surprisingly the viscosity is relatively unchanged despite the addition of 10 wt % particulate. This is unexpected since, by comparison, adding the same Al₂O₃ particles to water (10 wt % loading) increases the viscosity from 1.0 cP to 4.4 cP.

Table 3.3. Viscosity of various Deep Eutectic Solvents with various loadings of particulates of different particle size.

Liquid 1 ChCl: 2 EG	Density / g cm ⁻³	Viscosity / cP	Free volume /%
No particulates	1.108	17.3	16.9
10 wt % 0.05 μm Al ₂ O ₃	1.180	19.5	17.7
10 wt % 1-3 μm SiC	1.187	15.0	16.6

It has previously been shown that ionic liquids and DESs are viscous because the flux of ions is controlled by the availability of suitably sized holes to accommodate the movement of such large ionic species.⁴⁹ By calculating the volumes of the ionic and molecular species in the liquid and with a knowledge of the solution density it is possible to calculate the theoretical percentage of the liquid volume that is void. For the EG mixture this is approximately 16.9 % which is typical for most other ionic liquids. Interestingly ionic liquids have a much lower free volume than most molecular solvents (typically 22 - 26 %). It is proposed that the addition of particulates causes an increase in the effective free volume in the liquid.

This could result from the micron and sub-micron sized particles acting as local stirrers as they tumble through the fluid. To test this idea the density of DES suspension was measured using a volumetric flask. Note that the high particulate concentration makes most other methods very difficult. The free volume of the neat DES was calculated by modelling the size of the ions and subtracting this from the total volume occupied by the neat liquid. The same technique was used with the alumina / DES suspension. It was found that the mean free volume of the system was relatively unchanged when the particulates were added, **Table 3.3**. Since the packing density of the particulates is very high (compared to the equivalent

packing density of the ions in the neat liquid) this implies that there is effectively an increase in the free volume of the liquid component of the mixture. This argument is consistent with increased hole availability (size and probability) caused by addition of particulate and therefore with the observed viscosity measurements.

Given that the trend in peak currents, of the CVs presented in **Figure 3.7**, is not caused by increased liquid viscosity, it is most likely that the attenuation of voltammetric response is caused by physical blocking of the electrode surface by the insulating particulate mass *i.e.* effectively reducing the conducting electrode surface area.

Table 3.4 Composition of Cu/Al₂O₃ coating (wt. % Al₂O₃) produced from a 1 ChCl: 2 EG determined using QCM data as a function of solution loading and particle size.

Wt % Al ₂ O ₃ in solution	Wt % Al ₂ O ₃ in coating	
	0.05µm particles	1 µm particles
0.5	0.7	2.0
5	3.3	3.5
10	27.3	23.0

Also evident from **Figure 3.7** is some variation of peak potentials with the nature of deposit. This is most noticeable in the anodic stripping response. This is not surprising since the peak position is time-scale dependent; hence the Cu component of each composite is dissipated at a rate that is dependent on composition. The data for Al₂O₃ shown in **Table 3.4** are consistent with those presented previously for aqueous solutions.^{45,46,47} Two observations must be stressed; the loadings have been achieved without vigorous stirring of the solution and the silicon carbide particles are the largest yet reported in an electrodeposited composite.

3.3.2. Gravimetric analysis of the Cu composites

Electrochemical quartz crystal microbalance experiments were also used to obtain the mass / charge plots for copper deposition with various amounts of Al₂O₃ suspended in the ionic liquids. This is a new and novel use of the technique and permits real time *in-situ* monitoring of both copper deposition rate and the proportion of Al₂O₃ (or any particulate) incorporated into the composite since the particulate adds to the mass without consuming charge. This is important as it can address the issue of whether the composite material is settling on the surface or being

dragged there by the copper complexes. The liquids were all kinetically stable on the time scale of the experiment *i.e.* the Al_2O_3 did not settle out at any time during the experiment and this suggests that the sedimentation of Al_2O_3 is unlikely to be a major contributor to the overall rate of material inclusion.

Figure 3.8a shows the mass-charge plot for copper at -0.8 V for different solution phase loadings of $0.05 \mu\text{m}$ Al_2O_3 in 1 ChCl: 2 EG based liquid and **Figure 3.8b** shows the corresponding data for $1 \mu\text{m}$ Al_2O_3 . The most striking feature of these two figures is the similarity between the two systems. The particle size has little effect upon the overall mass of alumina in the deposit again suggesting that sedimentation is not the primary mechanism

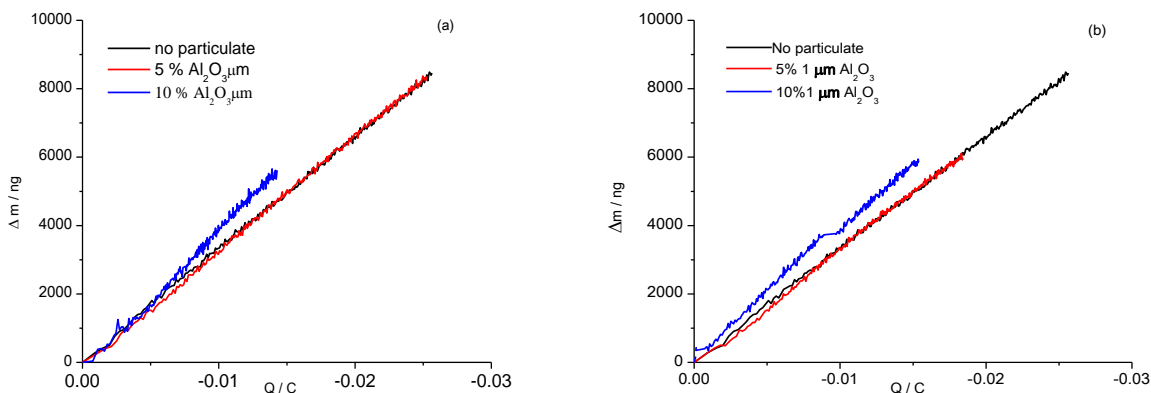


Figure 3.8. Mass-charge plots for copper composite deposition at -0.8 V and 0.02 M $[\text{CuCl}_2 \cdot 2\text{H}_2\text{O}]$ in 1 ChCl: 2 EG based liquid for different solution-phase loadings of; (a) $0.05 \mu\text{m}$ Al_2O_3 , $[dm/dQ = 3.38 \times 10^{-4}$ and $4.16 \times 10^{-4} \text{ g C}^{-1}$ for 5% and 10% loadings respectively] and (b) $1 \mu\text{m}$ Al_2O_3 , $[dm/dQ = 3.26 \times 10^{-4}$, 3.38×10^{-4} and $4.02 \times 10^{-4} \text{ g C}^{-1}$ for pure copper metal, 5% and 10% loadings respectively]

by which particles are incorporated into the metal. Assuming that high current efficiency for Cu deposition is maintained in the presence of the particulate it is possible to determine the proportion of particulate in the metal deposit from the slope of the linear correlations **Figure 3.8**. The results of these calculations for the data presented in **Figure 3.8** are shown in **Table 3.4**. The general trend relating solution loading with deposit composition is intuitive, however, the data show that at low solution loadings the larger particles are incorporated more effectively than the smaller ones but at higher loadings both particle types are partitioned preferentially into the metal deposit. The good linear correlation between the

charge and mass for all systems shows that the alumina is incorporated evenly throughout the film. The low settling rates compared to the drag rates also suggest that the composition of the deposit should be relatively independent of the substrate orientation. This was found to be the case for example in equivalent samples prepared perpendicular to one another. Representative SEM images for pure copper and Al_2O_3 composite coatings deposited from solutions with particulate loadings of 3%, 5% and 10% (w/w) are shown in **Figure 3.9**. These show that the surface morphologies are homogeneous and that the roughness correlates with particle density. Good agreement was observed between the Cu:Al percentage ratio, as measured by EDAX and the results presented in **Table 3.4**. Also, **Figure 3.9** shows that the copper layer is not microcrystalline as would be expected for the electrolytic deposition of copper from most molecular solvents. This confirms that under these conditions nanocrystalline growth results from progressive nucleation and leads to smooth, bright metallic materials.

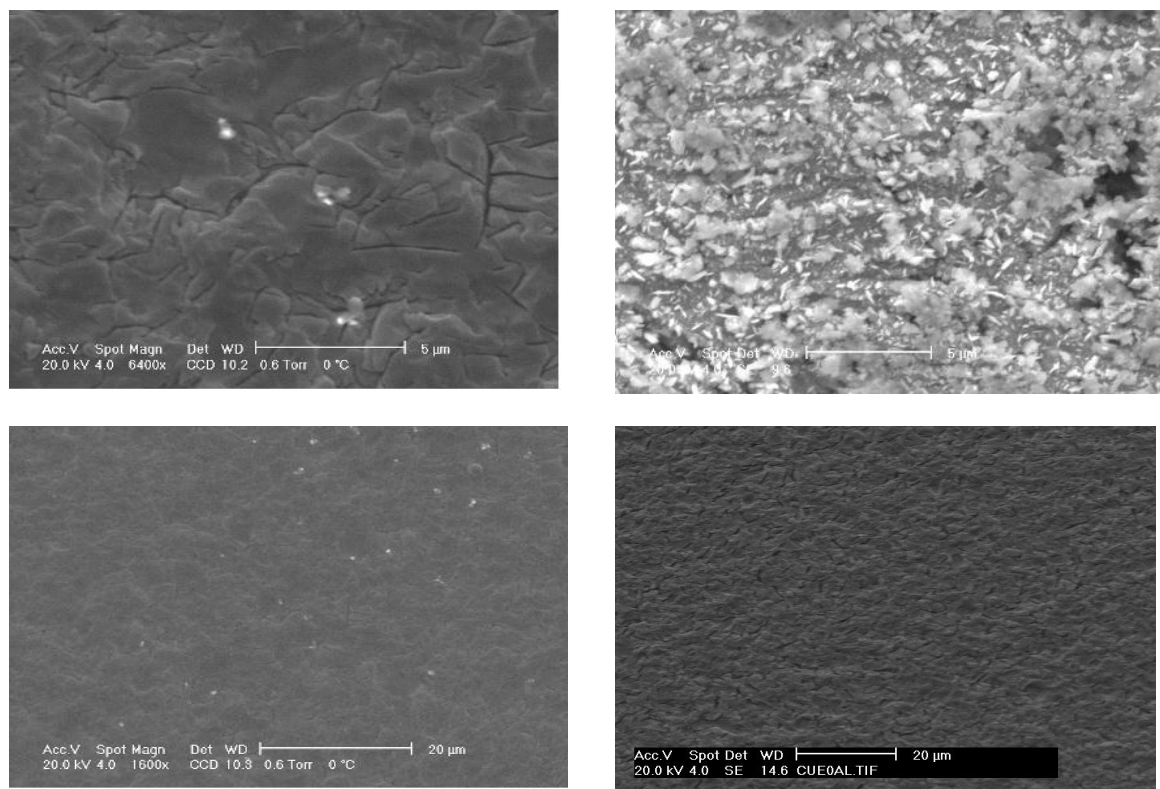


Figure 3.9. SEM images of copper films containing different loadings of Al_2O_3 : (top-left) 5% $0.05 \mu\text{m}$ Al_2O_3 (3% in film), (top-right) 10% $0.05 \mu\text{m}$ Al_2O_3 (27% in film), (bottom-left) 5% $1 \mu\text{m}$ Al_2O_3 (3% in film), (bottom-right) copper deposit with no Al_2O_3 . Deposition at -0.8 V and 0.02 M $[\text{CuCl}_2 \cdot 2\text{H}_2\text{O}]$ in $1 \text{ ChCl} : 2 \text{ EG}$ based liquid.

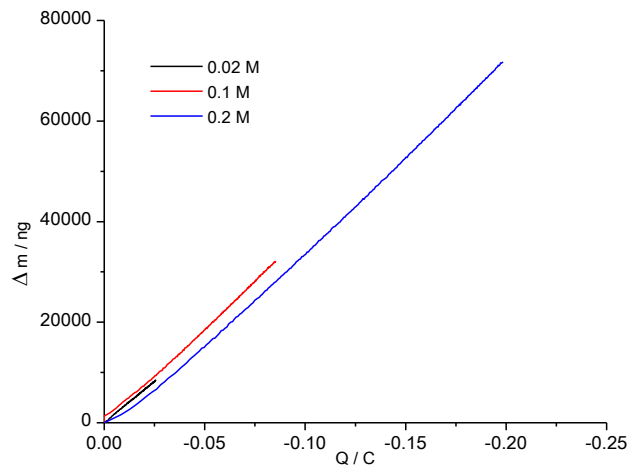


Figure 3.10. Mass-charge plots for copper deposition at an applied potential of -0.8 V over a range of $[\text{CuCl}_2 \cdot 2\text{H}_2\text{O}]$ concentrations but with constant solution phase loading (10 wt. %) of $0.05\ \mu\text{m Al}_2\text{O}_3$ in 1 ChCl: 2 EG mixture .

In the previous section the effect of the size and the concentration of alumina were discussed. Now the concentration was kept constant (10 % w/v) of 50 nm size while the concentration of Cu ions was varied. **Figure 3.10** shows that the amount of incorporated alumina in the Cu co-deposits almost the same loading that the amount of second phase loaded is independent of copper concentration as well as the time scale for all Cu concentrations. It has been noticed that the film deposits from 0.2 M Cu solution is 10 times greater than deposited from 0.02 M Cu solution.

3.3.3 Addition of a hard dispersed phase (SiC 1-3 μm)

In a separate experiment (similar to that shown in **Figure 3.10**), Cu deposition was investigated in the presence of 1-3 μm SiC. In this case, however, the particulate loading was kept constant, at 10% and the concentration of Cu ions was varied. The time scale of this experiment was also extended. These data are presented in **Figure 3.11**. Here all the mass-charge plots are again linear confirming that there is a uniform distribution of particulates throughout the film.

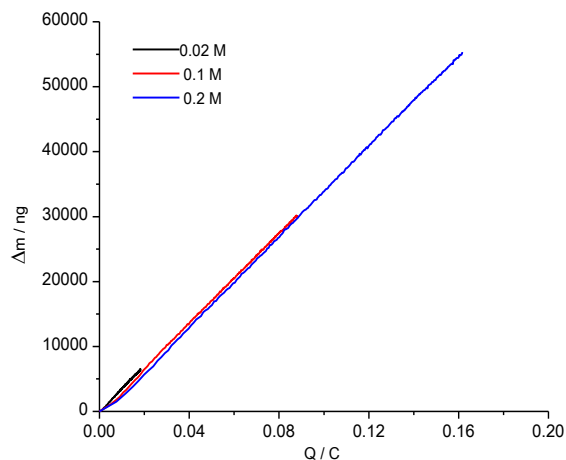


Figure 3.11. Mass-charge plots for copper deposition at an applied potential of -0.8 V over a range of $[\text{CuCl}_2 \cdot 2\text{H}_2\text{O}]$ concentrations but with constant solution phase loading (10 wt. %) of $1\text{-}3\ \mu\text{m}$ SiC in 1 ChCl: 2 EG mixture [mean slope $dm/dQ = 3.60 \times 10^{-4}\ \text{g C}^{-1}$, giving a composition of 9.4 % SiC].

It is important to note that the slopes, dm/dQ , for all 3 copper concentrations are essentially identical indicating that the Cu:SiC ratio is the same in each of the deposits despite that fact that the higher Cu concentration resulted in a 10 fold increase in the amount of copper deposited.

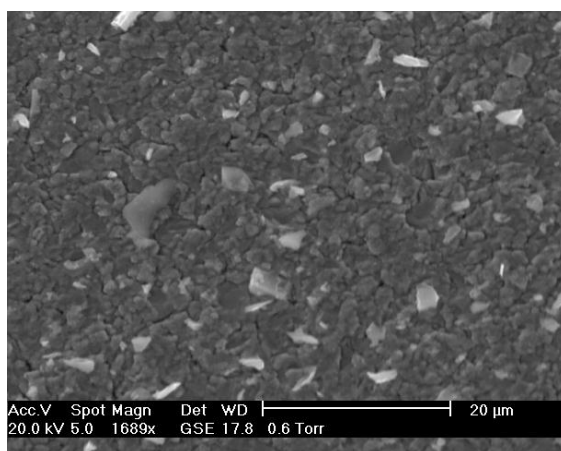


Figure 3.12. SEM micrograph of copper co-deposited film with SiC (1-3 μm).

The proportion of SiC in the film (9.4 wt %) was also in quantitative agreement with the solution loading for each of the three deposits and was independent of time scale as well as concentration

of copper. This shows clearly that the main mechanism for particulate inclusion is diffusional / convection caused by the concentration gradient of copper complex *i.e.* drag

3.3.4. Addition of a soft dispersed phase (polytetrafluoroethylene, PTFE 1 μ m)

In the previous section the incorporation of hard composites was investigated as a function of type and size with two types of ceramics; alumina and silicon carbide. In this section the loading of soft composite particles, PTFE was studied. The aim was to develop a self lubricating material, which registers a super-low friction coefficient. The use of these particles has been limited due to its poor mechanical properties, high linear expansion coefficient, bad thermal conductivity and high wear rate. The CV of CuCl_2 in 1 ChCl: 2 EG with the incorporation of PTFE particles is shown in **Figure 3.7**. Gravimetric investigation using EQCM was carried out with a particulate loading was 20 g / l instead of 10 wt % because the PTFE has low density. The concentration of copper was 0.1 M and these EQCM data are presented in **Figure 3.13**. The mass-charge plot is again linear confirming that the even distribution of the dispersed phase throughout the film.

It is important to note that mean slope $dm/dQ = 3.80 \times 10^{-4} \text{ g C}^{-1}$ which equates to a PTFE loading in the film of 14 wt %. This relatively high loading is surprising given that the PTFE particles float relatively quickly to the surface. Compared to studies with hard composite materials soft dispersed materials are less common. There are no direct comparisons of similar materials deposited from aqueous solutions although Balaji *et al.* did study 0.3 μm PTFE particles in brass deposited from an alkaline cyanide bath.⁵⁰ At low PTFE loadings the particulates were well dispersed, but as the loading increased they aggregated.

Figure 3.14 shows SEM images of a PTFE – copper composite and it is important to note that the distribution of particles is relatively homogeneous. This is an advantage compared with the aqueous counterparts. The underlying morphology of the copper is not affected by the particulates, which is unusual given the difference in hydrophobicity between PTFE and Al_2O_3 . The fact that PTFE floats on the ionic liquid reinforces the earlier observation that incorporation of particulates is not due to settling.

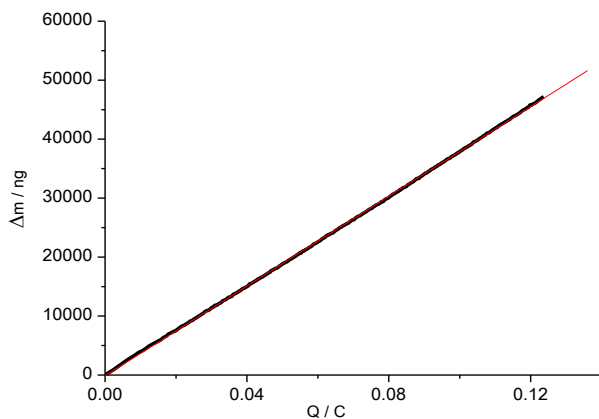


Figure 3.13. Mass-charge plots for copper composite deposition at an applied potential of - 0.8 V and 0.1 M[CuCl₂.2H₂O] with solution phase loading (20 g / L PTFE 1 μ m size in 1 ChCl: 2 EG mixture).

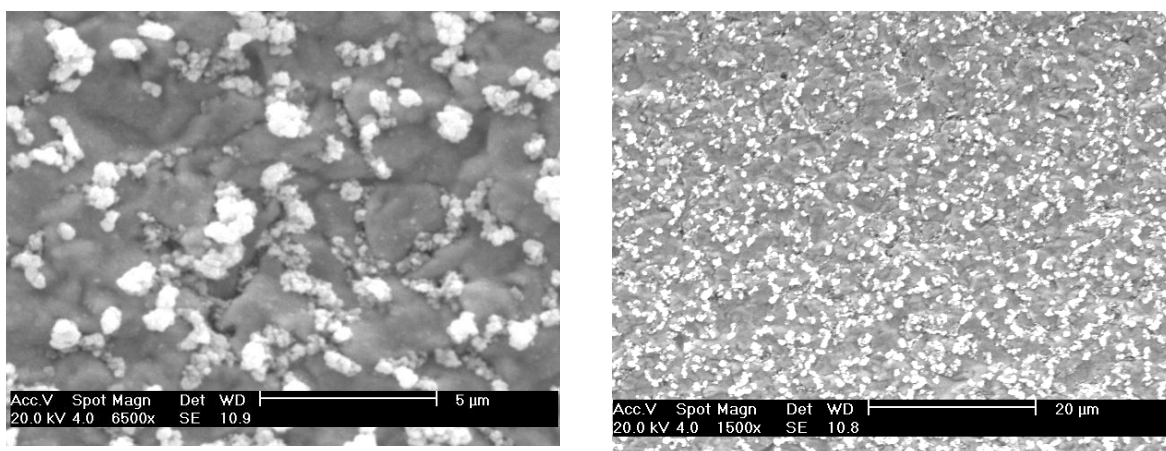


Figure 3.14. SEM microstructure of copper co-deposits film with PTFE 1 μ m size.

3.3.5. Use of Surfactants

Surfactants are ionic or molecular compound with charged or polar head groups (electrophilic) and long hydrocarbon tails (hydrophobic) that reduces surface tension. Two of their properties are useful in electrochemistry: adsorption at interfaces and aggregation into supra-molecular structures. Surfactants have previously been used in aqueous solutions for the deposition of particulates.^{51,52} Polymer particulates have been dispersed more evenly distribution throughout metal films using a variety of surfactants.⁵³

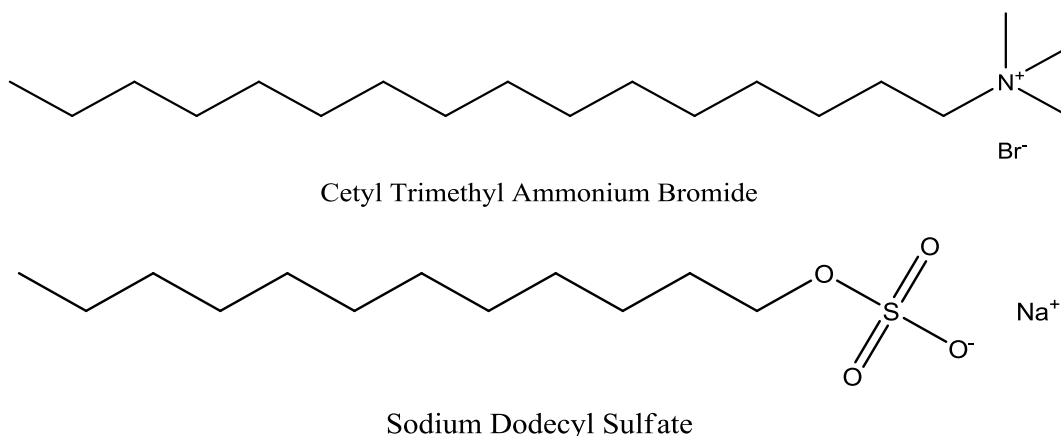


Figure 3.15. Surfactants used in this study

The influences of cationic and anionic surfactants, sodium dodecylsulfate (SDS) and hexadecyltrimethylammonium bromide (CTAB), on the electro-deposition of Cu and its composites with Al_2O_3 (50 nm size) and PTFE (1 μm size) was determined. The concentration of both particulates was 20 g / l with 1 and 3 mM additions for SDS or CTAB in 0.1 mol dm^{-3} $[\text{CuCl}_2 \cdot 2 \text{H}_2\text{O}]$ in Ethaline. **Figure 3.15** shows the chemical structure of CTAB and SDS.

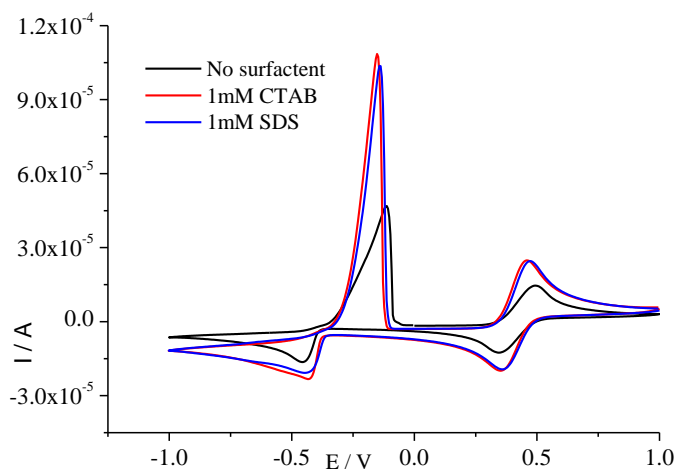


Figure 3.16. Voltammetry of $[\text{CuCl}_2 \cdot 2\text{H}_2\text{O}]$ in 1 ChCl: 2 EG (2 mm diam. Pt disk) with either 1mM SDS or 1mM CTAB at a potential scan rate of 10 mV s^{-1} . $[\text{CuCl}_2 \cdot 2\text{H}_2\text{O}] = 0.1 \text{ M}$ (with no particulate). (Potential versus Ag wire quasi-reference electrode).

Figure 3.16 shows the cyclic-voltammogram for the deposition of copper from IL solutions containing 1mM CTAB or 1 mM SDS (but no particulates). It can be seen that current is

significantly increased when the surfactants are added. The increasing current could be attributed to a double layer effect or a change in mass transport resulting from a decrease in viscosity. Work by Barron³² showed that the viscosity of these DESs decreased significantly when surfactants were added to them suggesting that the latter cause is responsible for the increased current.

3.3.6 Gravimetric analysis

Electrochemical quartz crystal microbalance experiments were used to obtain the mass / charge plots for copper deposition with and without composites in the presence of the two types of surfactants. **Figure 3.17** shows the mass-charge plot for copper at -0.8 V vs. Ag for both surfactants at two concentrations. The results showed that there was no significant change in the rate of deposition of copper when surfactant was added which is surprising given the change in the shape of the voltammogram in Figure 3.16.

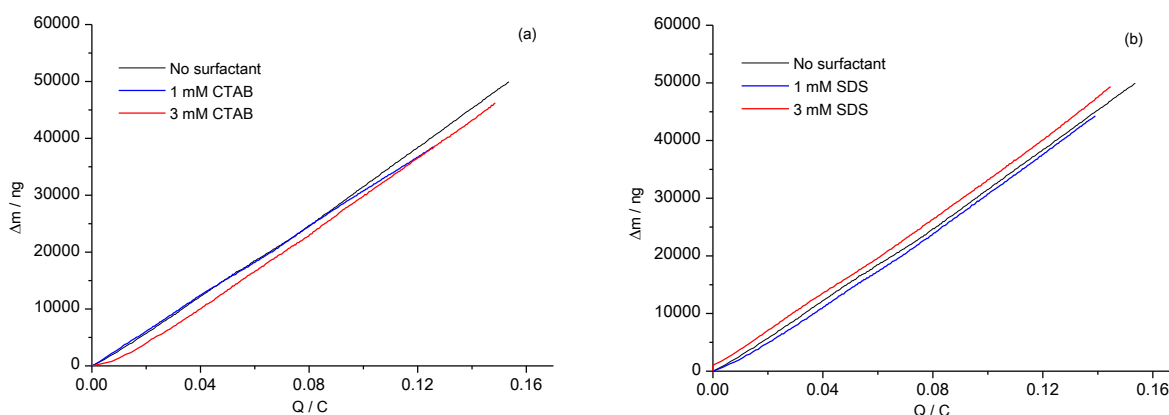


Figure 3.17. Mass-Charge plots for Cu deposits on a Au coated quartz crystal (10 MHz) with geometric area 0.23 cm^2 as a function of surfactant concentration and type at applied potential of -0.8 V from $0.1 \text{ M } [\text{CuCl}_2(\text{H}_2\text{O})]$ in 1 ChCl: 2 EG. (a) CTAB (b) SDS

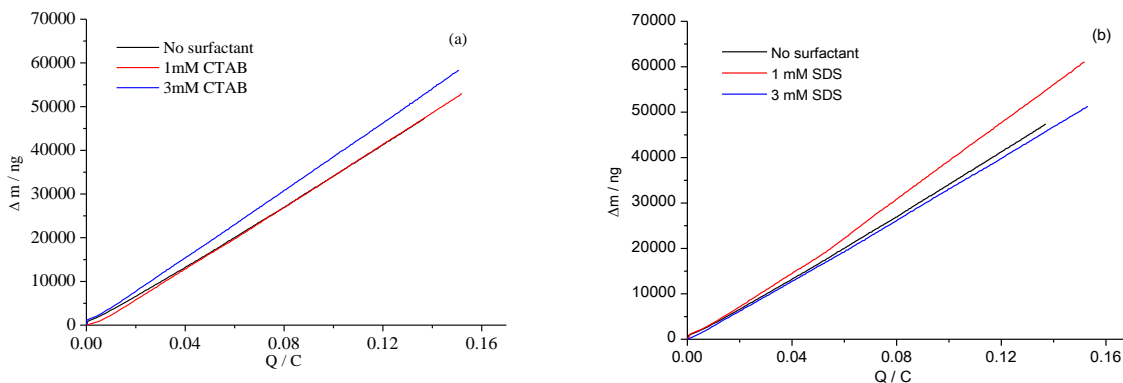


Figure 3.18. Mass-Charge for Cu / 20 g / l Al₂O₃ 50 nm size co-deposits on a Au coated quartz crystal (10 MHz) with geometric area 0.23 cm² as a function of surfactant concentration and type at applied potential of -0.8 V from 0.1 M [CuCl₂(H₂O)] in 1 ChCl: 2 EG. (a) CTAB (b) SDS

The above experiment was repeated using 20 g dm⁻³ Al₂O₃ (50 nm size) and the effects surfactants upon the particulate incorporation are shown in **Figure 3.18**. It can be seen that there are some changes although these are not consistent with a trend. In each case one surfactant concentration leads to an increase and the other did not, but it was not the same concentration in either case.

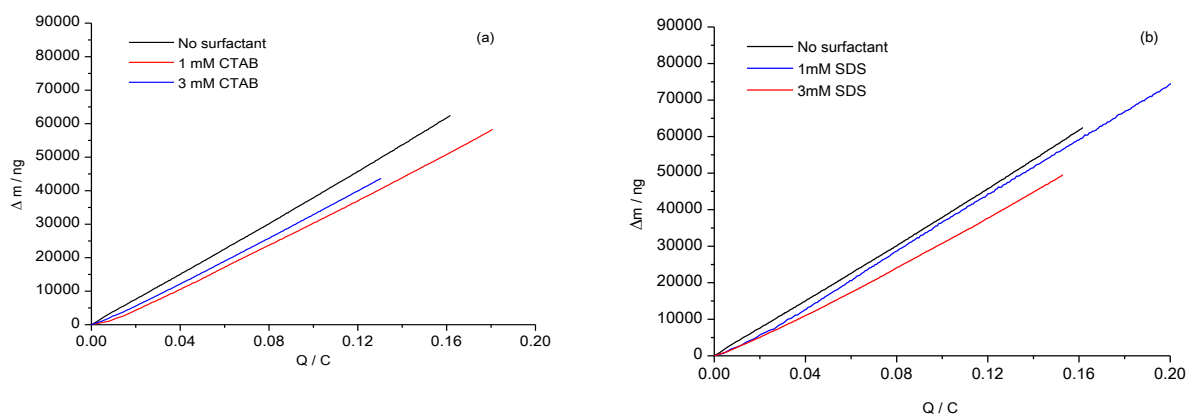
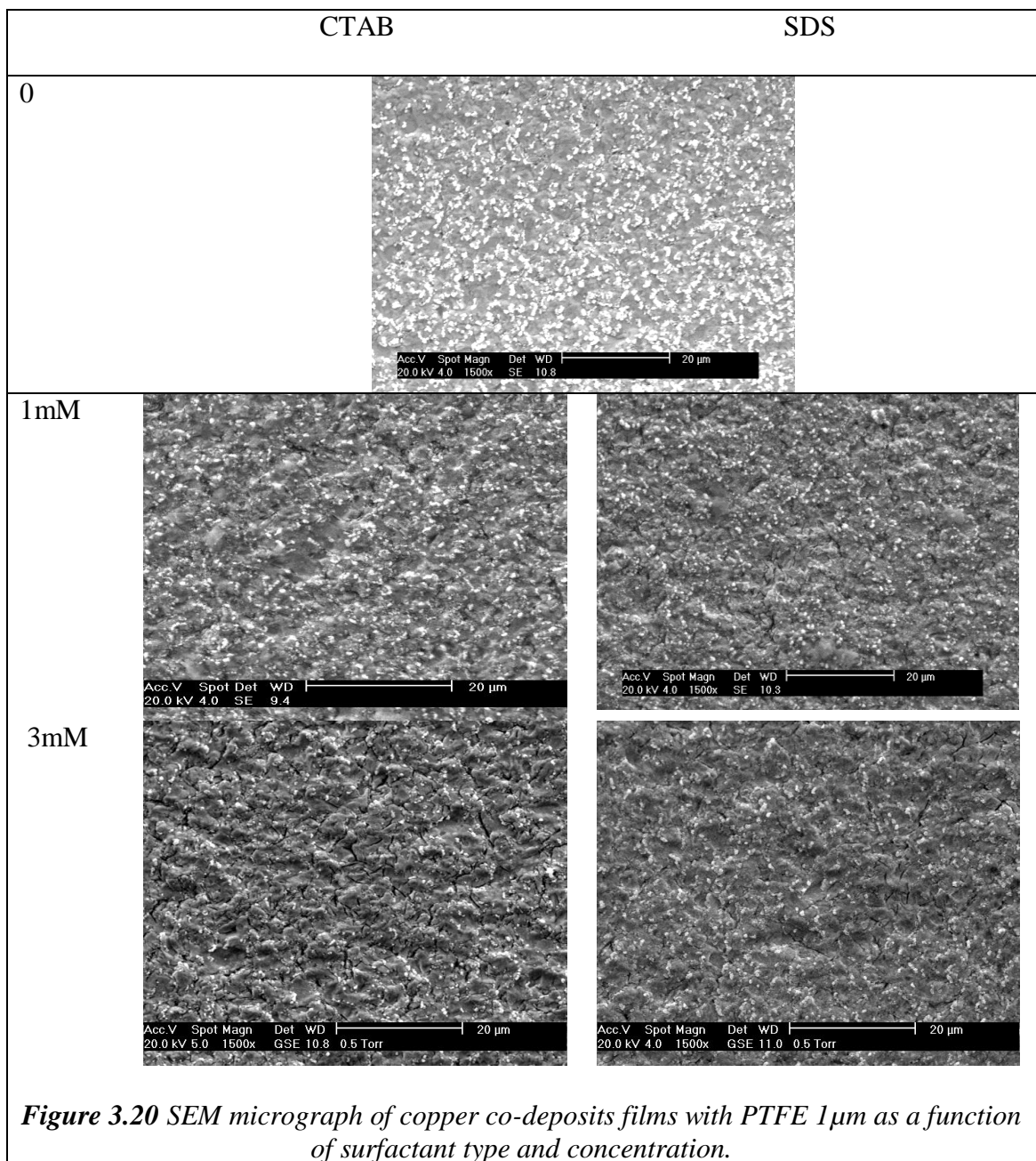


Figure 3.19. Mass-Charge plots for Cu/ 20 g / l PTFE 1µm size co-deposits on a Au coated quartz crystal (10 MHz) with geometric area 0.23 cm² as a function of surfactant concentration and type at applied potential of -0.8 V from 0.1 M [CuCl₂(H₂O)] in 1 ChCl: 2 EG. (a) CTAB (b) SDS

When surfactants were used to study the co-deposition of copper films with PTFE a different response was observed to that with hard materials. It has been seen that the amount of PTFE particulate in the Cu co-deposits films is decreased with addition of both cationic and anionic surfactants as shown in **Figure 3.19**. These results are underpinned with the SEM images. **Figure 3.20** shows SEM images copper co-deposits with 20 g dm^{-3} PTFE particulate as function of surfactant type and concentration. Qualitatively the particle density decreases as the surfactant concentration is increased. The origin for this is unknown but the incorporation of PTFE into nickel films from aqueous solutions was found to be particularly sensitive to the physical parameters. This is clearly an area that is in need of more in-depth study. It is clear, however that surfactants are not necessary for the dispersion of particles in ionic liquids and they do not lead to increased incorporation in the metal film.



3.4 Conclusions

This work shows that ionic liquids based on eutectic mixtures of choline chloride and hydrogen bond donors such as urea or ethylene glycol can be used as electrochemical solvents for the electrodeposition of copper. It has been shown that in both liquids the current efficiency for copper deposition is close to 100%. Composites of copper with Al_2O_3 and SiC have also been produced and it has been shown that the loading of these species in the resulting electroplated films is strongly dependent on the concentration of particulate in solution but largely independent of the concentration of copper metal ion or timescale. Gravitational settlement has been excluded as the main mechanism for particulate inclusion into the electrolytic deposits. The inclusion of suspended particles in the liquid is found to have negligible effect upon the fluid viscosity and it is proposed that this is because of the tumbling motion of the particles acting as micro-stirrers in the liquid. The advantages of using DESs for the incorporation of particulates into electrodeposited films are that the colloidal solutions are stable for longer periods and they lead to the deposition of homogeneous composites without the necessity of complex stabilisers in solution. The size of particulate that can be incorporated into the metal film is also larger than can be achieved using aqueous solutions.

3.5 References

- 1 P.C. Andricacos, C. Uzoh, J.O. Dukovic, J. Horkans and H. Deligianni, *Electrochemical Microfabrication*, **1998**, 42, 5.
- 2 P. C. Andricacos, *Interface*, **1998**, 7, 23.
- 3 “*The Canning handbook Surface Finishing Technology*”, W. Canning plc, in association with E. & F. N. Spoon Ltd., London – New York, **1989**.
- 4 I. Garcia, I. Franaer, J. Celis *Surf. Coat. Tech.* **2001**, 148, 171.
- 5 P.M. Vereecken, I. Shao, P.C. Searson, *J. Electrochem. Soc.* **2000**, 147, 2572.
- 6 M. Nishira, O. Takano, *Plat. Surf. Finish.* **1994**, 48.
- 7 L. Benea, P. Bonora, A. Borello, S. Martelli *Wear* **2002**, 249, 995.
- 8 R. T. Carlin, H.C. De Long, J. Fuller and P.C. Trulove, *J. Electrochem. Soc.*, **1998**, 145, 1598.
- 9 B. J. Tierney, W. R. Pitner, J.A. Mitchell, C. L. Hussey and G.R. Stafford, *J. Electrochem. Soc.*, **1998**, 145, 3110.
- 10 C. Nanjundiah and R.A. Osteryoung, *J. Electrochem. Soc.*, **1983**, 130, 1312.
- 11 F. Endres and A. Schweizer, *Phys. Chem. Chem. Phys.*, **2000**, 2, 5455.
- 12 P.-Y. Chen and I.-W. Sun, *Electrochim. Acta*, **1999**, 44, 441.
- 13 K. Murase, K. Nitta, T. Hirato and Y. Awakura, *J. Appl. Electrochem.*, **2001**, 31, 1089.
- 14 S. Zein El Abedin, A. Y. Saad, H. K. Farag, N. Borisenko, Q. X. Liu and F. Endres, *Electrochim. Acta*, **2007**, 52, 2746.
- 15 F. Endres, *Phys. Chem. Chem. Phys.*, **2002**, 3, 144.
- 16 A.P. Abbott, G. Capper, B.G. Swain and D. A. Wheeler, *Trans. Inst Metal Finish*, **2005**, 83, 51.
- 17 A.P. Abbott, G. Capper, .K.J. McKenzie and K.S. Ryder, *Electrochim. Acta*, **2006**, 51, 4420.
- 18 A.P. Abbott, G. Capper, K.J. McKenzie, . A. Glidle and K.S. Ryder, *Phys. Chem. Chem. Phys.*, **2006**, 8, 4214.
- 19 J.H. Liao, P.C. Wu and Y.H. Bai, *Inorg. Chem. Commun.*, **2005**, 8, 390.
- 20 A.P. Abbott, S. Nandhra, S. Postlethwaite, E.L. Smith and K.S. Ryder, *Phys. Chem. Chem. Phys.*, **2007**, 9, 3735.

- 21 A.P. Abbott, J. Griffith, S. Nandhra, C. O'Connor, S. Postlethwaite, K.S. Ryder and
E.L. Smith, *Surf. Coat. Tech.*, **2008**, 202, 2033.
- 22 A.P. Abbott, G. Capper, D.L. Davies, R. Rasheed and P. Shikotra, *Inorg. Chem.*, **2005**,
44, 6497.
- 23 A.P. Abbott, G. Capper, D.L. Davies, K.J. McKenzie and S.U. Obi, *J. Chem. Eng. Data*,
2006, 51, 1280.
- 24 A.P. Abbott, G. Capper, K.J. McKenzie and K.S. Ryder, *J. Electroanal. Chem.*, **2007**,
599, 288.
- 25 A.P. Abbott and K.J. McKenzie, *Phys. Chem. Chem. Phys.*, **2006**, 8, 4265.
- 26 S.Z. El Abedin and F. Endres, *American Chemistry Council, Chemistry Research*, **2007**,
40, 1106.
- 27 A.P. Abbott, K.S. Ryder and U. Koenig, *Trans. Inst Metal Finish.*, **2008**, 86, 196.
- 28 N.V. Plechkova and K.R. Seddon, *Chem. Soc. Rev.*, **2008**, 37, 123.
- 29 "Electrodeposition of Metals (Chapter 4)", T.J.S. Schubert, S.Z. El Abedin, A.P.
Abbott, K.J. McKenzie, K.S. Ryder and F. Endres, in "Electrodeposition in Ionic
Liquids", Edited by F. Endres, A.P. Abbott and D.R. Macfarlane, Wiley-VCH
Weinheim, **2008**, ISBN: 978-3-527-31565-9
- 30 "Technical Aspects (Chapter 11)", D.S. Silvester, E.L. Rogers, R.G. Compton, K.J.
McKenzie, K.S. Ryder, F. Endres, D. MacFarlane and A.P. Abbott in
"Electrodeposition in Ionic Liquids", Edited by F. Endres, A.P. Abbott and D.R.
Macfarlane, Wiley-VCH Weinheim, **2008**, ISBN: 978-3-527-31565-9
- 31 *CRC Handbook of Chemistry and Physics*, 66th Edition, Ed. Robert C. Weast, CRC
Press Inc., Florida **1986**.
- 32 J. C. Barron, PhD Thesis, University of Leicester, **2009**
- 33 A.P. Abbott, J.C. Barron, K.S. Ryder and E. L. Smith, *Trans. Inst Metal Finish*, **2008**,
87, 201.
- 34 D. Pletcher, *A first course in electrode processes*, The Electrochemistry Consultancy,
Hants, UK, page 163, **1991**.
- 35 T. Katase, K. Murase, T. Hirato and Y. Awakura, *J. Appl. Electrochem.*, **2007**, 37, 339.

-
- 36 C.S. Barin, A.N. Correia, S.A.S. Machado and L.A. Avaca, *J. Braz. Chem. Soc.*, **2000**,
11, 175.
- 37 P.S Salmon, W.S Howells and R. Mills, *J. Phys. C: Solid State Phys.*, **1987**, 20, 5727.
- 38 A.P. Abbott, G. Frisch and K.S. Ryder, *Annu. Rep. Prog. Chem., Sect. A: Inorg. Chem.*,
2008, 104, 21.
- 39 L.P. Battaglia, A. Bonamartini Orradi, G. Marcotrigiano, L. Menabue and G.C.
Pellacani, *Inorg. Chem.*, **1979**, 18, 148.
- 40 C. Amuli, M. Elleb, J. Meullemeestre, M.-J. Schwing and F. Vierling, *Inorg. Chem.*,
1986, 25, 856.
- 41 R.D. Shannon, *Acta Cryst.*, **1976**, A32, 751.
- 42 J.J. Lee, B. Miller, X. Shi, R. Kalishi and K.A. Wheeler, *J. Electrochem. Soc.*, **2001**,
148, C183.
- 43 O. Mann and W. Freyland, *J. Phys. Chem. C*, **2007**, 111, 9832.
- 44 T. Jiang, M.J. Chollier Brym, G. Dubé, A. Lasia and G.M. Brisard, *Surf. Coat. Tech.*,
2006, 201, 10.
- 45 A. Lozano-Morales and E.J. Podlaha, *J. Electrochem. Soc.* **151** (2004) (7), p. C478
- 46 E.J. Podlaha, *Nano Lett.* **1** (2001) (8), p. 413
- 47 E.J. Podlaha and D. Landolt, AESF SUR/FIN Annual Intern. Technical Conference,
1998.
- 48 E.J. Podlaha and D. Landolt, *J. Electrochem. Soc.* **144** (1997) (7), p. L200
- 49 A.P. Abbott, R.C. Harris and K.S. Ryder, *J. Phys. Chem B*, **2007**, 147, 4910.
- 50 R. Balaji, M. Pushpavanam, K. Yogesh Kumar and K. Subramanian, *Surf. Coat. Tech.*
201, 2006, 3205
- 51 L. Chen, L. Wang, Z. Zeng and J. Zhang, *Mat. Sci. Eng. A*. **2006**, 434, 319.
- 52 K. H. Hou, M. D. Ger, L. M. Wand and S. E. Ke, *Wear*, **2002**, 253, 994.
- 53 A. Hovestad, and L. J. J. Janssen, *J. Appl. Electrochem.*, **1995**, 6, 521.

Chapter 4: The Electrodeposition of Silver Composites using Deep Eutectic Solvents

4.1 Introduction

4.1.1 Silver composites

4.1.2 Silver deposition from ionic liquids

4.2 Electrodeposition of Silver

4.2.1. Electrodeposition of Ag / SiC (45-55 nm) composites

4.2.2 Electrodeposition of Ag / SiC (1-3 μm) composites

4.2.3 Electrodeposition of Ag / Al₂O₃ (50 nm) composites

4.2.4 Hardness of composite films

4.2.5 Wear analysis

4.2.6 Effect of LiF on hardness and friction coefficient of Ag / SiC films

4.3 Conclusion

4.4 References

4.1 Introduction

In the last chapter it was shown that composites with copper could be deposited efficiently and with a high particulate loading. In this chapter these ideas are expanded to a practical application, namely the deposition of silver composites for connectors.

The electrodeposition of silver is classified as one of the top metal coating in the global market. The reason behind is that it is a soft, white lustrous metal and has the ability of taking a high polish. The shiny and smooth surface, makes silver film coatings used mainly for their decorative property.

The electrodeposition of silver is usually carried out using a Zonax silver solution which is used primarily for the electronics industry and the Argentax process which is a high speed process used extensively in the silver plating of bearings. Both processes are electrolytic and use an electrolyte composed of silver cyanide and potassium cyanide. In solution these form the complex $\text{KAg}(\text{CN})_2$. The issue with this process the breakdown product of cyanide is carbonate which precipitates in the bath and leads to dull deposits. An alternate alkaline process used KOH and a series of proprietary complexing agents to deposit silver.

There is another method which is currently used which does not require an externally applied potential *i.e.* it is electroless. This is called the immersion or Sterling Silver process and it is commonly used for silvering printed circuit boards or small items such as buttons.¹

4.1.1 Silver composites

The majority of studies on the electrodeposition have concentrated on nickel as the metal matrix although a significant number have also investigated copper.^{2,3} In comparison the electrodeposition of silver composites is relatively unstudied. Suzuki *et al.*⁴ studied the the codeposition of Al_2O_3 particles from a AgSCN bath. It was found that the current density at low constant potential was increased compared to that without particles but the reverse was true at high overpotentials. It was concluded that the Al_2O_3 particles adsorbed on the electrode and suppressed Ag deposition.

Two studies also investigated the codeposition of TiO₂ with silver for the application as a photocatalyst. It was found that submicron-sized particles of TiO₂ could be incorporated into a silver film although the TiO₂ was formed by the anodic oxidation of a titanium substrate rather than dragging TiO₂ particles from the solution.^{5,6}

Pagetti⁷ and co-workers studied the incorporation of particulate ZrO₂ on the morphology and properties of silver deposits and reported of the addition of the second phase in the plating bath modifies the surface coating morphology, moreover the hardness increases with the incorporation of particles from 88 Hv for pure silver to 140 Hv with 13.8 % of ZrO₂.

4.1.2 Silver deposition from ionic liquids

The study of silver deposition in ionic liquids has emulated the development of ionic liquids. The first studies were carried out using the water sensitive chloroaluminate salts.^{8,9} Hussey⁸ studied the electrodeposition of silver on a variety of electrodes in the 2:1 aluminum chloride:1-methyl-3-ethylimidazolium chloride ionic liquid at 40 °C. Of the four materials studied, the silver deposition-stripping process was simple on platinum, dominated by underpotential deposition on gold and required large nucleation overpotentials on tungsten and glassy carbon. Instantaneous three-dimensional nucleation of silver was found on W whereas progressive three-dimensional nucleation predominated on GC. The bulk silver deposition-stripping process proceeds with virtually 100% efficiency at all four of the electrodes tested.

Endres⁹ *et al.* reported the first *in-situ* electrochemical-STM study on the electrodeposition of Ag on highly oriented pyrolytic graphite (HOPG). The ionic liquid was a 1.22:1 AlCl₃ 1-methyl-3-butyl-imidazolium chloride mixture with AgCl as the silver source. The nucleation of silver was shown with ultra-high resolution for the first time.

The development of water stable ionic liquids led to the study of Ag/Pd alloys by Sun *et al.* using 1-ethyl-3-methylimidazolium chloride-tetrafluoroborate.¹⁰ He *et al.* studied the electrochemical deposition of silver using BMIMPF₆ and BMIMBF₄ and found that progressive 3D nucleation was observed in BMIMPF₆ but in BMIMBF₄ neither instantaneous nor progressive nucleation models were followed. AFM showed that the

silver deposit consisted of dense nanoclusters which were less than 100 nm in diameter.¹¹

A similar study by Bardi *et al.*¹² used BMIMBF₄ to study the deposition of silver and they studied the effect of temperature upon the nucleation mechanism. It was found that 300 nm sized particles could be deposited using higher temperatures. Fu *et al.*¹³ studied the electrodeposition of silver in water in IL and IL in water microemulsions. The electrodeposits obtained from W/IL microemulsion system were found to be nanogranular, while those obtained from IL/W microemulsion system were planar. These differences in morphologies were attributed to the different environments for the silver ions. More recently silver has also been studied in the distillable ionic liquid, DIMCARB,¹⁴ 1-ethyl-3-methylimidazolium trifluoromethylsulfonate¹⁵, BMIM Tf₂N¹⁶ and butylmethylpyrrolidinium Tf₂N.¹⁷

The electroless (immersion) coating of silver on to copper has been studied in depth and was one of the first metal finishing processes to be scaled up to a commercial scale. In a series of articles, Abbott *et al.* showed that silver could oxidise copper and simultaneously be deposited on the copper surface.¹⁸ The growth of the silver coating was found to be a sustained process *i.e.* the silver film was nano-porous and allowed thick coatings of silver to be obtained without the need for a catalyst. The silver deposited by this method was nanocrystalline and gave a smooth shiny coating. A commercial plating line was constructed using two different concentrations of silver chloride in Ethaline to achieve rapid coating followed by a polishing step with a small particulate silver top-layer.^{19,20}

In this chapter the results obtained in the previous chapter with copper composites are directly compared with those of silver composites. Electrolytic deposition of silver films without and with composites from deep eutectic solvents was studied as a function of both size and type of particulate. In this study SiC (45-55 nm and 1-3 μm) are compared with Al₂O₃ (50 nm). The deposition was carried onto a nickel substrate. SEM-EDX was used to investigate the morphology of the surface of silver coating, the existence of the ceramics particles and digital holographic microscope was used to determine the roughness of the surface coating as well as for the wear volume removed after testing the wear rate. The hardness and wear resistance values of all the Ag coatings were also determined.

4.2 Electrodeposition of silver and silver composites coatings

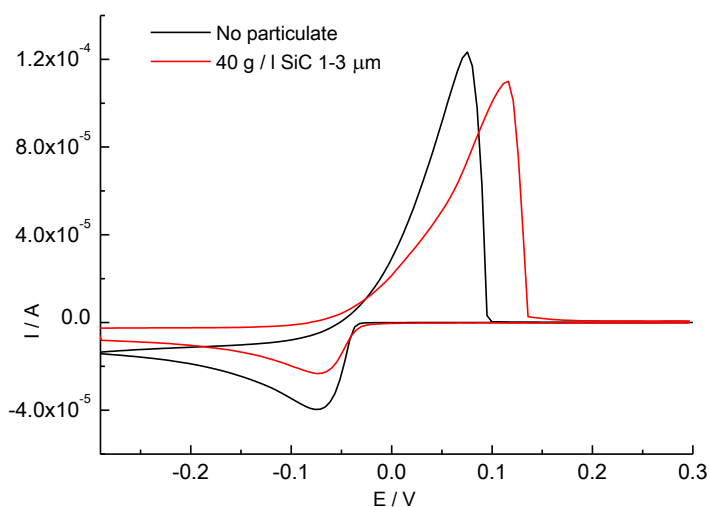


Figure 4.1 Voltammetry of AgCl in Ethaline (2 mm diam. Pt disk) with and without particulate at a potential scan rate of 20 mV s^{-1} . $[\text{AgCl}] = 0.1 \text{ mol dm}^{-3}$.

The cyclic voltammogram for the reduction of silver in Ethaline shows a reversible deposition and stripping signal (**Figure 4.1**). This contrasts with the deposition of other metals including zinc,²¹ nickel,²² aluminium²³ and to some extent copper (**Figure 3.1a**) where the cathodic and anodic peaks contain either a marked shoulder or a distinct second peak. These multiple peaks are thought to be due to the morphology of the deposit. **Figure 4.2** shows a scanning electron micrograph of a silver deposit obtained by the electrolysis of -1.20 V for 20 hours at 30 °C. The SEM image shows that the silver grows as large crystallites and the EDX analysis shows only silver in the deposit. The morphology contrasts markedly with the deposits for nickel, copper (**Figure 3.9**) and aluminium where the deposits are either amorphous or nanocrystalline. It has previously been shown that the nucleation of silver in 1 ChCl: 2 EG and 1 ChCl: 2 urea based liquid occurs *via* a progressive method.²⁴ Abbott *et al.* have recently analysed the nucleation mechanisms reported for various metals in a wide variety of ionic liquids.²⁵ It was shown that there was some commonality in the mechanism despite the differences in the anion, cation and electrode material. In general metals with a large negative reduction potential exhibit an instantaneous nucleation mechanism whereas those with a more electropositive reduction potential show a progressive nucleation

mechanism. This is thought to be associated with the adsorption of the quaternary ammonium cation on the electrode surface. Silver has a relatively positive reduction potential and its deposition has previously been studied in Bmim BF₄ where a very similar electrochemical response was reported as that shown in **Figure 4.1**. Bomparola *et al.*¹² showed that the silver also nucleated by a progressive mechanism. The large crystallite size is consistent with a progressive nucleation mechanism where a small number of nuclei start and keep on growing without developing new nuclei on the surface.

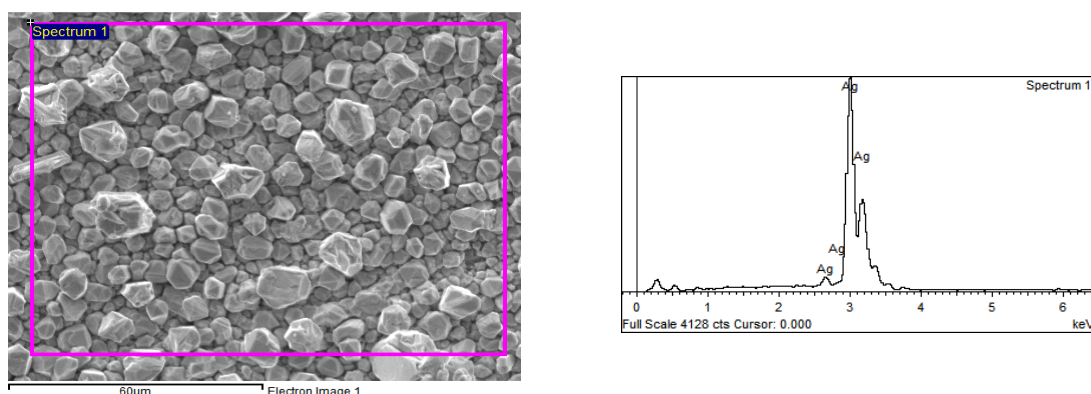


Figure 4.2 SEM microphotograph of electro-deposit Ag from 0.1 M AgCl, 1 mM SDS in 1 ChCl: 2 EG based liquid at -1.20 V. EDX in the right, profile for the area shown in the SEM image in the left.

4.2.1. Electrodeposition of Ag / SiC (45-55 nm) composites

The aim of this study was to investigate the effect of incorporation of ceramics in electrodeposited silver coatings on some mechanical properties such as Vicker's hardness, wear resistance and surface roughness of the films. The wear volume of the scar was also determined as well as the morphology of the worn surface.

Figure 4.3 (a) is an SEM image of a silver coating with SiC (45-55 nm particle size) dispersed in it. The SiC nanoparticles cannot be distinguished in the SEM micrographs however EDX mapping in **Figure 4.3** (b-d) shows that the SiC is evenly distributed throughout the material. It is important to note that the SiC particles are evenly distributed throughout the silver.

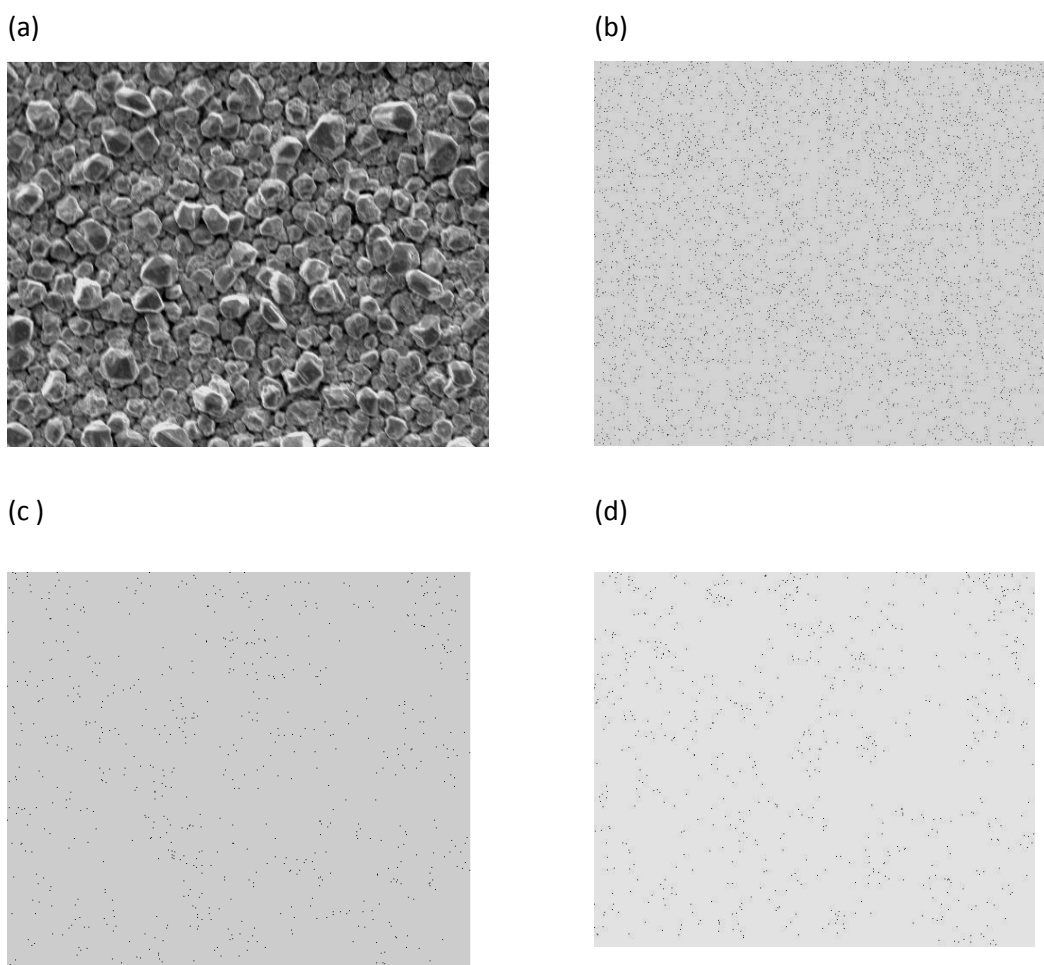


Figure 4.3 (a) SEM micrograph of Ag electrodeposits with SiC nano particles from 0.1 M AgCl, 1 mM SDS and 40 g/l SiC45-55nm in 1 ChCl: 2 EG based liquid at -1.20 V (b) EDX map image shows of (b) Ag (c) Si (d) C in the silver coating.

4.2.2. Electrodeposition of Ag / SiC (1-3 μm) composite

The above experiments were repeated using larger SiC particles. The aim was to try to incorporate the same amount of SiC into the silver film, but in this case the colloidal dispersion is aggregated into larger particles. **Figure 4.4** shows an SEM image of a silver/ SiC composite formed from the electrodeposition of potential applied -1.20 V for 20 hours at 30°C. It should however be noted that the comparison of SEM micrographs of Ag with and without SiC particles yields deposits with different morphologies. **Figure 4.2** shows large silver crystals obtained in the absence of particles and the addition of nano-SiC particles (**Figure 4.3a**) does not significantly affect the silver crystallite size. The inclusion of SiC microparticles with the same

experimental conditions leads to a much smaller grain size in the silver deposit (**Figure 4.4a**).

It has previously been shown² that the co-deposition of SiC particles results in an increase in the grain size of the silver deposits. This has been attributed to many factors^{3,4} including silver ion adsorption on the electrode surface. The effect of the particle on the morphology is thought to depend upon the nature of the particle for example whether the micro-particle is hydrophobic or hydrophilic.

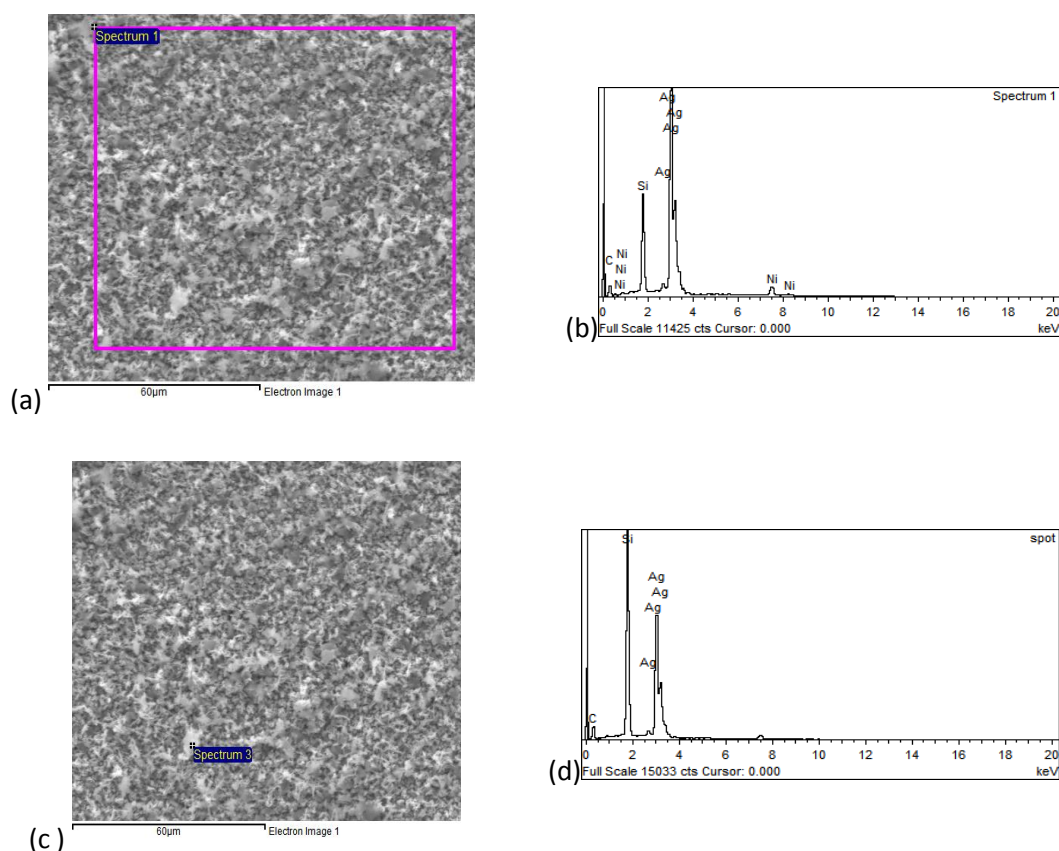


Figure 4.4 SEM micrographs of Ag deposit with SiC micro-particles from 0.1 M AgCl, 1 mM SDS and 40 g/l SiC1-3µm in 1 ChCl: 2 EG based liquid at -1.20 V (b) EDX profile for the area shown the SEM image (a). (c) SEM microphotographs of electro-deposit Ag with SiC micro-particles.(d) EDX profile for the area shown.

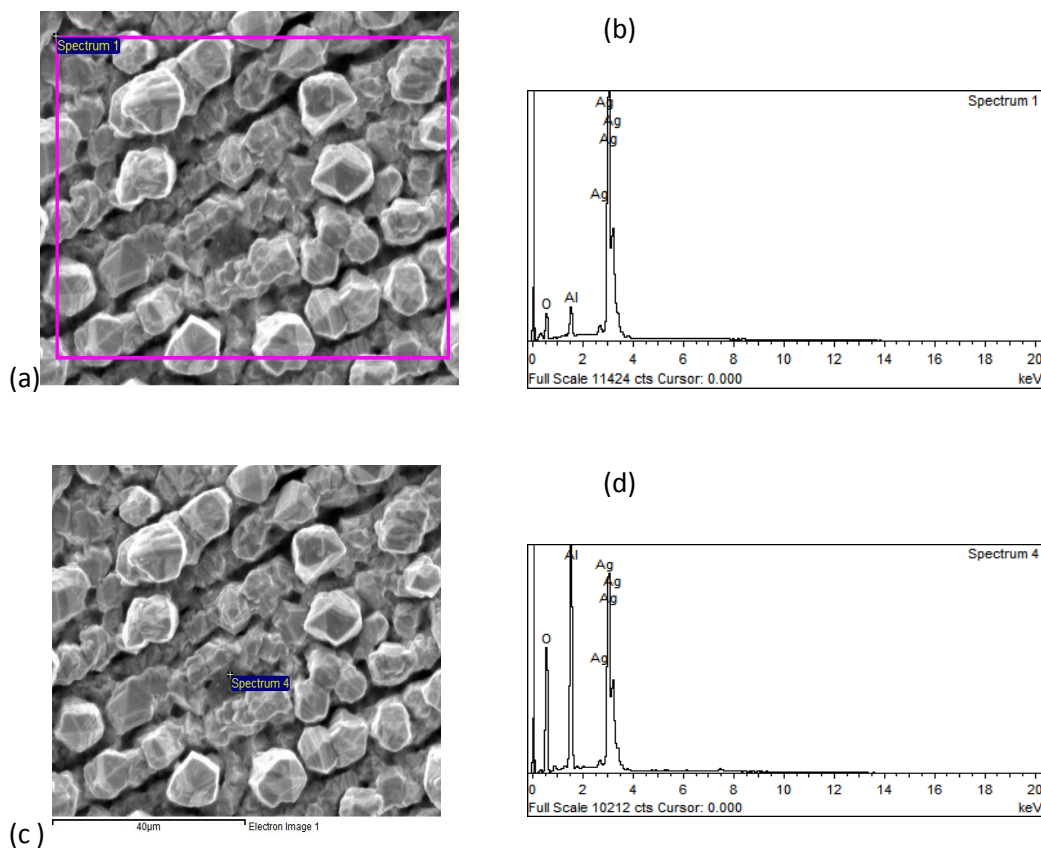


Figure 4.5. (a): SEM micrographs of Ag deposit with Al_2O_3 nano particles from 0.1 M AgCl, 1 mM SDS and 40 g / l Al_2O_3 50 nm in 1 ChCl: 2 EG based liquid at -1.20 V (b) EDX profile for the area shown the SEM image (a). (c) SEM microphotographs of electrodeposit Ag with Al_2O_3 nano particles. (d) EDX profile for the area shown.

4.2.3 Electrodeposition of Ag / Al_2O_3 50 nm film

The deposition of Ag/ Al_2O_3 (50 nm particle size) composites was obtained following bulk electrolysis at -1.20 V for 20 hours at 30°C with an Al_2O_3 loading of 40 g dm^{-3} . **Figures 4.5 (a)** and **(c)** show the SEM images of the deposits with spots showing the areas over which the EDAX analysis was taken. When a large samples area was taken the Al_2O_3 content was *c.a.* 5.5 %. The small spot in **Figure 4.5(d)** shows a very high concentration of Al_2O_3 (14 %). It is interesting to note that the morphology of silver with nano-alumina particles is similar to that obtained with the same size SiC particles.

4.2.4 Hardness of composite films

Figure 4.6 shows a comparison of microhardness data for Ag and Cu films with different sized and types of particulates. The results are rather surprising, but

demonstrate in all cases improved material properties from the composites. The hardness of the pure, electrodeposited material is lower than that of bulk metals (*c.f.* Ag = 60 Hv and Cu = 80 Hv). When silicon carbide particles are added the hardness of both copper and silver films is higher than that of the pure material and in the case of copper is higher than the bulk value. The hardness is almost doubled in the case of silver and almost three fold in the case of copper. What is unusual is that the hardness does not appear to change with particle size and comparing **Figures 4.3a** and **4.5a** it does not appear to change despite the large difference in substrate morphology. The incorporation of Al₂O₃ in contrast leads to harder coatings despite Al₂O₃ being softer than SiC. The hardness of the copper film was 4 times that of the pure electrodeposited film and twice that of bulk copper. Analogous results were also obtained for silver. It should however be noted that the hardness values for the composites shown in **Figure 4.6** are not only less than the silver/ zirconia composited reported in the literature⁷, but they are also less hard than the value reported for bulk silver deposited from aqueous solutions. This shows that the morphology of the metal matrix is the most important factor in controlling the hardness of a metal composite.

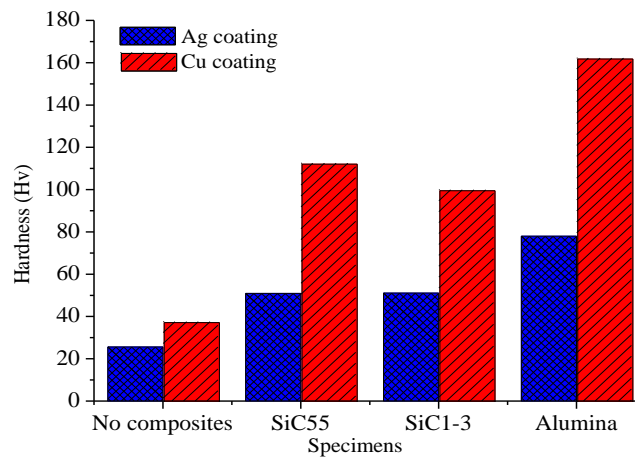


Figure 4.6 *Hardness comparison between Ag and Cu coating as function of type and particle size.*

There are three reasons for the increase in hardness^{26,27,28} particle-strengthening, dispersion-strengthening and grain refining. Particle-strengthening is related to the incorporation of hard particles at volume fraction above 20%. In this case, the load is

carried by both the matrix and the particles and strengthening is achieved because the particles restrain the matrix deformation. Dispersion-strengthening is associated with the incorporation of fine particles ($<1\ \mu\text{m}$) and volume fraction lower than 15%. In this case, the matrix carries the load and the small particles hinder dislocation motion. The third mechanism is related to the nucleation of small grains on the surface of the incorporated particles, resulting in a general structural refinement.

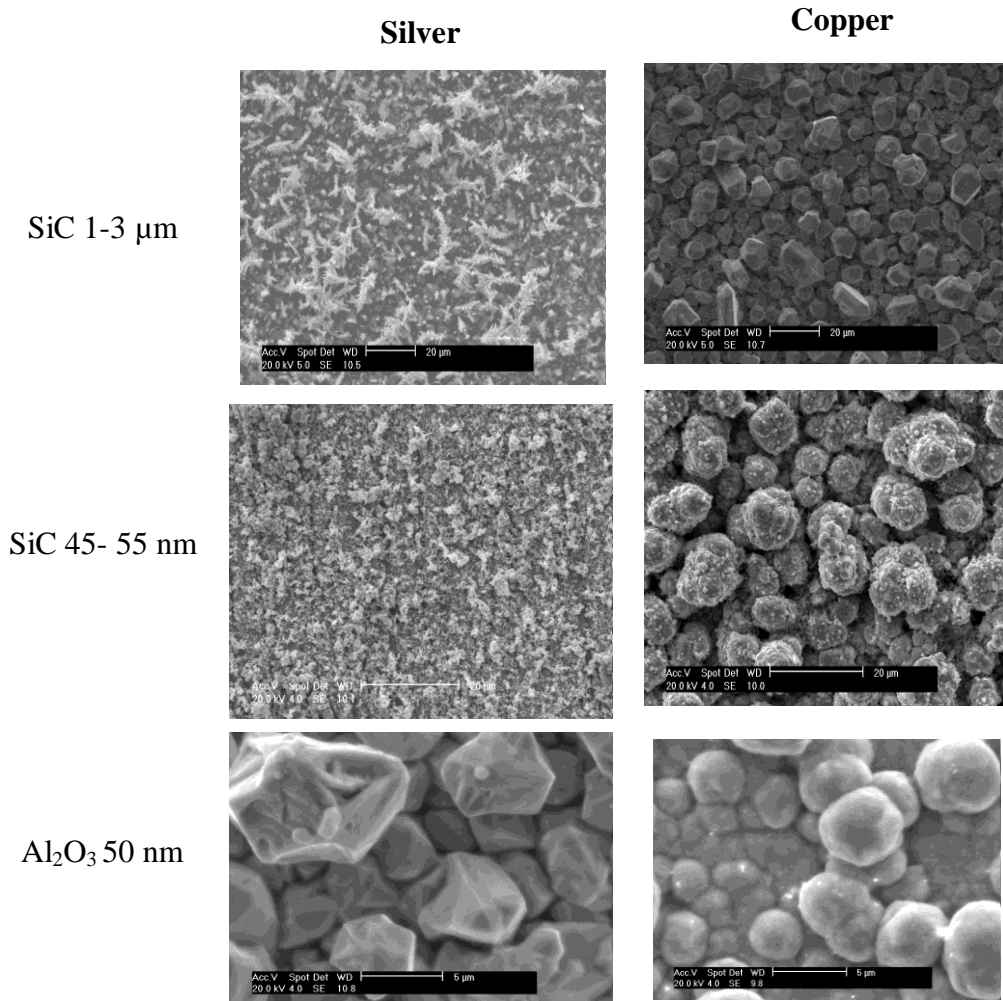


Figure 4.7 SEM micrographs for both Ag and Cu co-deposited films with SiC and alumina particles

It has been reported in literatures that the addition of lithium salts changes the mechanism of nucleation.²³ Work by Endres *et al.* showed that the addition of LiF had a significant effect upon the adherence the mechanical properties of deposited films. In the next chapter this is also demonstrated for nickel composites. **Figure 4.8** shows the change in morphology following the addition of LiF to electrodeposited silver/ SiC composites. It can be seen that the large microcrystalline silver particles formed with nanocrystalline SiC are not present when only 1 wt. % LiF is added to the DES. LiF does not appear to change the structure of the silver film formed with microcrystalline SiC. Clearly both the size of composite particle and the double layer structure affect the nucleation of silver.

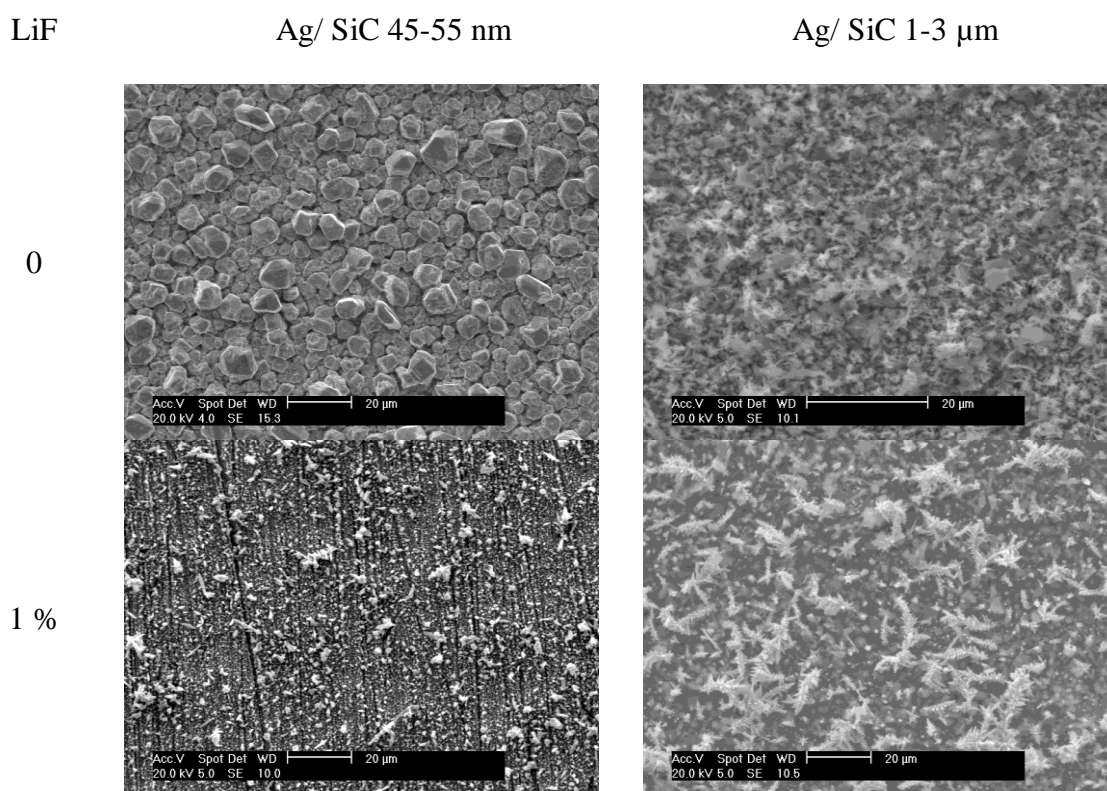


Figure 4.8 SEM micrograph of silver composites electrodeposited on a nickel substrate.

4.2.5 Wear analysis

The wear resistance of the coatings shown above were tested under dry sliding conditions in air at 25 °C for 12 min by the ball-on-disk method. An AS14 steel ball (diameter 5 mm) stylus was used under a load of 10 N. The slide distance was 5 mm

with a speed of 180 mm/ minute for 200 cycles. The morphology of the worn surface area was examined using SEM as shown below in various figures. For each sample the corresponding wear scar depth was determined using a profilometer as shown in **Table 4.1**. All the wear tests were confined within the coating thickness.

Coating	Depth (μm)
Ag	7.47 ± 1.41
SiC 1-3 μm	4.62 ± 0.19
SiC 45- 55 nm	4.64 ± 0.13
Al ₂ O ₃ 50 nm	3.73 ± 0.41

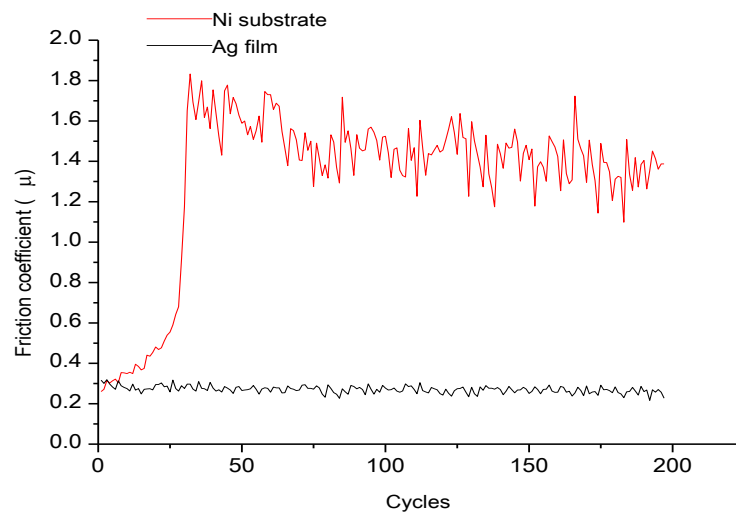


Figure 4.9 Plot showing the friction coefficient of a pure Ag coating and a nickel substrate.

Figure 4.9 shows the difference between the friction coefficients of silver and the nickel substrate. **Figure 4.10** shows that when the particulates are added to the silver film the friction coefficient increases. This is what would be expected since the soft silver is easily eroded and can be moved to form a flat surface thus decreasing friction. The particulates will have the opposite effect and therefore it is to be expected that the

friction coefficient increases as the test continues. This can be visually seen in the morphology of the worn surfaces. The pure silver surface is worn smooth, the nanoparticles have worn similar sized scratches in the surface while the micron size particles have gouged larger sized tracks from the surface.

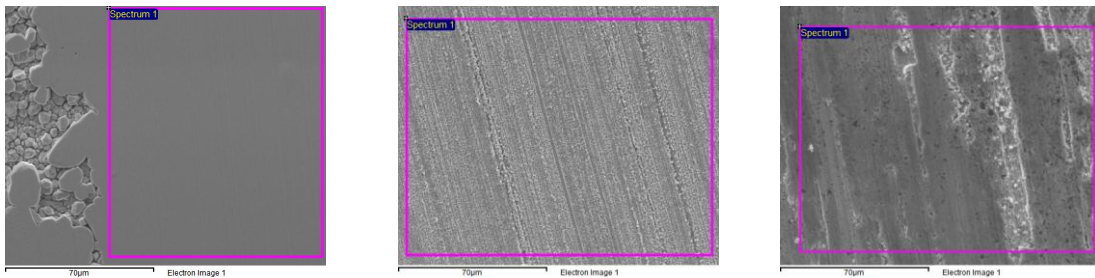
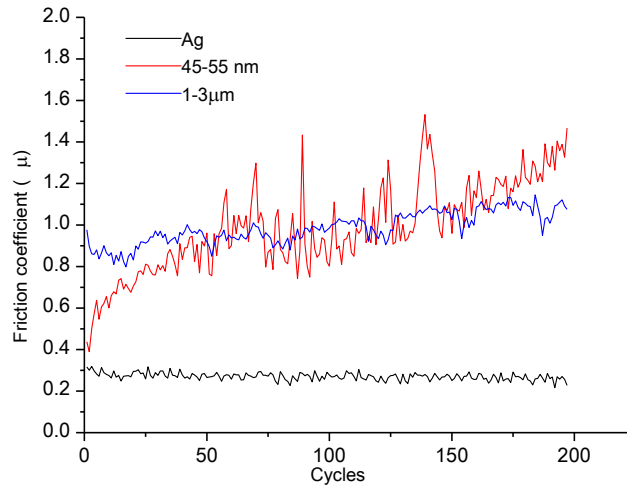
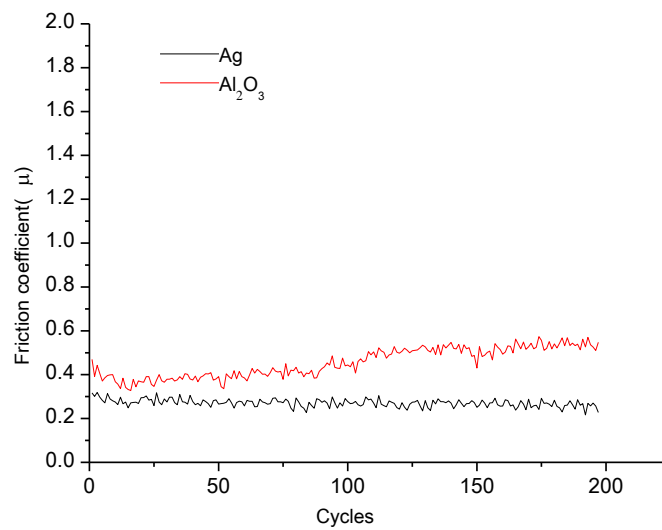


Figure 4.10 Plot to show the friction coefficient of Ag/ SiC composites as a function of particle size versus number of cycles where the complete cycle covers sliding distance of 1 cm length. SEM image for (a) worn surface of Ag only, (b) worn surface of Ag / SiC nano- particles coating, (c) worn surface of Ag / SiC -3 μm coating..

It has been observed that the influence of the second phase enhances the wear resistance compared to Ag coating without composites, as seen in Table 4.1. The incorporation of Al_2O_3 nanoparticles in silver coatings has the lowest wear rate although they are relatively similar to the SiC particles.

Figure 4.11 shows the affect of the addition of Al_2O_3 on the friction coefficient and the surface morphology of the worn surface. Comparing the results to those obtained with SiC it can be seen that the morphology of the surface following abrasion is similar in both cases. **Figure 4.11** shows that the friction coefficient for the Al_2O_3 composite starts with a value that is similar to the SiC composite shown in **Figure 4.10** however the friction coefficient does not increase to the same extent with repetitive cycling. The Al_2O_3 particles are less hard than SiC and therefore when the particles become detached they are less abrasive to the silver surface.



(a)

(b)

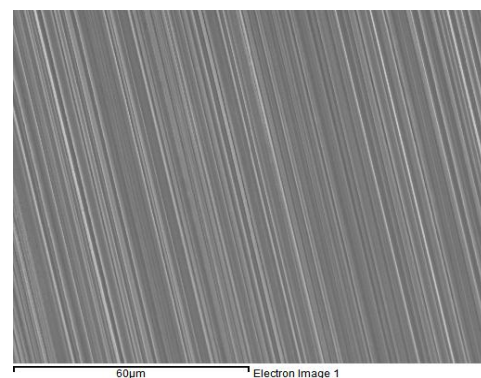
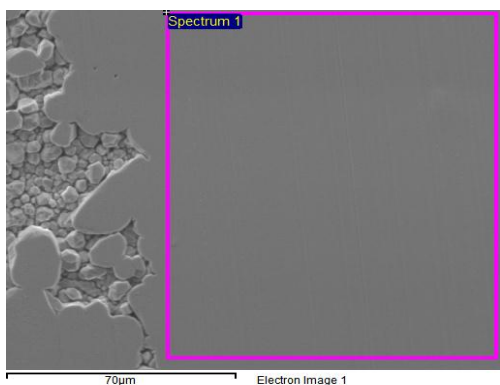


Figure 4.11 Plot of friction coefficient of a $\text{Ag}/\text{Al}_2\text{O}_3$ composite coating versus the number of cycles. SEM image for (a) the worn surface of Ag only, (b) the worn surface of $\text{Ag}/\text{Al}_2\text{O}_3$ composite coating.

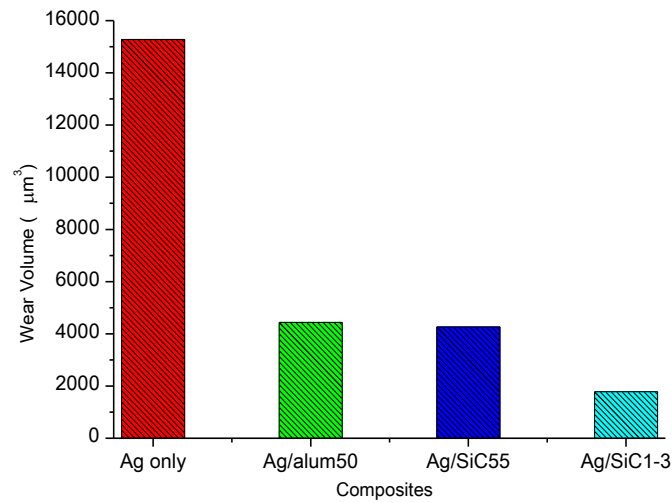


Figure 4.12 Bar chart for the wear volumes of various Ag coatings with composites as a function of size and type.

Figure 4.12 shows that the incorporation of composite particles decreases the wear volume by approximately 60 to 80 %. This is a significant result as it means that the aim behind this project namely the deposition of silver for electrical contacts with improved wear resistance should be possible.

The surface roughness of the films deposited in Sections 4.2.1 to 4.2.4 were determined using the technique of digital holographic microscopy (DHM). DHM images allow measurement of the surface profile which can help to assess basic problems such as contact distortion, friction, heat and electrical conduction, tightness of contact joints and positional accuracy.²⁹

The surface roughness of all the Ag coatings, without and with composites, was determined using a Digital Holographic Microscope (DHM) and the topography of the silver surface before and after the wear tests are shown in **Figure 4.13** and **4.14**. The surface roughness data obtained are listed in **Tables 4.2**. The 3 dimensional plots of the surface are shown in **Figure 4.14**. The average surface roughness (Sa) of the Ag coatings without composites was decreased in the test by approximately 35 nm.

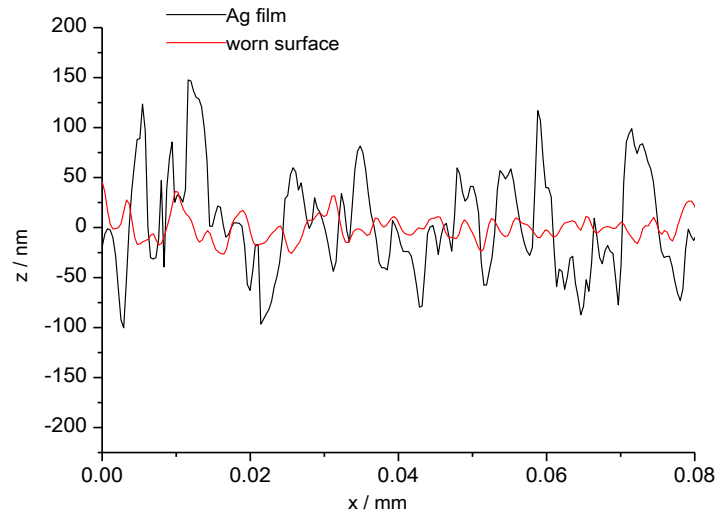
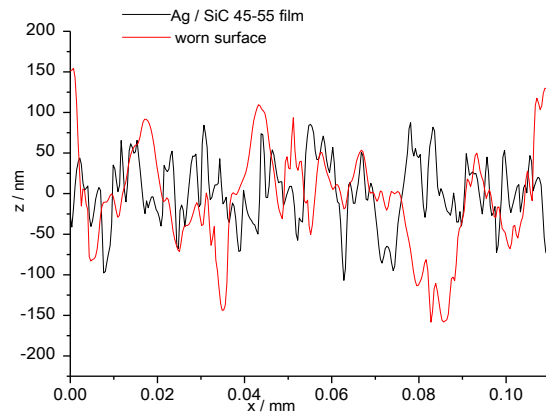


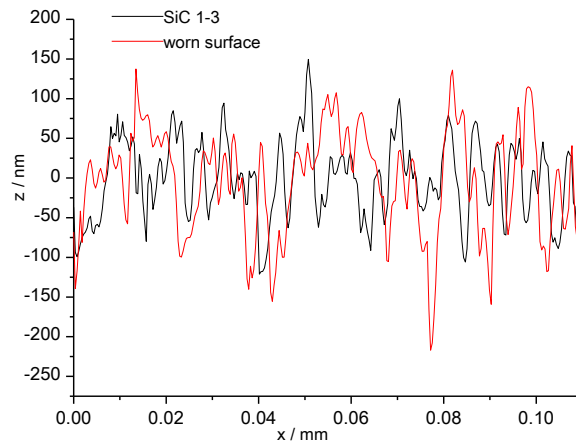
Figure 4.13 Surface roughness profile for the Ag coatings and the worn surface of Ag coatings where z represents the topology of the worn surface.

Table 4.2: the average surface roughness (S_a) of various coatings.

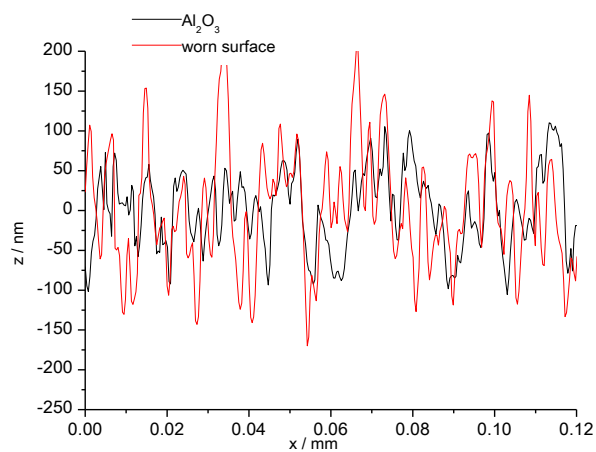
Coating	S_a / nm	S_a / nm (scar)
Ag	28.5	4.5
Ag/ Al_2O_3 50 nm	29.6	39.6
Ag/ SiC 45- 55 nm	36.5	35.0
Ag/ SiC 1-3 μ m	35.2	38.9
Ag/ SiC 45- 55 nm / 1% LiF	37.1	40.8
Ag/ SiC 1-3 μ m / 1% LiF	37.9	40.3



a

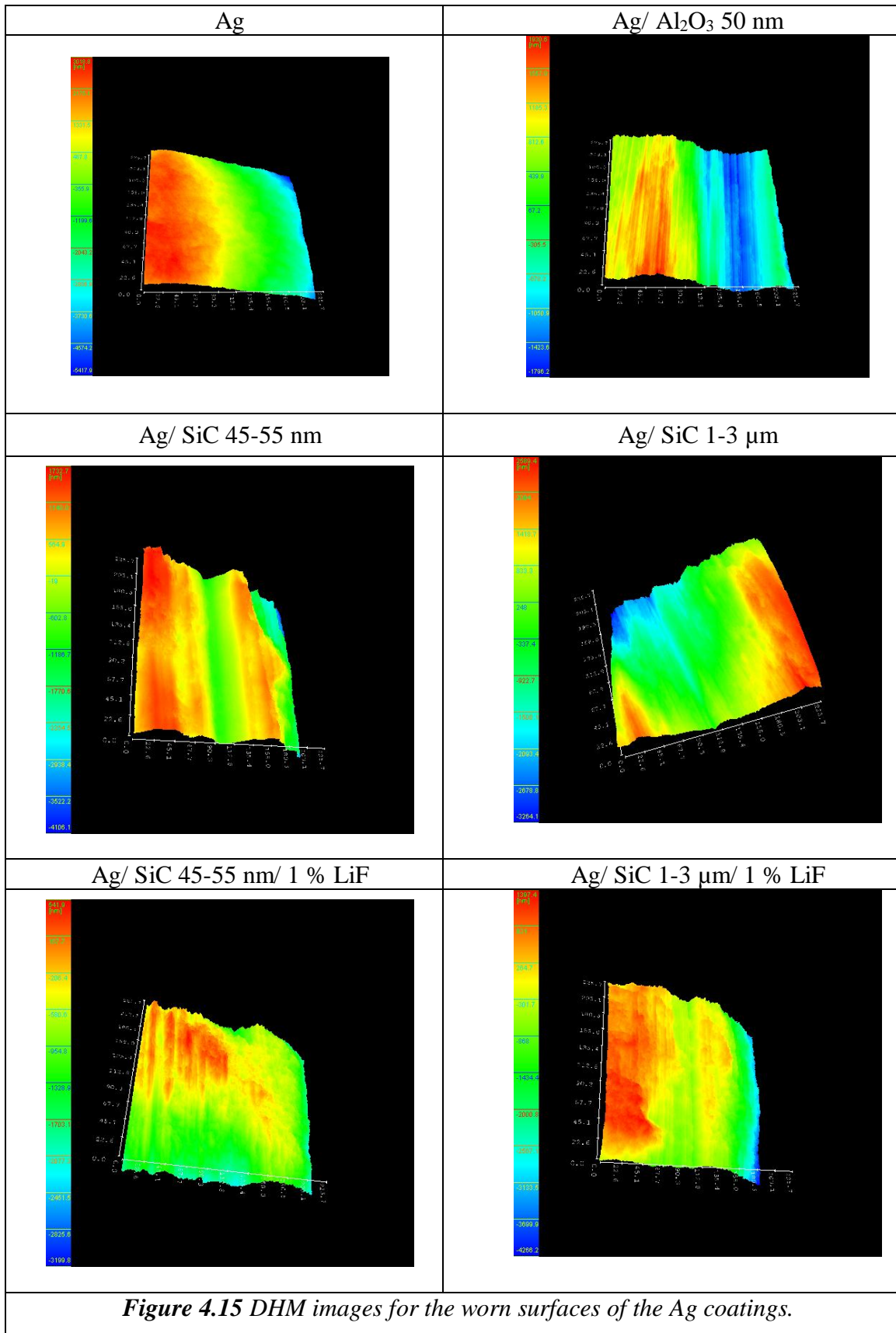


b



c

Figure 4.14 Surface roughness profile for the surface of a) Ag/ SiC 50 nm b) Ag/ SiC 1-3 μm c) Ag / Al_2O_3 50 nm before and after wear tests.



4.2.6 Effect of LiF on hardness and friction coefficient of Ag / SiC films

It has been reported that the addition of alkali metal fluorides such as LiF has a significant effect upon the electrodeposition of metals in high temperature molten salts.^{30,31,32,33} Furthermore the addition of LiF has been found to improve the mechanical properties of deposited films. Endres³⁴ and co-workers noticed that the morphology changed with the addition of LiF. **Figure 4.8** shows that the morphology of the silver changes with LiF added to the solution and this should have a significant effect upon the hardness of the composites. **Figure 4.16** shows that when LiF was added to the solution with nano-sized SiC particles the hardness approximately doubled from 51 Hv without LiF to 113 Hv with LiF. The same trend was observed with silicon carbide microparticles although the effect was larger and the hardness tripled from 51 Hv to 145 Hv. These hardness values are comparable with the values reported by Pagetti *et al* for Ag/ZrO₂ deposited from aqueous solutions.⁷

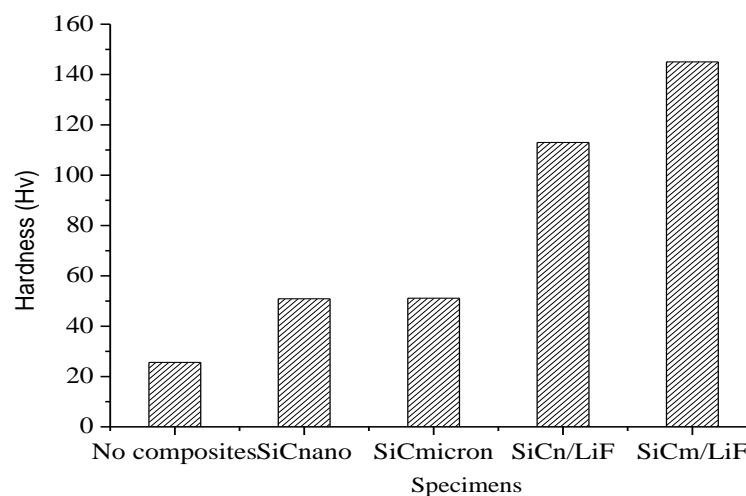
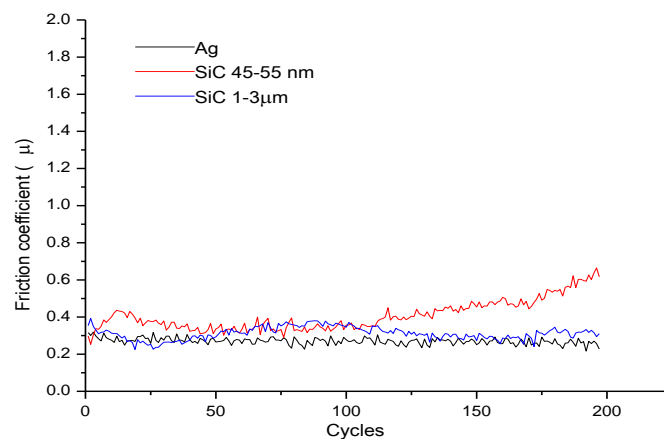


Figure 4.16 bar chart showing hardness of Ag composites with with SiC particulates deposited from 0.1 M AgCl, with 1 mM SDS and 40 g / l SiC in 1 ChCl: 2 EG based liquid(Ethaline) at -1.20 V with added 1 % LiF.

The friction coefficient is also affected significantly after adding LiF. Comparing **Figures 4.10** and **4.17** the average friction coefficient of silver deposits with silicon

carbide nanoparticles is decreased by roughly 0.6 and showed less roughness in the presence LiF. Using silicon carbide microparticles the average friction coefficient is reduced even more by 0.7 (which comparable to silver pure deposits). This is in a good agreement with what has been reported earlier for other types of composites. There could be two reasons why the hardness and the friction coefficient improve; one is the morphology change after addition of LiF which improves adherence of the film and the other is the amount of particulate distributed in the matrix.



(a)

(b)

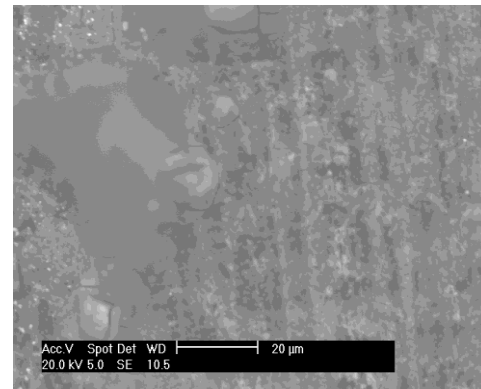
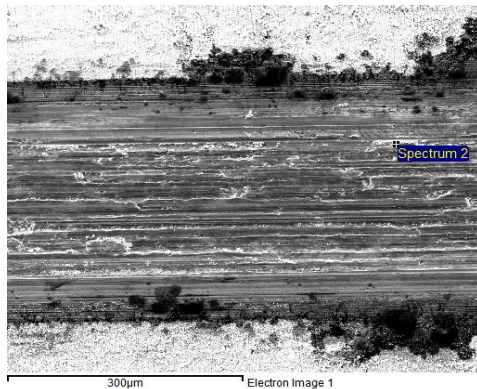


Figure 4.17 As Figure 4.10 but with the addition of 1 wt % LiF. (a) worn surface of Ag / SiC 50 nm composite, (b) worn surface of Ag / SiC 1 -3 μm coating..

Table 4.2 shows the comparison of the surface roughness between the Ag coatings and the worn surface with and without composites. It is clear that the average surface roughness of the worn surface decreases significantly compared to the as deposited surface. The silver is abraded from the surface and fills in the troughs on the surface.

The surface roughness of the worn surface of the silver composites is comparatively unchanged suggesting that the composite particles hinder the abrasion of the silver matrix. The similarity between the surface roughness values can be understood by the schematic diagram shown in **Figure 4.18**. Here the hard composite particles protrude from the soft silver matrix. If the particles are densely packed the large probe cannot grind away the soft silver between them and this results in a similar surface roughness.

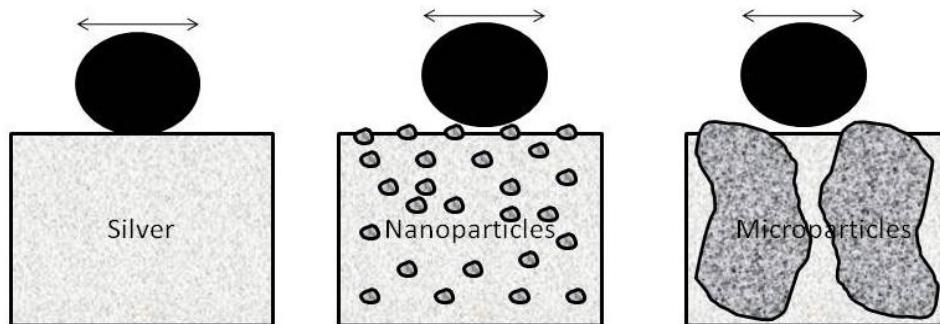


Figure 4.18: Schematic diagram of the wear experiment with composite silver

4.3 Conclusions

The aim of this chapter was to develop a silver composite which could be used in electrical connectors to impart improved wear resistance to frequently abraded interconnects. The results have shown that just as in the previous chapter, a large amount of particulate can be incorporated into the silver films. The as-deposited silver coatings are composed of dense micro-crystalline silver particles which are relatively soft. The incorporation of nano-sized SiC particles does not appear to affect the morphology of the silver matrix although it does roughly double the hardness of the film. An increase in the size of the SiC particles from 50 nm to 2 μm does not affect the hardness of the composite however, it does decrease the wear volume significantly. The incorporation of Al_2O_3 nano-particles has the biggest effect upon the hardness however the wear volume and morphology similar to the coatings with the same sized SiC particles. It can therefore be concluded that reducing the size of the silver crystals of the matrix appears to decrease the wear volume of the sample. To some extent this is what would be expected since the adhesion between larger particles will be less than that between smaller particles and the removal of removal of larger particles will lead to a larger wear volume.

4.4 References

-
- ¹ *The Canning Handbook Surface Finishing Technology* **1989**, F. N. Spon Ltd., London New York.
- ² C. T. J. Low, R. G. A. Wills and F. C. Walsh, *Surface and Coating Technology* **2006**, 201, 371.
- ³ A. Hovestad and L. J. J. Janssen, *Modern Aspect of Electrochemistry* **2005**, 38, 475.
- ⁴ Y. Suzuki, M. Wajima and O. Asai, *J. Electrochem. Soc.* **1986**, 133, 259
- ⁵ I. Boskovic, I. S. V. Mentus and M. Pjescic, *Electrochim. Acta* **2006**, 51, 2793.
- ⁶ K. Ui, T. Fujita, N. Koura, F. Yamaguchi, *J. Electrochem. Soc* **2006**, 153, C449.
- ⁷ P. A. Gay, P. Bercot and J. Pagetti *Surf. Coat. Tech.*, **2001**, 140,147.
- ⁸ X. Xu and C. L. Hussey, *J. Electrochem. Soc.*, **1992**, 139, 1295.
- ⁹ F. Endres, W. Freyland and B. Gilbert, *Ber. Buns. Ges.* **1997**, 101, 1075.
- ¹⁰ C. C.Tai, F. Y. Su and I. W. Sun, *Electrochim.Acta* **2005**, 50, 5504.
- ¹¹ P. He, H. Liu, Z. Li, Y. Liu, X. Xu, Xiudong and J. Li, *Langmuir* **2004**, 20, 10260.
- ¹² R. Bomparola, S. Caporali, A. Lavacch and U. Bardi, *Surf. Coat Tech.*, **2007**, 201, 9485.
- ¹³ C. Fu, H. Zhou, W. Peng, J. Chen and Y. Kuang, *Electrochem. Commun.***2008**, 10, 806.
- ¹⁴ A. I. Bhatt, A. M. Bond, *J. Electroanal. Chem.* **2008**, 619.
- ¹⁵ S. Z. El Abedin and F. Endres, *Electrochim. Acta* **2009**, 54, 5673.
- ¹⁶ T. Murakami, Y. Kogo, K. Waku, H. Hayashi and A. Kishimoto, *Electrochemistry* **2009**, 77, 645.
- ¹⁷ N. Serizawa, Y. Katayama and T.Miura, *J. Electrochem. Soc.*, **2009**, 156, D503
- ¹⁸ A. P. Abbott, J. Griffith S. Nandhra, C. O'Connor, S. Postlethwaite, K. S. Ryder and E. Smith, *Surf. Coat Tech.*, **2008**, 202, 2033
- ¹⁹ A. P. Abbott, S. Nandhra, K. S. Ryder and E. Smith *Phys. Chem. Chem. Phys.* **2007**, 9, 3735
- ²⁰ E. L. Smith, A. P. Abbott, J. Griffin, R. C. Harris, C. O' Connor and K. S. Ryder, *Circuit World* **2010**, 36, 3-9
- ²¹ A. P. Abbott, J. C. Barron, K. S. Ryder and E. L. Smith, *Trans. Inst. Metal Finish* **2009**, 87, 201.

-
- 22 A. P. Abbott, K. El Ttaib, K. S. Ryder and E. L. Smith, *Trans. Inst. Metal Finish*
2008, 86, 234.
- 23 A. P. Abbott, F. Qiu, H. M. A. Abood, R. M. Ali and K. S. Ryder, *Phys. Chem.*
Chem. Phys. **2010**, 12, 1862.
- 24 M. Azam, University of Leicester, unpublished results.
- 25 A. P. Abbott, J. C. Barron, K. S. Ryder and A. F. Silva, submitted for publication.
- 26 T. Lampke, B. Wielage, D. Dietrich and A. Leopold, *Appl.Surf. Sci.* **2006**, 253, 2399
- 27 Q. Feng, T. Li, H. Yue, K. Qi, F. Bai and J. Jin *Appl.Surf. Sci.* **2008**, 254 ,2262
- 28 H. Gül, F. Kılıc, S. Aslan, A. Alp, H. Akbulut *Wear* **2009**, 267, 976.
- 29 E. S. Gadelmawla, M. M. Koura, T. M. A. Maksoud, I. M. Elewa, H. H. Soliman *J.*
Mat. Proc. Tech. **2002**, 123, 133.
- 30 A. J. B. Dutra, J. C. Vazques and A. Spinola, *Min. Eng.***1993**, 6, 663.
- 31 P. Chamelot, P. Taxil and B. Lafage, *Electrochim. Acta* **1994**, 39, 2571.
- 32 P. Chamelot, P. Palau, L. Massot, A. Savall, P. Taxil, *Electrochim. Acta* **2002**, 47,
3423.
- 33 F. Lantelme, A. Barhoun, G. Le, J. P. Besse *J. Electrochem. Soc.***1992**, 139, 1255.
- 34 S. Zein El Abedin, H. K. Farag, E. M. Moustafa, F. Endres, *Phys. Chem. Chem.*
Phys. **2005**, 7, 2333.

Chapter 5: The Electrodeposition of Nickel and Nickel Composites using Deep Eutectic Solvents

5.1 Introduction

5.2 Nickel electrochemistry

5.2.1 Cyclic voltammetry

5.2.2 Chronocoulometry

5.2.3 Under-potential deposition (UPD) of nickel

5.2.4 Bulk electrolysis and morphology

5.3 Addition of brighteners: ethylene diamine

5.3.1 Speciation

5.3.2 Cyclic voltammetry

5.3.3 Chronocoulometry

5.3.4 Under-potential deposition (UPD) of nickel

5.3.5 Bulk electrolysis and morphology

5.4 Addition of brighteners: sodium acetylacetonate

5.4.1 Cyclic voltammetry

5.4.2 Chronocoulometry

5.4.3 Under-potential deposition (UPD) of nickel

5.4.4 Bulk electrolysis and morphology

5.5 Composites

5.5.1 Nickel/ SiC composites

5.5.1 Nickel/ PTFE composites

5.6 Anodic behaviour of nickel in Ethaline and Reline

5.7 Conclusions

5.8 References

5.1 Introduction

The previous two chapters have focussed on the electrodeposition of composite materials with relatively soft metal phases. The majority of metal composites deposited from aqueous solutions have involved the incorporation of hard particulates into nickel.^{1,2,3,4} Nickel has been the metal of choice because of its ductility, simplicity of electrodeposition and combination of anti-corrosive behaviour with enhanced wear resistance. This has largely been obtained through the incorporation of ceramic particles such as alumina, titania or silicon carbide.⁵ The composite materials can be tuned to provide other properties including magnetic, fluorescent, photocatalytic or piezoelectric attributes.⁶

While the deposition of composites has been carried out since the 1920s, it is only relatively recently that the codeposition of nickel has been studied in depth. Numerous models have been proposed for the incorporation of particles into metal films and these have been summarised in a review by Low *et al.*⁷ Numerous improvements to bath formulation and plating conditions have meant that the deposition of nano and micron-sized particles can now be achieved with up to 15 % by volume.^{8,9,10}

The main difficulty to be overcome with high particulate incorporation is in the agglomeration of particles in the metal film. One method of overcoming this issue is to use ultrasound to break up the particle clusters.^{11, 12} Steinhäuser *et al.* suggested that the incorporation of particulates into nickel coatings could improve the corrosion resistance of the material.¹³ This is thought to result from changes induced in the structure of the nickel film,¹⁴ however other studies report that particulates cause an increase in the number of defects and internal stress.^{15,16} The improvement in material strengthening, improved hardness and improved wear resistance are well documented.^{17,18,19,20} The subject of composite electrodeposition has been reviewed in several articles.^{7,21,22}

While the majority of important metals have been studied in ionic liquids, relatively few studies have been made into the deposition of nickel. Gou and Sun²³ studied the electrodeposition of nickel and nickel–zinc alloys from the zinc chloride-1-ethyl-3-methylimidazolium chloride. They found that although NiCl₂ dissolved in the pure chloride rich 1-ethyl-3-methylimidazolium chloride ionic melt, metallic nickel could

not be obtained by electrochemical reduction of this solution. The addition of zinc chloride to this solution enabled the electrodeposition of dense, compact and adherent nickel coatings. A similar study by Deng *et al.*²⁴ used 1-ethyl-3-methylimidazolium-dicyanamide as the electrolyte. The electroactive species was found to be $[\text{Ni}(\text{DCA})_4]^{2-}$ and the nucleation was found to occur by a 3D progressive mechanism. The grain size was found to increase with increasing deposition potential.

A related study on the co-deposition of multi-walled carbon nanotubes in nickel was published following the publication of the results in this chapter and those in Chapter 3. Martis *et al* reported, the electrodeposition of Ni/MWCNT coatings from a choline chloride/ urea based DES. They noted that the nano-tubes formed stable dispersion both in the pristine and oxidized form and these were well distributed throughout the nickel film. The MWCNTs affected the crystallinity and roughness of the film.²⁵

In this chapter, the electrolytic deposition and morphologies of metallic Ni coatings from ionic liquids based on a ChCl: 2 ethylene glycol and a ChCl:2 urea eutectic mix were investigated. Changes in morphology and composition have been investigated by the addition of brighteners and changing the ionic liquid used in the deposition process. Cyclic voltammetry and chronocoulometry together with AFM and SEM were used to probe the mechanism of deposition and the structure of the Ni deposits.

5.2 Nickel electrochemistry

5.2.1. Cyclic voltammetry

Figure 5.1 shows the cyclic voltammogram for the reduction of 0.2 mol dm^{-3} $\text{NiCl}_2 \cdot 6\text{H}_2\text{O}$ in Ethaline and Reline at 20°C on a Pt electrode as a function of sweep rate. It is clear that the reversibility of the deposition process is different in the two liquids. In the EG eutectic, the difference between the onset voltage of deposition and the onset of dissolution is smaller than in the urea eutectic. It is proposed that this is due to differences in ligand activity between the two liquids. There is a strong coordination between the urea and chloride ions which effectively decreases the activity of chloride compared with EG.

Figure 5.1 also shows that the deposition is quasi-reversible in both liquids. The electrochemistry of most p and d block elements has been studied in both of these liquids and it was found that metals in groups 3–5 (Sc–V) cannot be electrodeposited

within the potential window of the ionic liquid. Those in groups 6–8 (Cr–Fe) can be reduced but not stripped whereas Co, Ni and Pd all give a quasi-reversible deposition response. The majority of the remaining elements (Cu, Ag, Zn, Hg, In, Sn and Bi) show reversible deposition and stripping responses. The reason behind this is not known but is thought to result from the speciation of the metal complexes in solution. Metals in periods 3–8 predominantly have octahedral complexes whereas those in groups 11–15 tend to form linear or tetrahedral species. The quasi-reversible metals such as Ni are variable and tend to be either square planar or octahedral depending upon the ligand.²⁶

The reduction process for nickel is difficult to quantify but the onset potential is approximately -1.1 V vs. Ag. Comparison with the aqueous redox couple is difficult owing to the difference in speciation but $E^0(\text{Ag}^+/\text{Ag}^0) - E^0(\text{Ni}^{2+}/\text{Ni}^0) = 1.03$ V. What is notable about the Ni redox process is that the potential for the onset of reduction differs from that for oxidation by about 0.5 V. The reduction waves are not clearly defined like those previously observed with other metals such as Cu and Ag in the same IL and the anodic scan shows that there are two oxidative processes. A similar anodic response has been observed for zinc in the EG eutectic. In the Zn case, the presence of two anodic processes was unambiguously ascribed to two different morphologies of metals being deposited and stripped using *in situ* atomic force microscopy.^{27, 28} The less anodic stripping peak was found to be due to the deposition of nano-deposits whereas the more anodic peak was due to the deposition of bulk metal.

Figure 5.1 also shows that the shape of the Ni stripping peaks depends upon sweep rate in both liquids showing that the processes were kinetically slow. It should also be noted that the current on the anodic sweep is slow to return to zero, inferring that some material is strongly bound to the electrode surface.

Comparison of **Figure 5.1a** and **5.1b** show a similar response with Reline *i.e.* a poorly defined reduction waves and two anodic processes. It should be noted that the stripping peaks occur at larger over-potential. This can only really be due to two possible differences:

- (i) The morphologies of the deposits.
- (ii) The nature of the ligand involved in solvation process.

Since Cl⁻ is the major ligand in both cases, it is less likely to be due to latter of these.

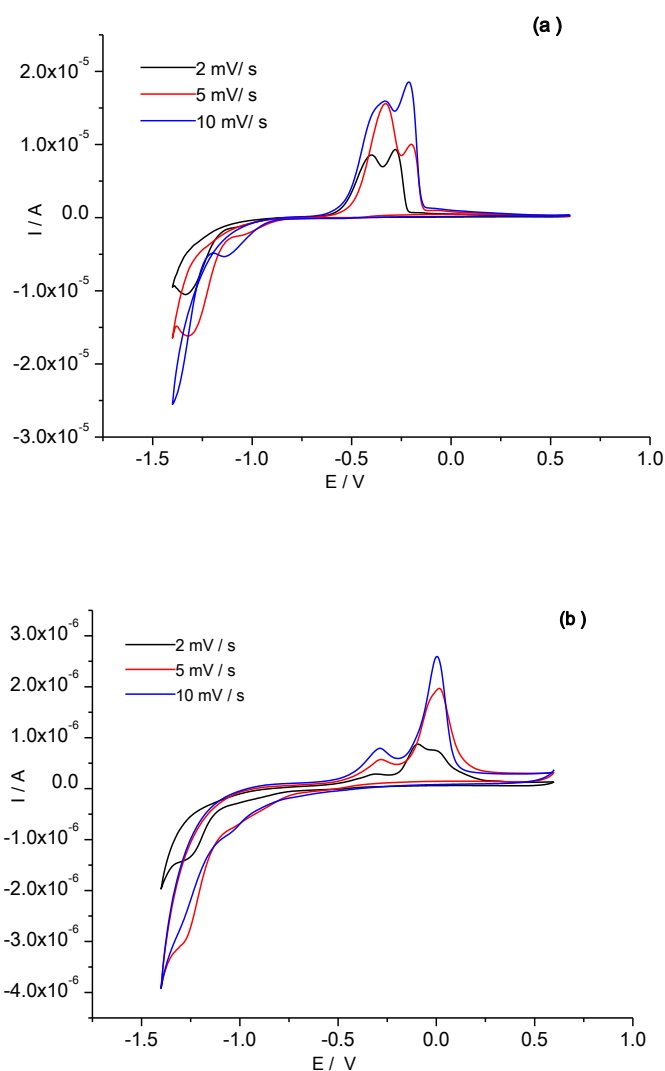


Figure 5.1 Cyclic voltammograms for a Pt disc (1.0 mm diameter) electrode immersed in 0.2M [NiCl₂·6H₂O] in a) Ethaline and b) Reline as a function of sweep-rate (potential versus Ag wire quasi-reference electrode).

5.2.2. Chronocoulometry

Figure 5.2 shows the charge/time transient for a Pt electrode immersed in Ethaline and Reline containing NiCl₂·6H₂O (0.2 M) for a potential step from +1 V (held for 10 s) to -1 V for 30 min. The charge/time transients are relatively linear but if the processes are 100% current efficient, the slopes of the curves should be proportional to the diffusion coefficients of the two Ni complexes. A similar response was observed for copper and the ratio of the dQ/dt plots was exactly the same as the ratio of the diffusion coefficients (obtained from the Cu^{2+/+} redox couple) showing that the

deposition process is mass transport limited. No similar internal redox couple exists for Ni but it is reasonable to assume that NiCl_3^- has a similar diffusion coefficient to CuCl_3^- . The ratio dQ/dt plots in **Figure 5.2** were found to be 5: 1, which is significantly smaller than to the ratio of D (10.6). This analysis assumes that the process is 100% current efficient which is clearly not valid since gassing can be observed at the cathode. It was observed that both ILs decomposed at about the same potential as Ni was reduced.

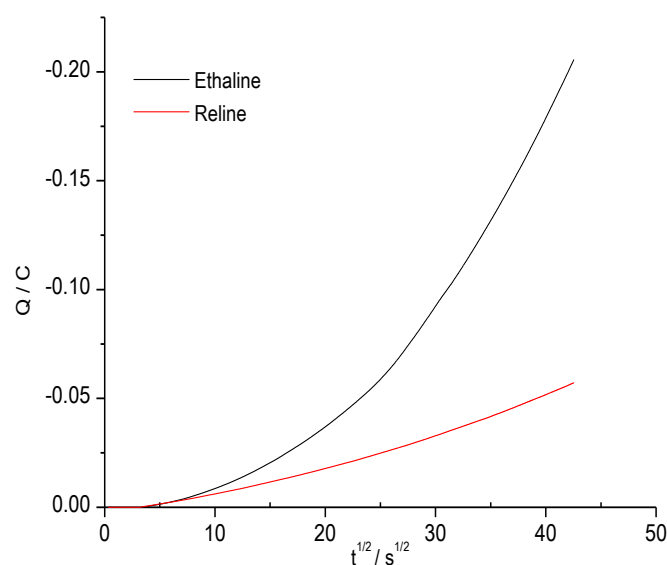


Figure 5.2 Chronocoulometry of $0.2 \text{ mol dm}^{-3} [\text{NiCl}_2 \cdot 6\text{H}_2\text{O}]$ in both 1 ChCl: 2 EG (black line) and 1 ChCl: 2 urea (red line) based liquids for potential steps from 1.00 V for 10s followed by a step to -1.00V for of ca. 30 min (1.0 mm diam. Pt wire).

This is apparently similar to the response observed for Cu. Using the same analysis as in **Figure 5.2** the ratio of deposition rates in the two ionic liquids was found to be 5.1, which is similar to the ratio of D in **Table 3.1**. It could be concluded that Ni deposition is mass transport controlled in the same way that Cu was found to be, although there is a difference between the concentrations in the **Figure 3.3**. However the rate of Ni deposition was considerably faster than for Cu which is unexpected given the difference in thermodynamics between the two metals. Clearly the above analysis assumes 100% current efficiency.

5.2.3 Under-potential deposition (upd) of nickel

Figure 5.3 show that for both ionic liquids upd of Ni is observed and it would appear that the upd process in Ethaline is reversible. The comparison of upd with and without addition of brightener is discussed in section 5.4.3.

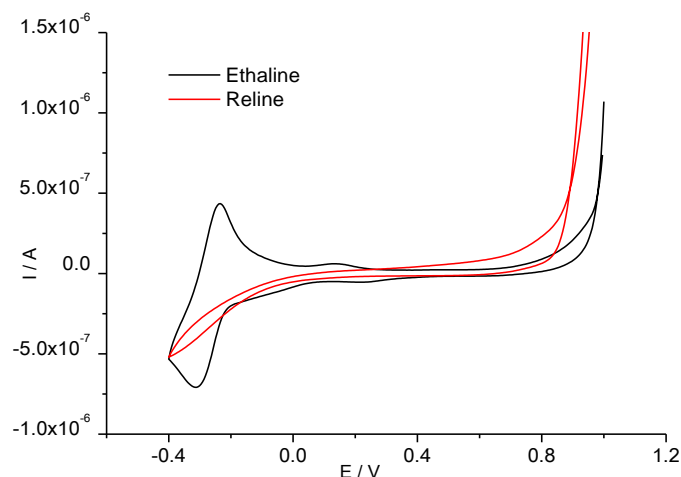


Figure 5.3 Under potential deposition of $[NiCl_2 \cdot 6H_2O]$ in Ethaline and Reline on a 1.0 mm diam. Pt wire at a scan rate 5 mV/s.

5.2.4 Bulk electrolysis and morphology

The electrodeposition of nickel was carried out at -2.50 V for 2 hours at 30 °C on copper substrates in Ethaline and Reline. Both experiments produced black deposits which were adherent. **Figure 5.4** shows the optical photographs of the samples together with the SEM and AFM images. The deposits show no sign of macroscopic crystal. This is typical of the electrodeposition of metals from ionic liquids.²⁹ The deposit morphologies are similar in both liquids. It has recently been reported that zinc forms different structures in Ethaline and Reline. In the former plate-like structures are observed whereas the latter produces small rice-like structures. This was thought to be due to the specific adsorption of chloride ions on the electrode surface which poisoned certain crystal faces. The addition of brighteners with strong hydrogen bonding ability suppressed this and led to brighter surfaces. Since this type of morphology is not observed with nickel it is concluded that specific adsorption of chloride is not a major factor.

It is interesting to note that the morphology of the nickel deposit in Figure 5.4 is almost identical to that reported using 1-ethyl-3-methylimidazolium-dicyanamide by Deng *et al.*²⁴

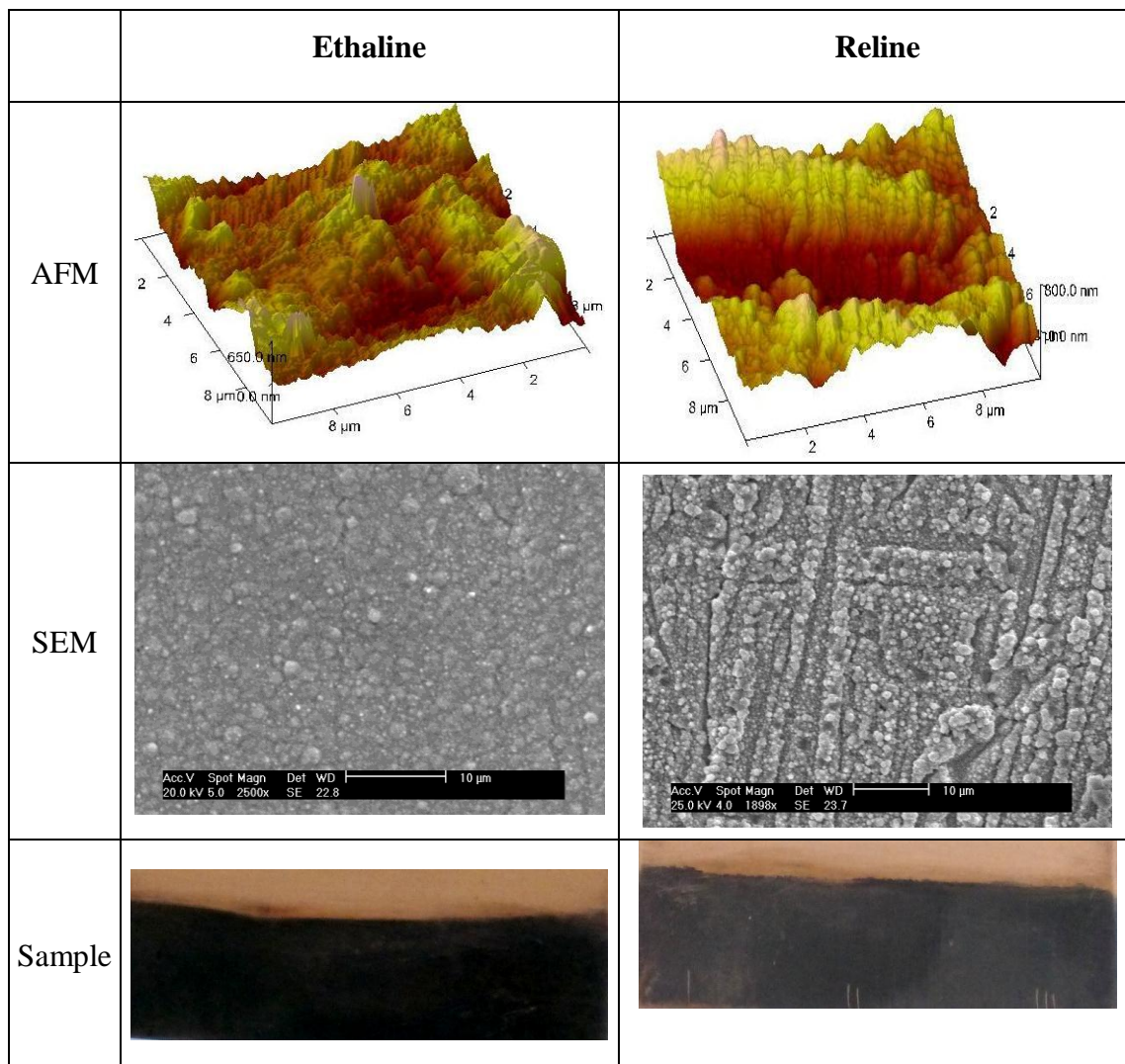


Figure 5.4 shows the comparison Ni deposition on a copper substrate from a solution containing $0.2 \text{ mol dm}^{-3} \text{ NiCl}_2 \cdot 6\text{H}_2\text{O}$ in both Ethaline and Reline using AFM and SEM.

5.3 Addition of brighteners: ethylene diamine

Brighteners are commonly used in aqueous electrodeposition and they tend to function by one of three methods; adsorbing at the electrode-solution interface, modifying viscosity or changing speciation. Speciation is difficult to identify with

great certainty because it is impossible to isolate the species and so *in-situ* techniques have to be used. Speciation in ionic liquids is the subject of two reviews by Hardacre *et al.*³⁰ and Abbott *et al.*³¹

5.3.1 Nickel speciation

Determining speciation in ionic liquids is not trivial because it is impossible to evaporate the solvent to leave the metal complex. One method that has previously been used is fast atom bombardment mass spectrometry (FAB-MS). FAB-MS for the Ethaline IL containing $\text{NiCl}_2 \cdot 6\text{H}_2\text{O}$ shows that the only anionic Ni containing species is NiCl_3^- . No cationic Ni species were observed showing that the naked or hydrated ions are not stable in solution. This is the same as that observed for most metal complexes obtained by dissolving metal halides in these types of ionic liquids. When a metal salt of the form M^{x+}Cl_x is dissolved in an ionic liquid, FAB-MS usually shows that the predominant species is $\text{M}^{x+}\text{Cl}_{x+1}$. This may however be an artefact of the ionisation technique which will destroy any weak complexes. Interestingly, FAB-MS also shows the cluster ChCl_2^- but no Cl.EG^- whereas in the urea based liquid, the ChCl_2^- cluster is small but the Cl.urea^- is the largest signal confirming the fundamental difference between the chloride speciation. As highlighted in the previous reviews,^{30,31} the data from FAB-MS is often contradicted by data from other techniques. Dissolution of ZnCl_2 in these liquids shows that the main species is ZnCl_3^- with a small amount of Zn_2Cl_5^- . Analysis using EXAFS showed that $[\text{ZnCl}_4]^{2-}$ was the main species. Similar results have also been found for CuCl_2 .

Very little is known about the electrochemistry of nickel containing species in ionic liquid. As previously shown knowledge of speciation is vital to understand redox processes.

FAB-MS for NiCl_2 in Ethaline shows peaks at 165 and 295 which correspond to NiCl_3^- and Ni_2Cl_5^- respectively. The other signals were minor ones that could not be identified. FAB MS data in Reline showed only the peak at 165. The relative intensities of these signals were relatively unchanged with the addition of 1, 2 and 3 mole equivalents of en. As discussed in section 5.2 the main species in the absence of en is NiCl_3^- . Uv-visible spectrum (**Figure 5.5**) of this solution has an absorbance maximum at 415 nm. In water NiCl_2 gives a maximum at 722 nm corresponding to

containing complexes are present, but standard spectroscopic techniques cannot give conclusive evidence of this. It is, however, clear to say from simple visual inspection that the addition of en changes the speciation of nickel to some extent.

5.3.2 Cyclic voltammetry

Figure 5.6a shows the C.V for Ni(II) in Ethaline and the subsequent effect of mole equivalents additions of ethylene diamine (en). It is well known that en acts as a strong ligand for most transition metal ions. The aim of this experiment was to create a more stable Ni complex thus suppressing upd and decreasing the ability of the metal to nucleate. **Figure 5.6a** shows that cathodic process is relatively unaffected by the addition of en. The larger cathodic current with 3 mole equivalents of en is due to the decomposition of uncomplexed en. This suggests that there is excess en in the system and shows that the equilibrium



does not lie completely to the right of the equation.

It is notable that the addition of amine causes a significant decrease in the anodic response. This could be due to the decreased amount of deposition occurring when en is added. It noticeable, however, that with three mole equivalents of en no stripping occurs, although the Ni is still being deposited. This suggests that the presence of en affects the complex formed when the metal strips from the electrode surface. One possible explanation could be that the presence of en causes $[\text{Ni(en)}_3]^{2+}$ to be formed and this could be difficult to strip from the electrode surface. When the metal is stripped from the electrode there will be a competition between the nickel ion and the ligands in solution and these are either en or Cl^- . Clearly en is the stronger ligand but there is a higher concentration of Cl^- .

Comparison of the effects of en in Reline with those in Ethaline it can be seen that qualitatively the cyclic voltammograms appear to be similar, however, the anodic signal is proportionately smaller for Reline than Ethaline. The second anodic peak is also at a larger over-potential for Reline than Ethaline and it is also noticeable that the third mole equivalent of en does not result in the large cathodic current suggesting that it is probably bound to the nickel centre. This suggests that **Equation 5.1** lies

more to the right with urea and may be because the chloride is more strongly bound to the urea as was the case observed with zinc by Barron.²⁷

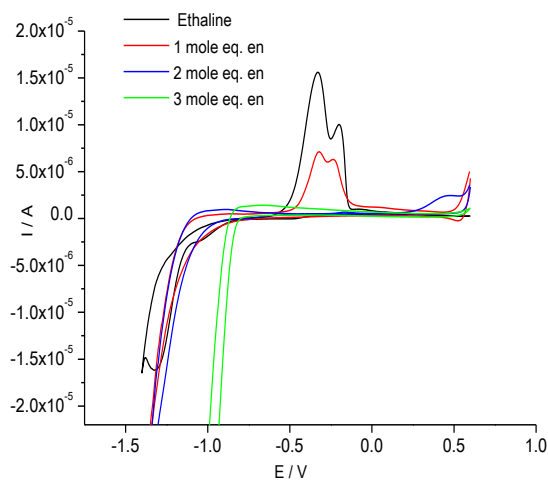


Figure 5.6a Cyclic voltammogram for a Pt disc (1.0 mm diameter) electrode immersed in 0.2M $[\text{NiCl}_2 \cdot 6\text{H}_2\text{O}]$ in Ethaline as a function of various mole equivalents of en at sweep rate 5 mV/s (potential versus Ag wire quasi-reference electrode).

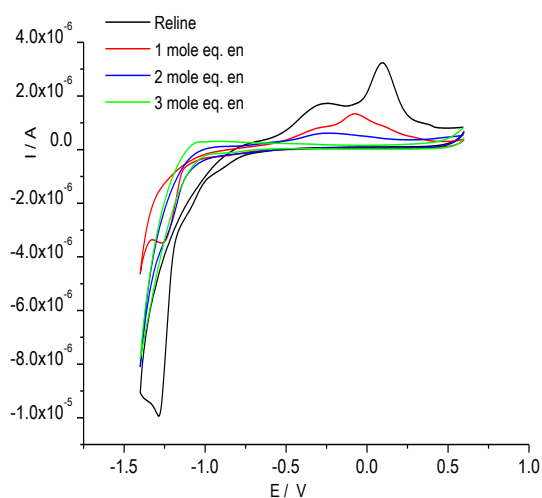


Figure 5.6b Cyclic voltammogram for a Pt disc (1.0 mm diameter) electrode immersed in 0.2M $[\text{NiCl}_2 \cdot 6\text{H}_2\text{O}]$ in Reline as a function of with various mole equivalents of en at sweep rate 10 mV/s (potential versus Ag wire quasi-reference electrode).

5.3.3 Chronocoulometry

Figure 5.7 shows the charge/time transients for a Pt electrode immersed in a Ethaline and a Reline ILs containing $\text{NiCl}_2 \cdot 6\text{H}_2\text{O}$ (0.2 M) for a potential step from +1 V (held for 10 s) to -1 V for 30 min. The charge/time transients are nonlinear suggesting that the process is not solely diffusion control.

Comparison with **Figure 5.2** of the chronocoulometry data for the ILs with and without the addition of en shows that when en is added, there is a significant decrease in current and the associated growth rate is also decreased, suggesting that the en stops the formation and growth of Ni nuclei.

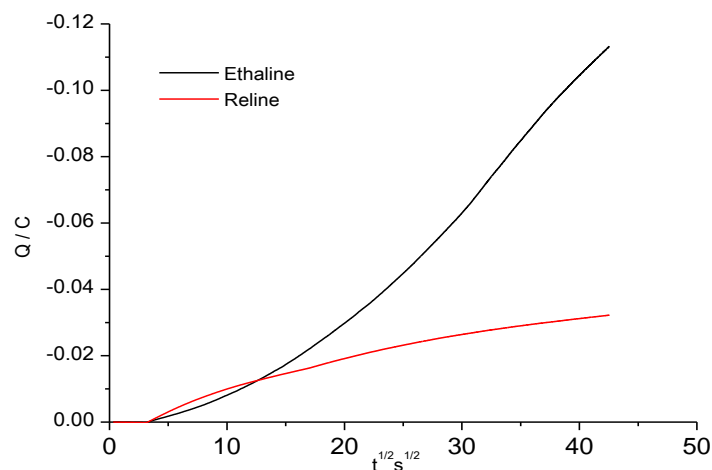


Figure 5.7 Chronocoulometry of $0.2 \text{ mol dm}^{-3} [\text{NiCl}_2 \cdot 6\text{H}_2\text{O}]$ in both Ethaline Reline with 3 equivalents en for potential steps from 1.00 V for 10s followed by a step to -1.00V for of ca. 30 min.

5.3.4 Under-potential deposition of nickel

Figure 5.3 shows that a significant amount of under-potential deposition occurs when $\text{NiCl}_2 \cdot 6\text{H}_2\text{O}$ is reduced in Ethaline and Reline and in the former this is reversible. The occurrence of UPD in ionic liquids has been shown to have a significant effect upon deposit morphology. Abbott *et al.* demonstrated that an electrode which was immersed in a chloroaluminate ionic liquid at the open circuit potential was subject to upd.³² If the deposition potential was applied and then the sample was immersed further into the liquid the portion which had been above the level of the liquid i.e. had not experience upd had a very different morphology to that which had been immersed.

Figure 5.7 shows that when en is added to the solution the upd is suppressed in both Ethaline and Reline. The addition of 1 equivalent of en to the Ethaline solution also had a marked effect upon the oxidative chemistry of the nickel species. An apparent reversible one electron oxidation process occurs at *c.a.* 0.56 V. A second equivalent of en shifts the redox potential wave positive to 0.92 V. It is proposed that this process corresponds to the oxidation of the Ni(II) centre to form a Ni(III) complex. While it is not common for Ni complexes it has previously been reported for en complexes. The addition of a third equivalent of en suppresses the oxidation behaviour of the solution.

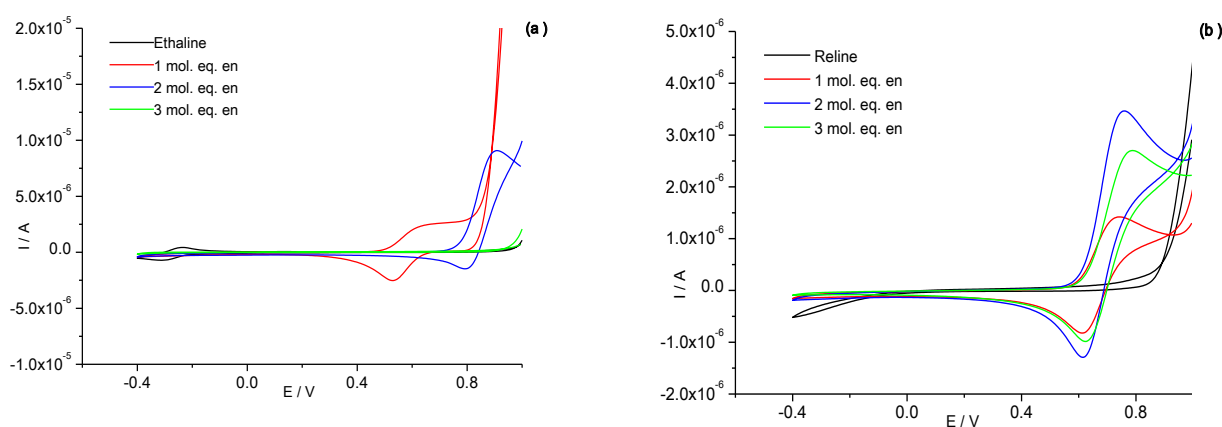


Figure 5.8 under potential deposition and anodic response of 0.2 mol dm^{-3} $[\text{NiCl}_2 \cdot 6\text{H}_2\text{O}]$ with various equivalents en in (a) Ethaline and (b) Reline at a scan rate of 5 mV/s .

Repeating this experiment with Reline shows that a reversible oxidation occurs at 0.7 V. The current roughly doubles when a second equivalent of en is added but the current subsequently decreases when a third equivalent of en is added. In contrast to the Ethaline case the redox potential does not change when the second and third equivalent of en are added to the Reline solution. It is difficult to speculate on the cause of this difference because the changes occurring in speciation are difficult to quantify. It does, however allow some general conclusions to be drawn. Firstly, en changes the speciation in solution and this is also affected by the number of equivalents in solution and secondly the solution composition is dependent upon the nature of the hydrogen bond donor and this suggests that the activity of chloride ions is important in governing speciation.

5.3.5 Bulk electrolysis and morphology

The effect of the additives upon the morphology of the nickel deposits was analysed in an analogous method to that carried out in Section 5.2.4. Bulk deposition was carried out onto Cu substrates by holding at -2.50 V for 2 h from both Ethaline and Reline. The deposits obtained are shown in **Figure 5.9**. Comparing these images with those obtained in the absence of en, it was seen that the deposits appear more grey and metallic than those in the absence of en.

Figure 5.9 also shows SEM images of deposits from liquids with different mole equivalents of en. The Ni deposit from Ethaline without the addition of en was black and consisted of particles of varying sizes. The addition of en led to a smaller distribution of particle sizes and greater leveling of the surface. The particles are hemi-spherical in shape and tend to be *ca.* 1 μm in diameter. Further addition of en decreased the small scale surface roughness. In fact, although some of the features appear to be larger as a consequence of adding more en (**Figure 5.9**), these larger features are made up from clusters of much smaller crystallites. The images for the addition of the same mole equivalent of en in Reline are similar to those obtained for Ethaline, although the deposits appeared optically brighter. This difference in brightness could be partially due to the fact that the coatings are thinner. In conclusion, the SEM images do however show that the surfaces were significantly smoother with the addition of en. It can be seen that en suppresses up and nucleation, and therefore leads to a smoother surface finish.

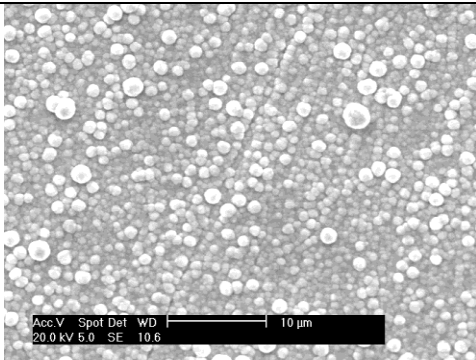
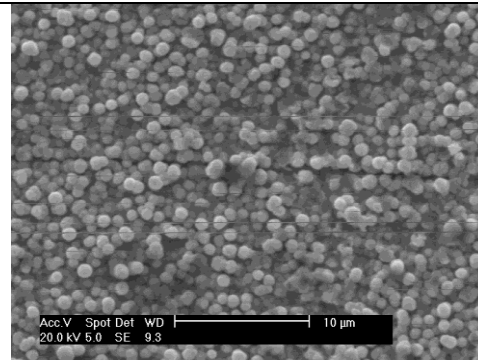
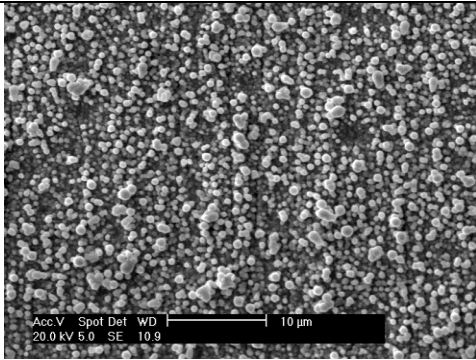
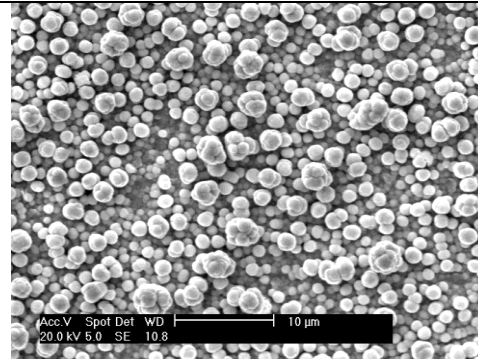
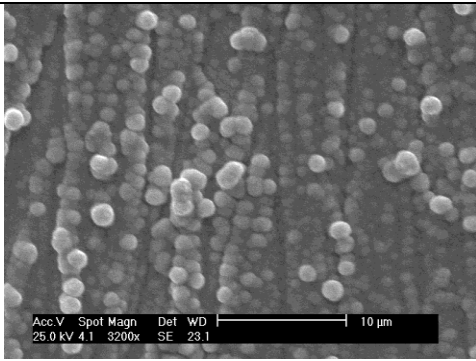
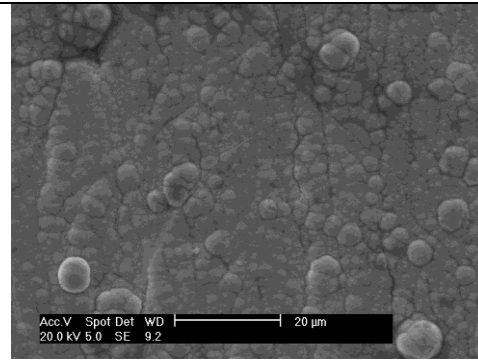
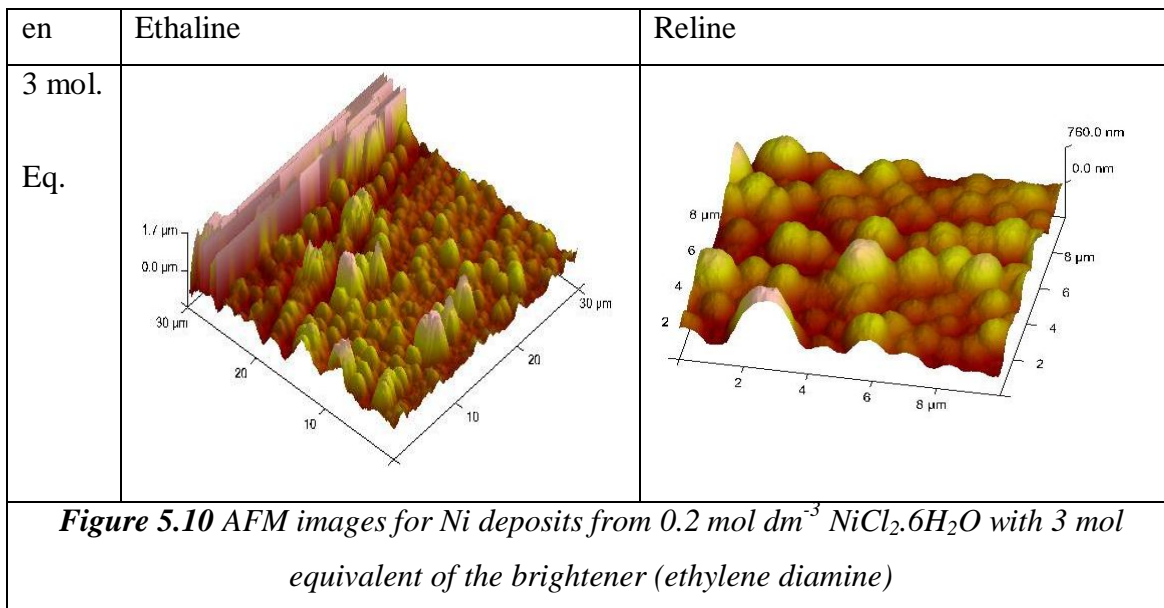
NiCl ₂ :en	Ethaline	Reline
1:1		
1:2		
1:3		
Sample		

Figure 5.9 Scanning electron micrographs of Ni deposited on Cu from solution containing $0.2 \text{ mol dm}^{-3} \text{ NiCl}_2 \cdot 6\text{H}_2\text{O}$ in both Ethaline and Reline with various mole equivalents of en.

The AFM results in **Figure 5:10** show more clearly the change in surface roughness that occurs when en is added as a brightener. Comparison with **Figure 5.4** shows that the angular topography has been replaced with a regular series of hemispherical growths.



One advantage of ionic liquids listed above is the ability to deposit metals onto substrates that usually passivate or are water sensitive. **Figure 5.11** shows a photograph of an aluminium sample which was coated directly in a similar manner to the copper samples shown above. The relatively dull appearance is a consequence of the rough substrate that was used.

Figure 5.11 Photograph of a nickel layer deposited onto an aluminium substrate following electrolysis of $\text{ChCl} : 2 \text{ EG}$ containing 0.2 mol dm^{-3} with 3 mol equivalents of en at an applied potential of -2.5 V for 120 min.



5.3.6 Effect of addition of LiF

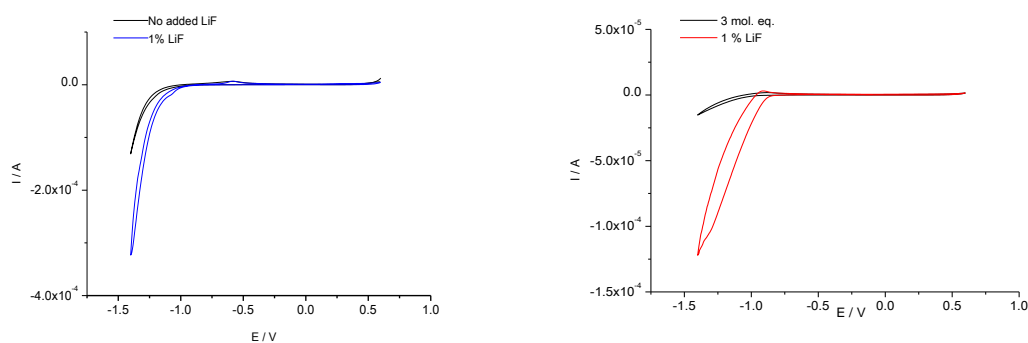
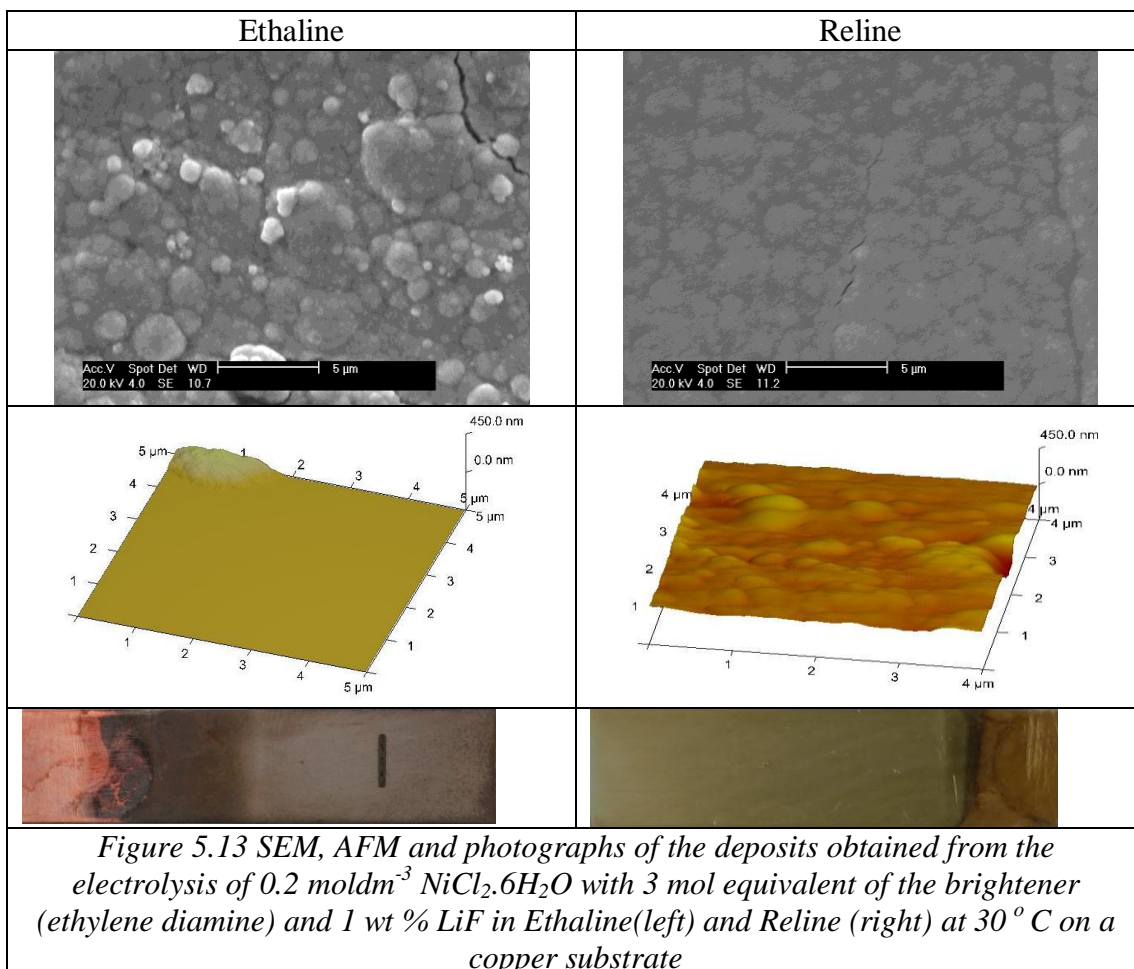


Figure 5.12 Cyclic voltammogram of $0.2M$ $NiCl_2 \cdot 6H_2O$ with 3 mol equivalent of the brightener (ethylene diamine) and 1 wt % LiF in Ethaline(left) and Reline (right) at $30^\circ C$ on a Pt electrode($v=20$ mVs^{-1}).

In previous work it has been shown that the addition of lithium salts significantly affects the structure of the deposit. Abbott *et al.*³² showed that the addition of LiCl to an imidazolium chloroaluminate system changed the deposit from nanocrystalline to microcrystalline. This is thought to be due to the change in the double layer properties.

Figure 5.12a and **b** show the reduction of $NiCl_2 \cdot 6H_2O$ in Ethaline and Reline in the presence of LiF. There is a significant change in the cathodic current and the onset potential for reduction. This is in line with previous results for the addition of LiCl to chloroaluminate ionic liquids.³² It was proposed that this was due to the Li^+ ion adsorbing at the electrode solution interface and affecting the nucleation mechanism. In the previous case this led to a black, macrocrystalline deposit whereas in the case of nickel a bright, nano-crystalline deposit is observed. This can be seen visually and through SEM and AFM images in **Figure 5.13**.



Comparing **Figure 5.13** with **Figure 5.9**, it is clear that the LiF has a marked effect upon the morphology and surface topography of the samples. This ties in well with the results shown in Chapter 4 and suggests that the effect is not metal specific. It is also unusual given that silver is reduced above the pzc and nickel below the pzc. The large nodules which were characteristic of the en system are removed with the addition of LiF and the surface roughness is significantly decreased. The smooth surface is what leads to the mirror like finish of the sample.

5.4 Addition of brighteners: sodium acetylacetonate

The effect of adding sodium acetylacetonate (Na acac) as a complexing agent to both Ethaline and Reline was investigated and compared with the results for the addition of en. The rationale behind this approach was that Ni is well known to form the dark green nickel(II) acetylacetonate complex $[\text{Ni}(\text{acac})_2]$ with the acac ligand and it would

be interesting to compare the neutral complex with the various en complexes studied in the previous section.

5.4.1 Cyclic voltammetry

The cyclic voltammogram for the two ionic liquids containing acac are shown in **Figure 5.14a**. In Ethaline and Reline the voltammograms with acac look qualitatively similar to each other and to those with en. The cathodic nucleation loop in Ethaline is slightly more positive than in Reline but the anodic sweep shows two peaks which are at similar potentials in both liquids. The anodic sweep using en as a ligand results in two peaks which are at different potentials suggesting that the species stripped from the electrode is different from that when en is the ligand. It can be assumed that the main species stripped from the electrode surface when no ligand is present is a chlorometallate species. The stripping potentials observed when there is a ligand present are different and so it can be inferred that the main species being stripped from the electrode surface involve the ligand being bound to the metal centre.

FAB-MS results in Ethaline and Reline show NiCl_3^- as the dominant signal in both liquids. Ethaline shows minor Ni containing fragments at 369 and 486 whereas in Reline a signal at 269 corresponding to $[\text{Ni}(\text{acac})\text{Cl}_2]^{2-}$ was observed. There is an obvious colour change from pale green to dark green that occurs following the addition of sodium acetylacetonate (Na acac). **Figure 5.5** shows that the visible spectrum peak positions and the relative intensities change following the addition Na acac. While the Ni acac complex is clearly formed some NiCl_3^- (or more probably NiCl_4^{2-}) is probably still in solution so further investigation is required.

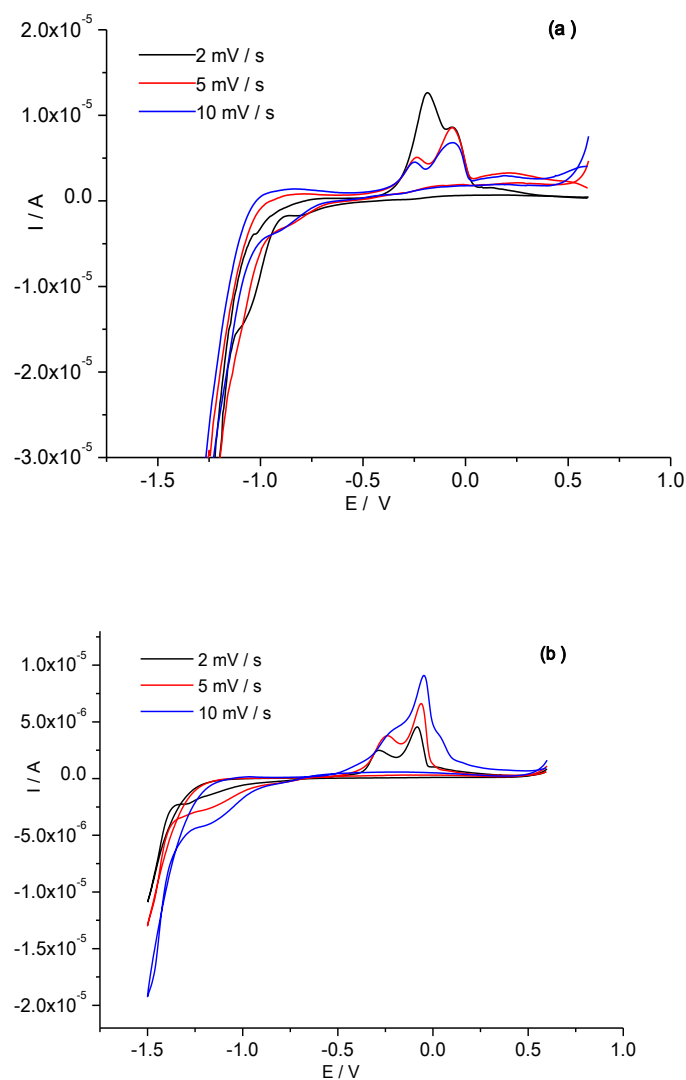


Figure 5.14 Cyclic voltammogram for a Pt disc (1.0 mm diameter) electrode immersed in 0.2M [NiCl₂·6H₂O] in a) Ethaline and b) Reline as a function of sweep-rate with 2 equivalents of acac (potential versus Ag wire quasi-reference electrode).

5.4.2 Chronocoulometry

Figure 5.15 shows the charge/time transient for a Pt electrode immersed in a Ethaline and a Reline containing NiCl₂·6H₂O (0.2 M) for a potential step from +1 V (held for 10 s) to -1 V for 30 min. The plot of charge vs. $t^{1/2}$ is nonlinear for Ethaline showing that it is not mass transport controlled. The charge passed for the same experiment using en (**Figure 5.7**) showed a smaller charge with Ethaline but a larger charge with

Reline. This clearly shows that speciation and viscosity both play a role in the rate of Ni deposition.

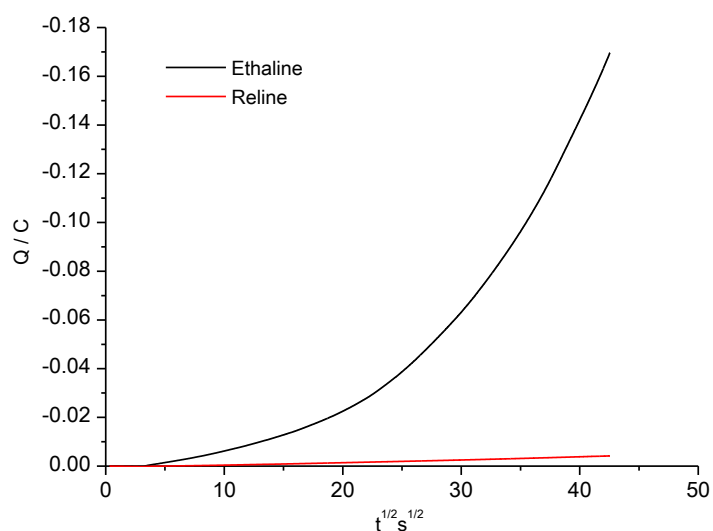


Figure 5.15 Chronocoulometry of $0.2 \text{ mol dm}^{-3} [\text{NiCl}_2 \cdot 6\text{H}_2\text{O}]$ in both Ethaline and Reline IL with 2 mole equivalents acac for potential steps from 1.00 V for 10s followed by a step to -1.00V for of ca. 30 min ($1.0 \text{ mm diam. Pt wire}$).

5.4.3. Under-potential deposition of nickel

Figure 5.16 show that UPD is still observed with the acac complex. Comparing **Figure 5.16** to **Figures 5.3** and **5.8** it can be seen that the upd in Reline is more significant than with en or with no ligand. The reason for this could be that complexes formed by acac are less stable than those formed by en which is due to the ring size *i.e.* en forms five membered ring which the most optimum ring size while acac forms six membered ring which is less stable. It is notable that the upd in Reline is a partially reversible process.

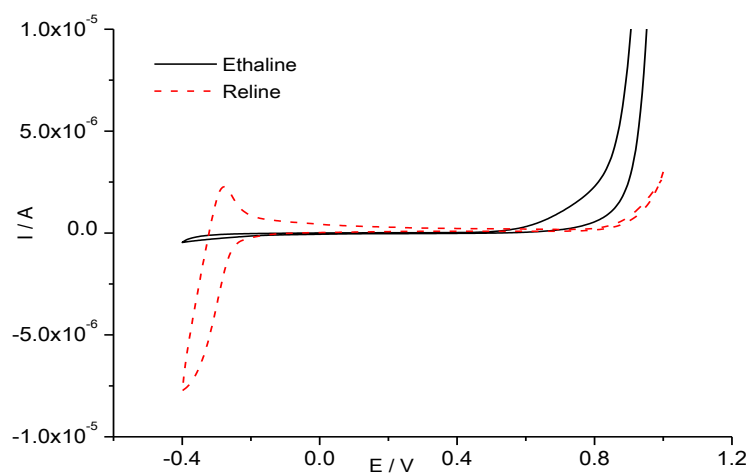


Figure 5.16 under potential deposition and anodic region of 0.2 mol dm^{-3} $[\text{NiCl}_2 \cdot 6\text{H}_2\text{O}]$ with 2 equivalents acac in Ethaline and Reline at scan rate 5 mV s^{-1} .

5.4.4. Bulk electrolysis and morphology

Bulk electrolysis was carried out on a copper substrate for 2 hours from a solution of 0.2 mol dm^{-3} $\text{NiCl}_2 \cdot 6\text{H}_2\text{O}$ with 2 mol equivalents of acac in both Ethaline ($E = -2.5 \text{ V}$) and Reline ($E = -1.2 \text{ V}$). **Figure 5.17** shows the SEM and AFM images for Ni films deposited from Ethaline and Reline in the presence of acac as an additive and it confirms that the addition of acac has a significant effect as a brightener.

The SEM images show a completely different morphology to those presented above for either no ligand or with en. The addition of acac to an Ethaline solution results in a surface which appears to be micro-cracked with an unusual order to the cracking pattern in the surface. In Reline there is no such cracking and the small crystallites are in the order of 10 to 100 nm. Although the AFM images of the surface suggest that the particle size is more random, comparison with the earlier sections shows that they are smaller and the undulation in the z-direction is less than that seen previously. This makes the surface appear visually more uniform and hence brighter. In aqueous electroplating the rationale commonly employed is to attempt to make the crystals that make up the deposit larger but more flat. In ionic liquids the deposition tends to result in smaller crystallites and the aim is to produce particles that pack closer together and do not lead to large fluctuation in the z-direction.

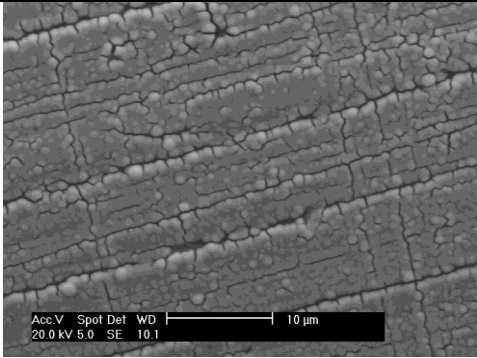
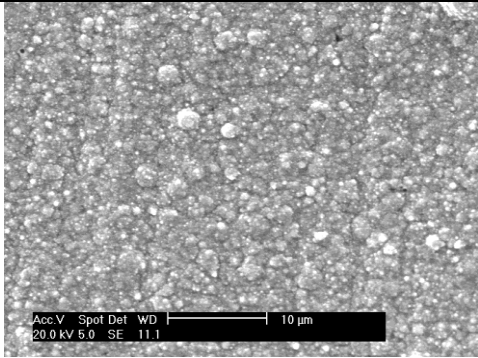
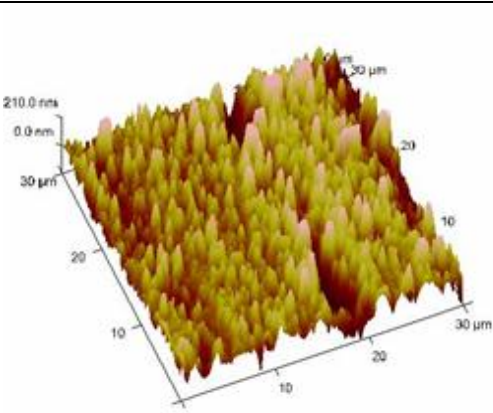
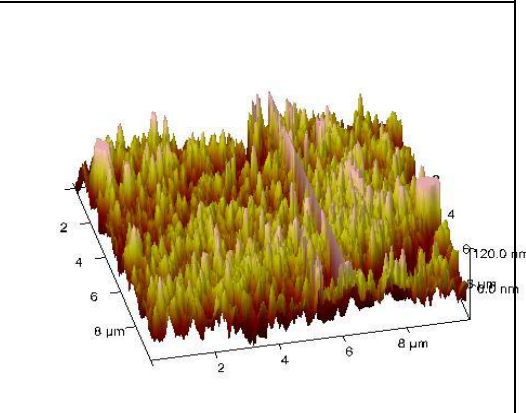
	Ethaline	Reline
SEM		
AFM		
<i>0</i>		
<i>acac</i>		

Figure 5.17: SEM, AFM images and photos of Ni deposited on Cu from solution containing $0.2 \text{ mol dm}^{-3} \text{ NiCl}_2 \cdot 2\text{H}_2\text{O}$ in both Ethaline and Reline with added of Na acac.

5.5 Nickel composites

In the previous chapters it has been shown that ionic liquids based on eutectic mixtures of choline chloride and hydrogen bond donors such as urea or ethylene glycol can be used as electrochemical solvents for the electrodeposition of copper and silver composites. In the current study this has been extended to Ni which has a wider application as functional coatings in practical applications. Also important is that such metals often have current efficiencies that are significantly lower than 100 % even in IL solvents. This precludes the use of EQCM as a quantitative tool and makes analysis and quantification more challenging.

As discussed in the introduction, there have been numerous studies on the formation of nickel composites from aqueous solution and most have involved the use of nanometer sized aluminium oxide or silicon carbide. In general the electrodeposition of nickel composites can lead to metal coatings with different morphologies and mechanical properties.^{7,21} Furthermore the type of particulate, size, and the amount involved in the metal coatings as well as the deposition variables such as pH, current densities, organic additives like surfactants, temperature, and stirring all affect the properties of the metal composites coatings.

5.5.1 Nickel/ SiC composites

Exactly as observed with copper and silver in **Chapters 3** and **4** the inclusion of particulates in solution does not change the shape of the voltammograms, but it does increase the cathodic current which is again thought to be due to the decrease in solution viscosity (not shown).

Bulk electrolysis was carried out at an applied potential of -2.50 V on a copper substrate for 20 hours from a solution of 0.2 mol dm^{-3} $\text{NiCl}_2 \cdot 6\text{H}_2\text{O}$ with 3 mol equivalents of ethylene diamine and 1 wt % LiF in both Ethaline and Reline at 50°C . The deposits obtained were bright and reflective. The incorporation of particulates does not appear to change the brightness of the deposit significantly. As in the previous sections the solutions were not stirred so that the deposition conditions were simplified.

Figure 5.18 and **Figure 5.19** show the scanning electron micrographs of the nickel coatings deposited on a copper substrate from Reline and Ethaline respectively. It is

clear that the morphology of the Ni deposits is similar from both ionic liquids *i.e.* composed of very small crystallites. Unlike the examples shown in **Figure 5.9** with just en added as a ligand, the incorporation of LiF appears to be producing micro-sized cracking in the coating. As described above, this tends to be unusual in ionic liquids but examples have been observed in chloroaluminate systems and these have been associated with internal stress in the coating.³² The incorporation of SiC particles has relatively little effect upon the general morphology of the nickel films and cracks are still observed which at times can penetrate all the way to the substrate surface. Evidence of SiC particles in the plan view of the coatings can be observed although it is more obvious in the cross-sectional views. As observed with the deposition of copper composites the distribution of particulates is shown to be relatively even throughout the deposit. It was not possible to quantify the rate of particulate deposition using electrochemical quartz crystal microbalance because the deposition of nickel is not 100 % current efficient although total composite loading was estimated from EDAX analysis.

Some of the cross-sectional images of composites deposited from Ethaline show that the particulates concentrate at the beginning of the deposition process which would be consistent with a liquid of lower viscosity where the diffusion layer is rapidly depleted of SiC particulates. These are relatively large particles (1-3 μm) with a high density (3.21 g cm^{-3}). The Reline results show greater uniformity in the particulate distribution because the liquid is more viscous. Settling should not be a significant effect because the electrodes are all ordered vertically in the liquid, however, setting may slowly deplete the vertical distribution of particles in the liquid. Note that the solutions were not stirred during deposition.

Table 5.1 SiC present in the nickel films as a function of solution loading.

SiC wt % in solution	SiC mol % in the film	
	Ethaline	Reline
10	1.66	4.65
20	9.39	14.15
30	3.59	5.65

Table 5.1 lists the percentage SiC incorporated in the nickel films as a function of SiC in the liquid. It can be seen that in general the composite in the liquid is related to the

amount in the solution, however, the amount incorporated at higher solution loading is less than expected. This is generally in line with the results observed for copper and silver in Chapters 3 and 4 showing that the main mechanism of composite incorporation is drag.

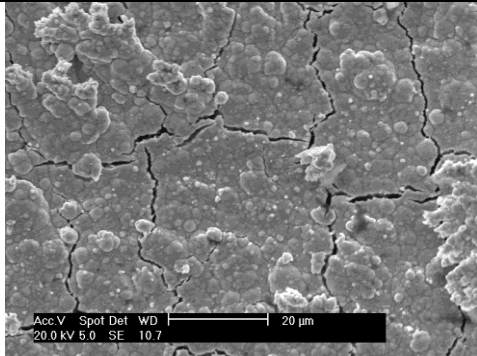
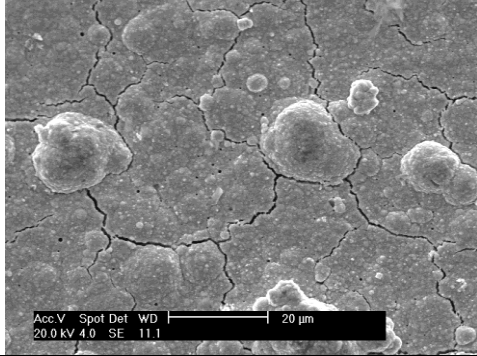
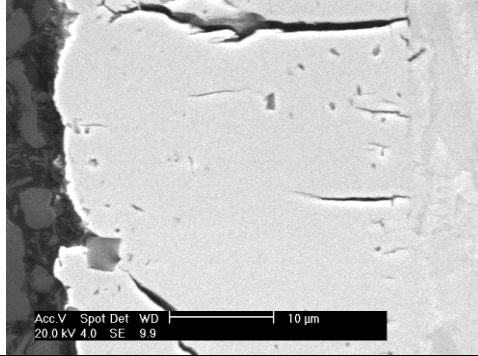
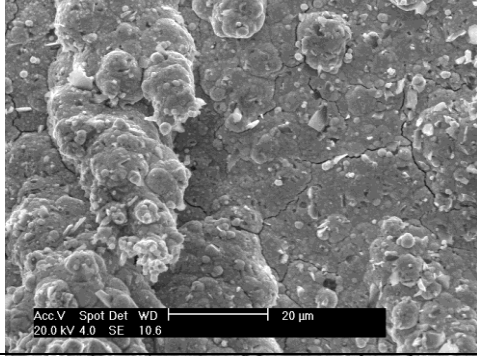
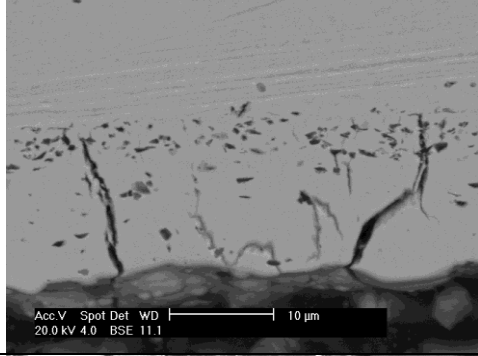
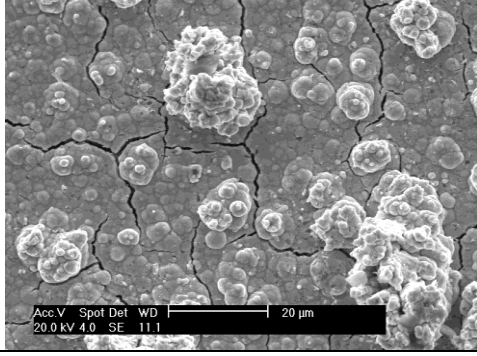
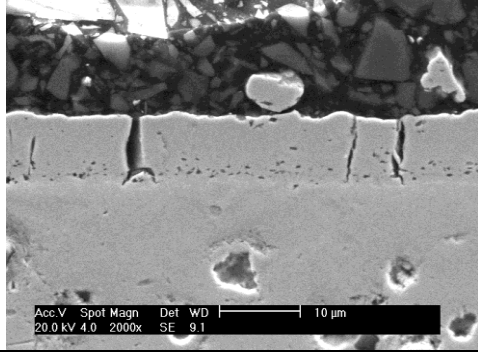
%SiC	Ethaline	
	Surface	Cross-section
0		
10		
20		
30		

Figure 5.18 SEM images for Ni deposited on a copper substrate from 0.2M NiCl₂.6H₂O with 3 mol equivalent of the brightener (ethylene diamine) and 1 wt % LiF at 50°C with and without SiC 1-3μm from Ethaline with an applied potential of 2.5 V.

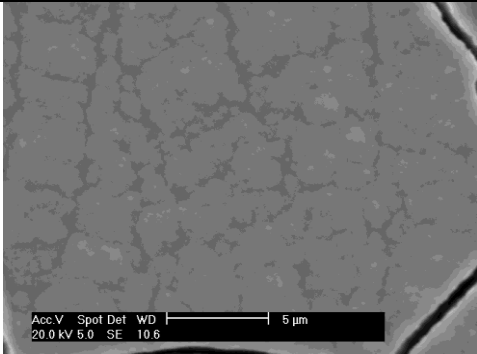
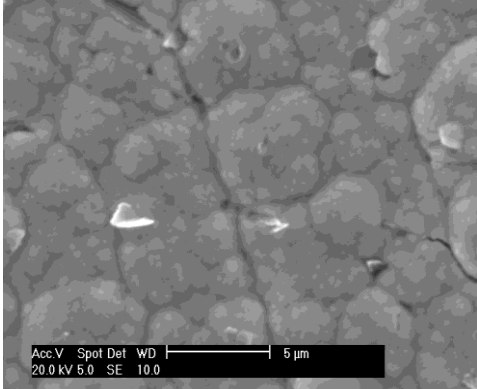
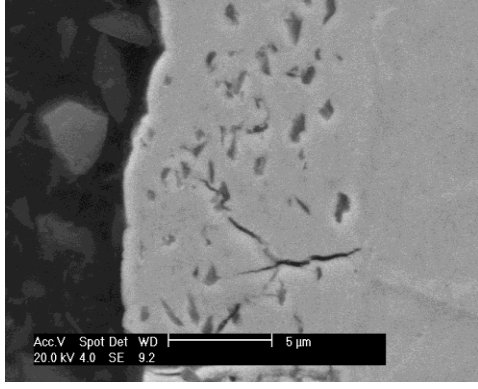
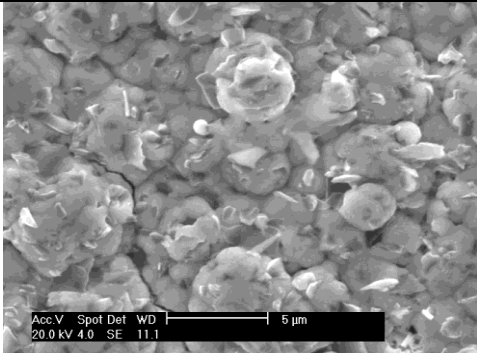
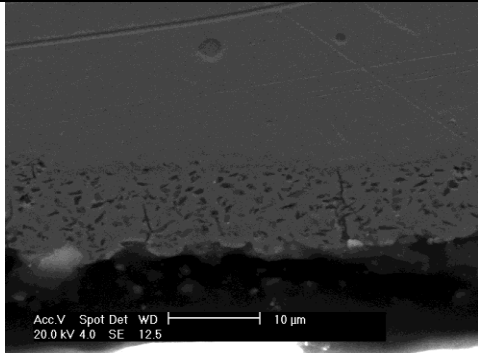
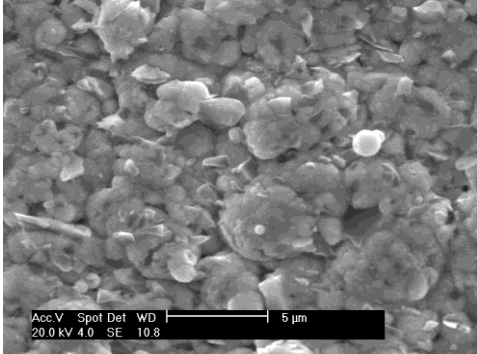
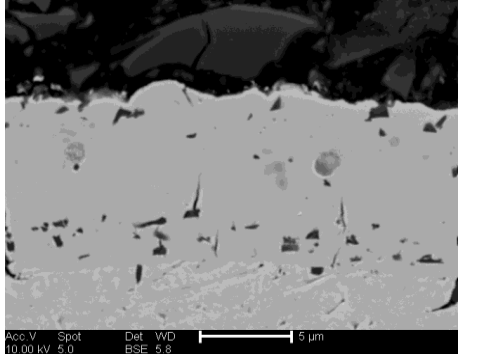
SiC %	Reline	
	Surface	Cross-section
0		
10		
20		
30		

Figure 5.19 SEM images for Ni deposited on a copper substrate from 0.2M NiCl₂.6H₂O with 3 mol equivalent of the brightener (ethylene diamine) and 1 wt % LiF at 50°C with and without SiC 1-3μm from Reline with an applied potential of 2.5 V.

Low concentrations of particulates do not appear to affect the morphology of the nickel layer however the addition of 20 wt % SiC affects the surface morphology in both liquids. It is assumed that a high density of the large particles disrupts the

nucleation mechanism and may act as a site to promote nucleation. The change in morphology following the incorporation of particles is similar to that observed in aqueous solutions.²⁰ The cross-sectional images of particulates in **Figures 5.18** and **5.19** should be treated with some caution because the sectioning process can lead to smearing of the nickel which does not show the true particle distribution (see below).

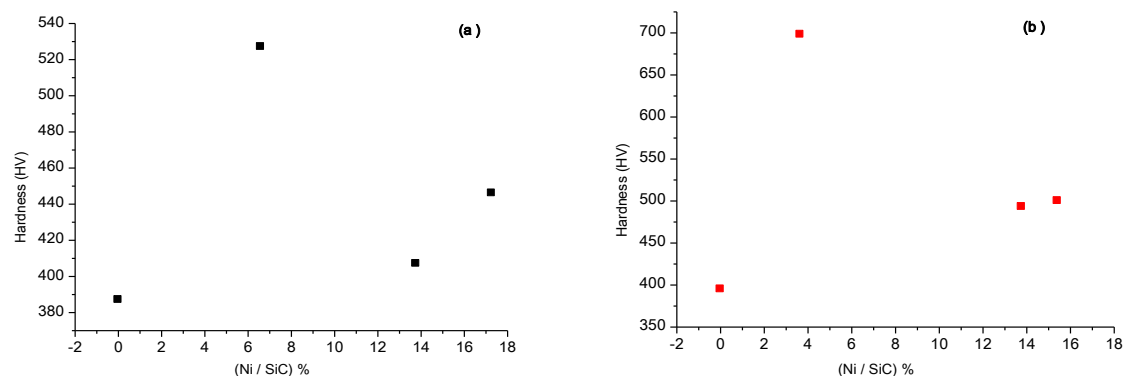


Figure 5.20 Vickers hardness of pure nickel and composite Ni–SiC coatings containing SiC 1-3 μ m particle size plotted vs. the (Ni / SiC) % of co-deposited Ni / SiC coating (a) Ethaline (b) Reline.

Figure 5.20 shows the Vickers hardness of the films shown in **Figures 5.18** and **5.19**. As expected the hardness of the films increases as the amount of composite incorporated increases. The hardness of the films deposited from Ethaline and Reline without composite particles are comparable with those deposited from aqueous solutions.¹⁷ It is known that the hardness of nickel films can range from 200 to 600 Vickers depending on the crystal size. Microcrystalline nickel is less hard than nanocrystalline material.

As the amount of SiC in solution is increased the solution of the composite film thus deposited increases. This is also in line with films prepared using aqueous solutions. Garcia *et al.*¹⁷ reported the incorporation of SiC particles (ranging from 0.3 to 5 μ m) into Ni deposited from a Watts' nickel solution. They reported the incorporation of up to 20 vol. % SiC which resulted in a hardness of 460 Vickers. In general it was found that the larger particles resulted in harder surfaces.

Figure 5.20 shows that the films deposited from Reline are harder than those deposited from Ethaline due largely to the increase amount of SiC. The hardness of films deposited using 20 % SiC in solution should be noted (700 Vickers).

Comparable hardness has been reported but this has required high temperature annealing of the sample.³³

Hardness is only one aspect of the surface properties; it is also important to consider the friction coefficient and wear volume. The friction coefficient is a parameter that describes the ratio of the friction force between two surfaces and the force pressing them together. The wear volume is the amount of material lost during a wear experiment under standard conditions.³⁴ **Figure 5.21** shows the friction coefficient of the films from **Figures 5.18** and **5.19**. It is interesting to note that the friction coefficient is largely unaffected by the incorporation of composite materials. This suggests that the surface roughness remains roughly the same, which corresponds with the SEM and AFM results shown above.

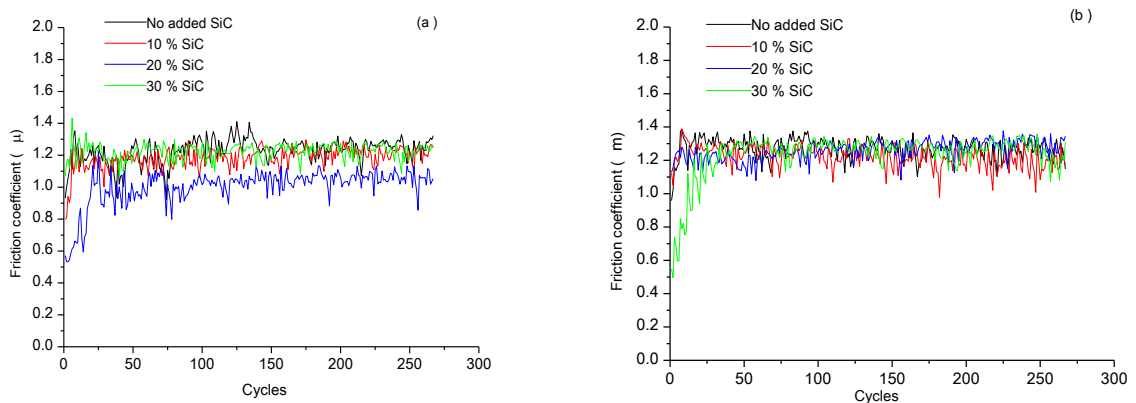


Figure 5.21 shows friction coefficient versus number of cycles where the complete cycle represents sliding distance of 1 cm length for Ni/ SiC 1-3 μm size co-deposits (a) Ethaline (b) Reline.

Figure 5.22 shows the wear volume of the samples shown in **Figure 5.18** and **5.19** and as expected the wear volume decreases when SiC is incorporated. The wear volume correlates relatively well with the hardness values as can be seen in **Figure 5.23**. Similar correlations have been shown by Garcia *et al.*¹⁷ and again it was shown that the larger particles were more effective at decreasing the wear volume of samples.

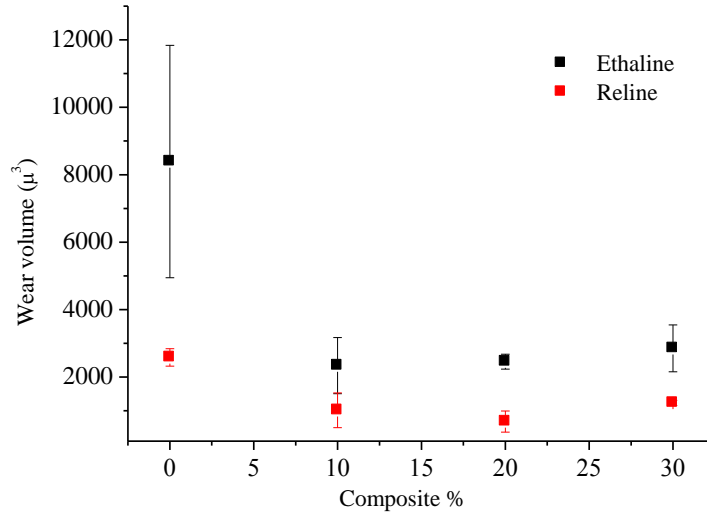


Figure 5.22 wear volume vs. composite % for Ni deposited on a copper substrate from 0.2M NiCl₂.6H₂O with 3 mol equivalent of the brightener (ethylene diamine) and 1 wt % LiF at 50°C with and without SiC 1-3μm from Ethaline and Reline with an applied potential of 2.5 V.

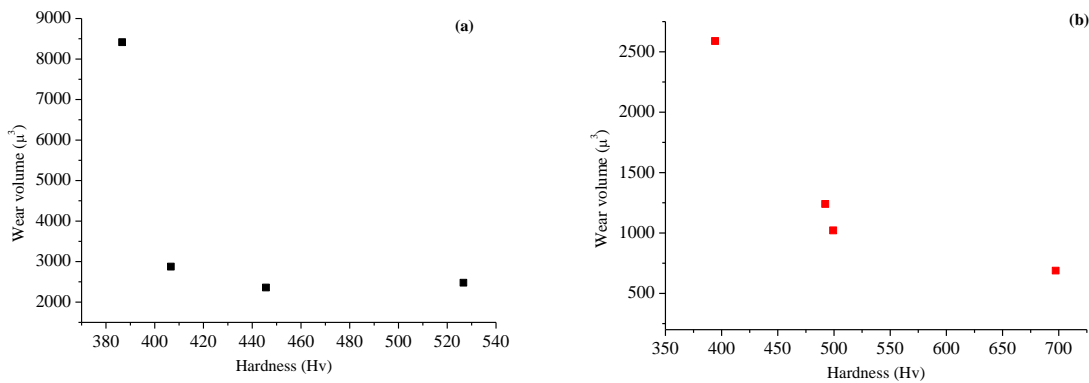


Figure 5.23 Vickers hardness of composite Ni-SiC coatings containing SiC 1-3μm particle size plotted vs. the wear volume of co-deposited Ni / SiC coating (a) Ethaline (b) Reline.

The structure of the nickel composite can be more clearly observed following the wear test. **Figure 5.24** shows clearly the particulate structure of the composites. This is a more effective way of revealing the composite distribution because the cross-section images shown in **Figures 5.18** and **5.19** were obtained by polishing the sectioned samples which can lead to smearing of the nickel layer which masks the particulate structure.

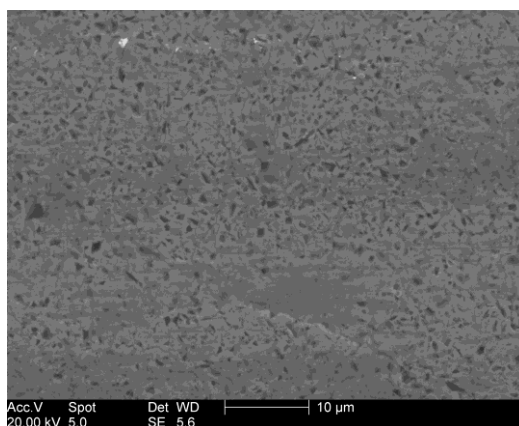


Figure 5.24 SEM images for worn surface of Ni co-deposited on a copper substrate from 0.2M NiCl₂.6H₂O with 3 mol equivalent of the brightener (ethylene diamine) and 1 wt % LiF in Ethaline at 50°C with 20 % SiC 1-3μm with an applied potential of 2.5 V.

5.5.2 Nickel/ PTFE composites

Wear resistance can be affected by the incorporation of either hard or soft particles. In comparison to hard composite materials there are comparatively fewer studies using polymeric materials dispersed in nickel films.^{35,36,37,38} Many require the use of surfactants to stabilise the polytetrafluoroethylene, PTFE, particles.³⁹ Bercot *et al.*³⁸ modelled the amount of particulate in the film as a function of current density, solution loading and electrode rotation rate and found that the maximum amount of PTFE that could be practically incorporated was about 10 vol. %.

In this section nickel was co-deposited with PTFE particles from Ethaline and Reline. PTFE particles with a 1 μm diameter were suspended in a similar manner to the SiC particles in the previous section. The main operational difference was that a slightly higher temperature was needed to stabilise the colloidal dispersion.

Figure 5.25 shows the morphology of the Ni composite films grown using the same conditions as shown in **Figure 5.18** and **Figure 5.19** but this time using varying loadings of PTFE particles. As previously, there is no discernible structure to the Ni film. The sample grown from Ethaline is more micro-cracked than the corresponding one grown from Reline. The particles are not evident from the simple SEM image, which is surprising since PTFE showed up clearly in **Figures 3.14** and **3.20**. **Figure 5.26** shows the elemental composition maps of the film grown from Reline (after wear testing) and it is evident from the fluorine map that the PTFE particles are there in high concentration and they are evenly distributed throughout the material.

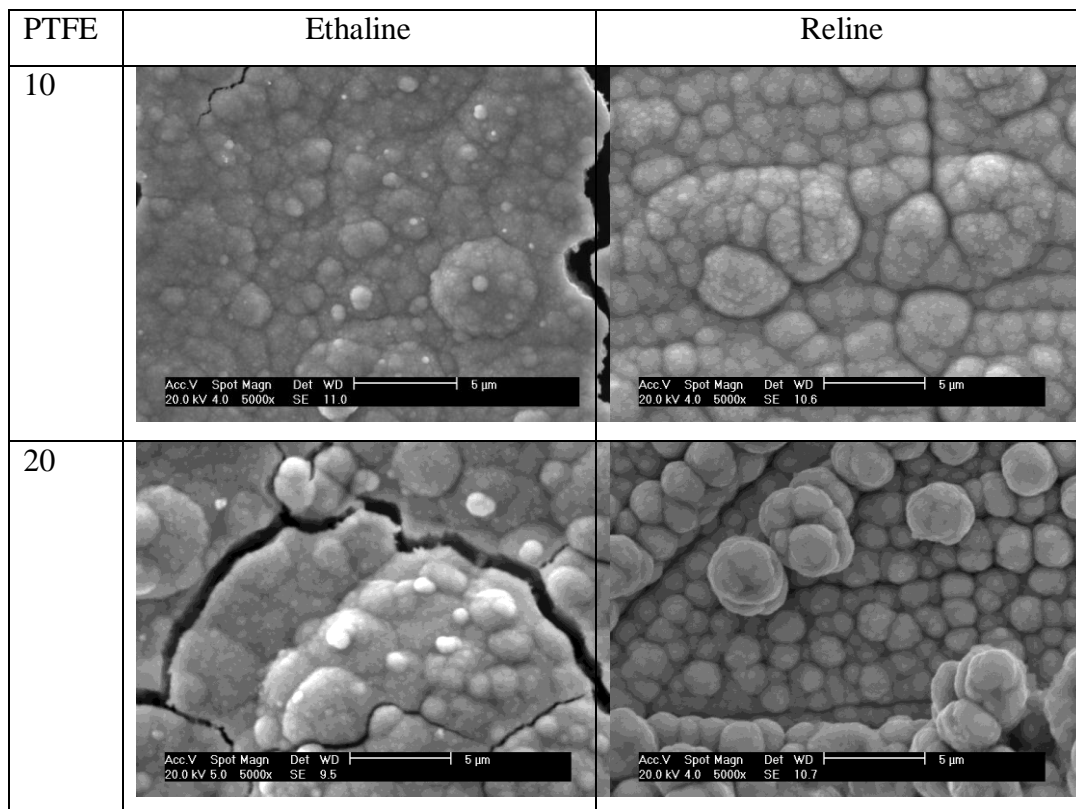


Figure 5.25 SEM images for Ni deposited on a copper substrate from 0.2M $\text{NiCl}_2 \cdot 6\text{H}_2\text{O}$ with 3 mol equivalent of the brightener (ethylene diamine) and 1 wt % LiF at 50°C with and PTFE 1μm with an applied potential of 2.5 V.

The observation that the nodular morphology is common to both the PTFE and SiC composites suggests that the nucleation of nickel is not dependent upon the surface properties of the colloidal particles. The poor wettability of the PTFE particles by either the nickel or the ionic liquid does not appear to affect the way in which they are incorporated in the film.

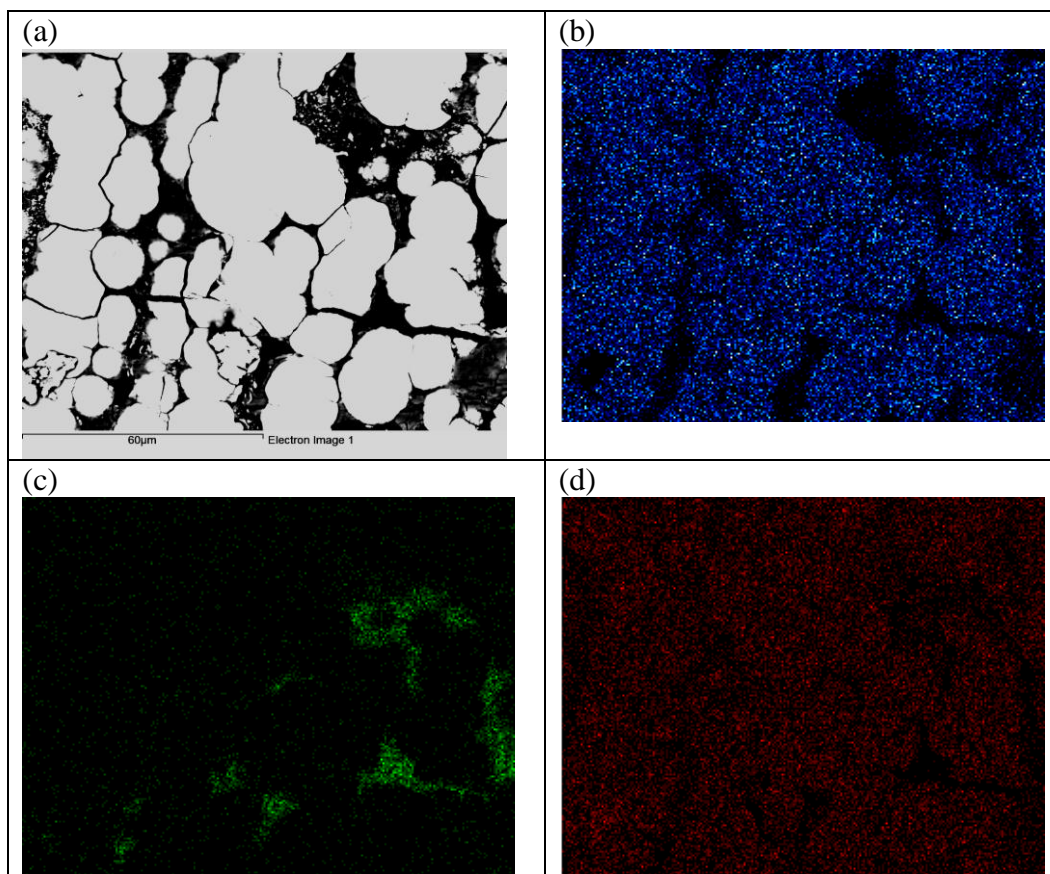


Figure 5.26 (a) SEM micrograph of worn surface of Ni/ PTFE electrodeposits on a copper substrate from 0.2M NiCl₂.6H₂O with 3 mol equivalent of the brightener (ethylene diamine) and 1 wt % LiF at 50°C and with 20 g / l PTFE 1µm size in Reline with an applied potential of 2.5 V. EDX map images shows (b) Ni (c) C (d) F.

In contrast to the samples with SiC particulates, those with PTFE showed a decrease in hardness increasing PTFE loading.

In an analogous manner to the SiC composites the friction coefficient of the Ni / PTFE composites was determined. Unlike the SiC films the PTFE particles did cause a change in friction coefficient confirming that they are incorporated in the film despite the SEM images not showing their presence. The higher PTFE loaded sample deposited from Ethaline shows an initial friction coefficient of approximately 0.4 compared to that of 1.4 without PTFE. The friction coefficient however rises to 1.4 after approximately 60 cycles. This shows that they are easily worn away and do not remain smeared on the surface. The results for Reline show that the friction coefficient starts at approximately the same value as the film deposited from Ethaline, but the value rises more rapidly to that of bulk nickel.

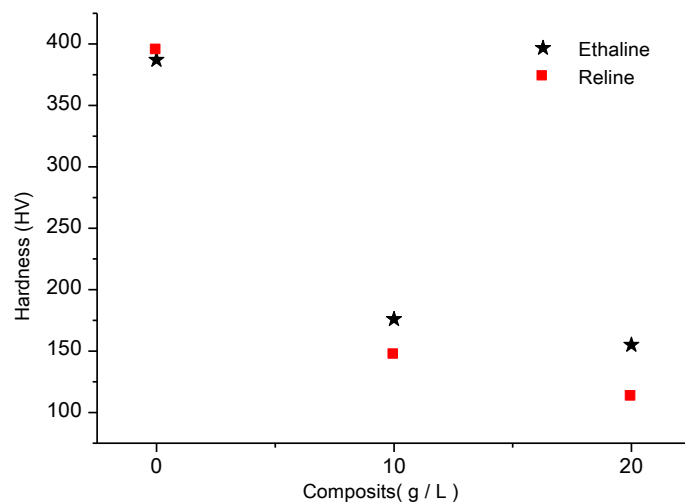


Figure 5.24 Vickers hardness of composite Ni/PTFE $1\mu\text{m}$ coatings containing PTFE $1\mu\text{m}$ particle size plotted vs. the wear volume of co-deposited Ni / PTFE coating.

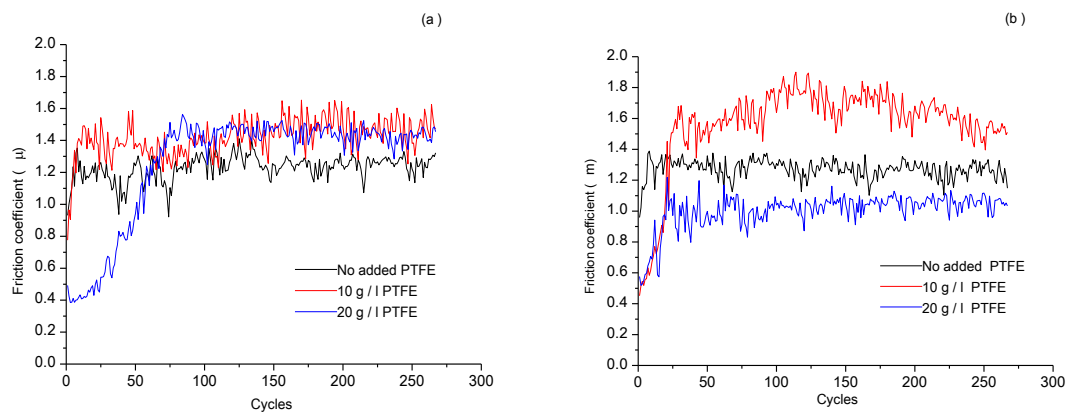


Figure 5.25 shows friction coefficient versus number of cycles where the complete cycle represents sliding distance of 1 cm length for Ni/ PTFE $1\mu\text{m}$ size co-deposits (a) Ethaline (b) Reline.

This section has shown that both hard and soft particulates can be incorporated into nickel films. The incorporation of SiC yields hard, wear resistant coatings whereas PTFE can decrease the friction coefficient.

5.6 Anodic properties nickel in Ethaline and Reline

Many electroplating processes use soluble anodes and the final part of this section deals with the anodic dissolution of nickel to determine whether soluble anodes are possible with this type of liquid. It was previously been shown^{40,41} that the electropolishing of stainless steel (iron, chromium and nickel alloys) leads to a semi-passivation of the electrode surface and limits the current at the electrode surface.

Figure 5.26 shows the linear sweep voltammogram for a nickel electrode in Ethaline. It can be seen that a peak in the current is observed at about 0.25 V which is similar in shape to that observed previously for stainless steel although the peak occurs at about 0.6 V for stainless steel.^{40,41} It is also interesting to compare the peak potential for dissolution with that for nickel stripping in **Figure 5.1a**. The stripping response following deposition has two anodic peaks which it was proposed resulted from different morphologies. These two peaks are 300 and 600 mV less positive than that observed for bulk metal. The same differences were recently observed for the corresponding aluminium case.³² This tends to reinforce the suggestion that the smaller the particle size the more cathodic (easier) the oxidation process. This is in agreement with the previous study by Smith *et al.*²⁸ Bulk electrolysis of the electrode at +0.5 V resulted in a dark green film forming on the electrode surface in a similar manner to that found with stainless steel.

The addition of LiF greatly increases the peak current suggesting that the fluoride ligand aids solubility or the Li^+ decreases the tendency for the electrode to passivate. Passivation does still occur albeit at a larger anodic overpotential. The trans-passive corrosion current increases steadily showing that the nickel is still able to dissolve.

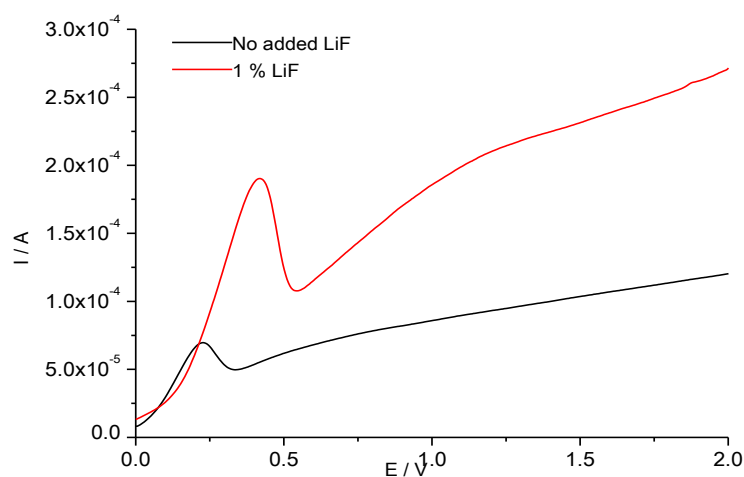


Figure 5.26 Linear sweep voltammogram (scan rate 20 mVs^{-1}) for a Ni wire disc in Ethaline.

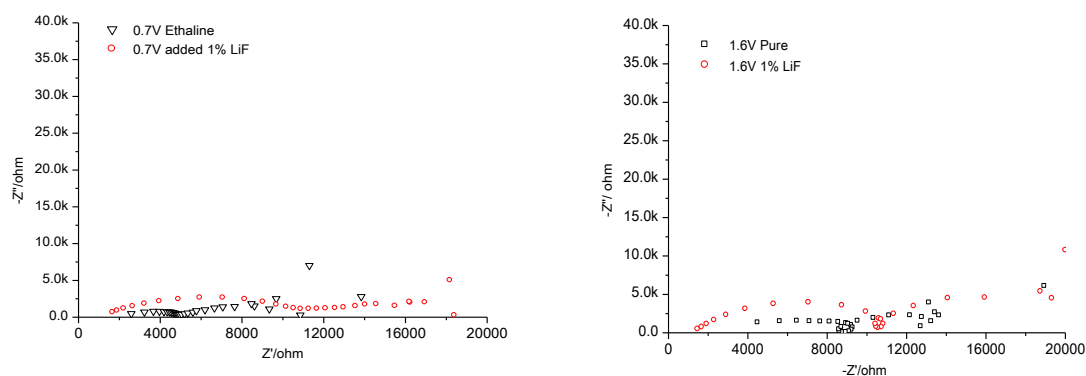


Figure 5.29 AC impedance spectra for a polished Nickel disc electrode immersed in fresh Ethaline and with added 1 % LiF. Measured at a single potential of 0.7 V and 1.60 V (vs. Ag wire reference).

AC impedance spectroscopy (**Figure 5.29**) is qualitatively the same as that observed for stainless steel confirming that the dissolution of nickel proceeds by an insoluble film forming on the electrode surface. Electrolysis of a nickel sheet in Ethaline for 10 minutes at 40°C resulted in a mirror finish showing that nickel can be electropolished like stainless steel. Bulk deposition of nickel from any of the liquids listed above using nickel anodes led to a bright (mirror) nickel finish showing that soluble anodes can be used for nickel deposition and electropolishing of nickel and nickel based alloys can be carried out in Ethaline.

5.6 Conclusions

This chapter has shown that nickel can be electrodeposited from eutectic base ionic liquids. FAB-MS shows that the major species present is NiCl_3^- . For deposition of Ni, the shape of the stripping peaks depends upon sweep rates, illustrating that the process is kinetically slow. The morphology and composition can be changed by the judicious choice of IL and the addition of complexing agents such as ethylene diamine and acetyl acetonate as brighteners. Both additives suppress UPD of Ni and lead to smaller particulate deposits. The addition of a small amount of LiF also significantly improved the deposit morphology. The direct deposition of nickel on aluminium was observed for the first time.

The electrodeposition of nickel composites was demonstrated using both silicon carbide and PTFE as the dispersed phase. Well dispersed particulates were obtained without the need for surfactants or solution stirring. The properties of these composite films were at least as good as those reported in the literature for aqueous solutions. The main advantage of using ionic liquids is that the particulates dispersions are much

more stable in solution and lead to more even particle dispersion. The tendency for ionic liquids to lead to smaller metal grain sizes is also thought to improve the hardness of the films.

5.7 Reference

-
- ¹ N. Guglielmi, *J. Electrochem. Soc.*, **1972**, 119, 1009.
- ² J.P. Celis and J.R. Roos, *J. Electrochem. Soc.*, **1977**, 124, 15
- ³ J.P. Celis, J. Fransaer, *Interfinish-96 World Congress, 10–12 September, 1996*, The Institute of Metal Finishing, Birmingham, **1996**, p. 377.
- ⁴ T. Hayashi, *Interfinish-96 World Congress, 10–12 September, 1996*, The Institute of Metal Finishing, Birmingham, UK, **1996**, p. 461.
- ⁵ A. Hovestad and L.J.J. Jansen, *J. Appl. Electrochem.* **1995**, 25, 519.
- ⁶ Y. Müller, P. Schmutz, T. Lampke and A. Leopold, *Metalloberfläche* **2006**, 60, 40.
- ⁷ C. T. J. Low, R. G. A. Wills and F. C. Walsh, *Surf. Coat. Tech.* **2006**, 201, 371.
- ⁸ E. Broszeit, G. Heinke and H. Wiegand, *Metall.* **1971**, 25, 470.
- ⁹ W. Ruythooren, K. Attenborough, S. Beerten, P. Merken, J. Fransaer, E. Beyne, C. Van Hoof, J. De Boeck and J.P. Celis, *J. Micromech. Microeng.* **2000**, 10, 101.
- ¹⁰ K. S. Teh, Y. T. Cheng and L. Lin, *J. Micromech. Microeng.* **2005**, 15, 2205.
- ¹¹ M. E. Hyde and R. G. Compton, *J. Electronal. Chem.* **2002**, 531, 19.
- ¹² S. H. Yeo, J. H. Choo and K. H. A. Sim, *J. Micromech. Microeng.* **2002**, 12, 271.
- ¹³ S. Steinhäuser, B. Wielage and T. Lampke, *Phys. Chem. Mech. Mat.*, **2004**, 4, 489.
- ¹⁴ I. Garcia, A. Conde, G. Langelaan, J. Fransaer and J.P. Celis, *Corr. Sci.* **2003**, 45, 1173.
- ¹⁵ V. Medeliene, *Surf. Coat. Tech.* **2002**, 154, 104.
- ¹⁶ N.K. Shrestha, K. Sakurada, M. Masuko and T. Saji, *Surf. Coat. Tech.* **2001**, 140, 175.
- ¹⁷ I. Garcia, J. Fransaer and J. P. Celis, *Surf. Coat. Tech.* **2001**, 148, 171.
- ¹⁸ F. Erler, C. Jakob, H. Romanus, L. Spiess, B. Wielage, T. Lampke and S. Steinhäuser, *Electrochim. Acta*, **2003**, 48, 3063.
- ¹⁹ E.W. Brooman, *Galvanotechnik* **2005**, 12, 2843.
- ²⁰ L. Du, B. Xu, S. Dong, H. Yang and W. Tu, *Wear*, **2004**, 257, 1058.

-
- 21 M. Musiani, *Electrochim. Acta*, **2000**, 45, 3397.
- 22 J.P. Celis, J.R. Roos, C. Buelens and J. Fransaer, *Trans. Inst. Met. Finish.*
23 **1991**, 69 133.
- 24 S. P. Gou and I.-W. Sun, *Electrochim. Acta*, **2008**, 53, 2583.
- 25 M.-J. Deng, I-W. Sun , P.-Yu Chen, J. K., Tsai and W. Ta, *Electrochim. Acta*,
26 **2008**, 53, 5812.
- 27 P.Martis, V. S. Dilimon, J. Delhalle, Z. Mekhalif, *Electrochim. Acta* **2010**, 55,
28 5407
- 29 A. P. Abbott, G. Frisch, J. Hartley and K. S. Ryder, *submitted for publication*.
- 30 A. P. Abbott, J. C. Barron and K. S. Ryder, *Trans. Inst. Metal Finish.*, **2009**,
31 87,201.
- 32 E. L. Smith, J. C. Barron, A. P. Abbott and K. S. Ryder, *Anal. Chem.* **2009**, 81,
33 8466.
- 34 F. Endres, A. P. Abbott and D. MacFarlane, Eds., *Electrodeposition of Metals*
35 *from Ionic Liquids*, Wiley VCH, Weinheim, **2008**.
- 36 C. Hardacre, *Annu. Rev. Mater. Res.*, **2005**, 35, 29.
- 37 A. P. Abbott, G. Frisch, and K. S. Ryder, *Ann. Rep. Prog. Chem., Section A:*
38 *Inorg. Chem.* **2008**, 104, 21.
- 39 A. P. Abbott, F. Qiu, H. M. A. Abood, R. M. Ali and K. S. Ryder, *Phys.*
40 *Chem. Chem. Phys* **2010**, 12, 1862.
- 41 S. J. Kim and H. J. Yoo, *Surf. Coat. Technol.*, **1998**, 108-109, 564.
- J. A Williams *Engineering Tribology* **1994**, Oxford university press
- M.Shoeib, *Corr. Prev. & Control* **2002**, 49, 141.
- T. Ibe, H. Kiyokawa, Y. B. Chong, S. Yonezawa and M. Takashima, *Mat. Sci.*
Res. Int. **1998**, 4, 148.
- G. N. K.Bapu, S. Ramesh and S Mohan, *Plating Surf. Finish.* **1995**, 82, 86.
- P. Bercot, E. Pena-Munoz and J. Pagetti, *Surf. Coat. Tech.* **2002**, 157, 282.
- Z. Abdel Hamid and A. M. A. Omar, *J. Surf. Detergents* **2003**, 6, 163.
- A. P. Abbott, G. Capper, K. J. McKenzie and K. S. Ryder, *Phys. Chem. Chem.*
Phys., **2006**, 8, 4214.
- A. P. Abbott, G. Capper, K. J. McKenzie and K. S. Ryder, *Electrochim. Acta*,
2006, 51, 4420.

Chapter 6: Summary and Future Work

6.1 Summary

6.1.1 Cu and Cu composites

6.1.2 Ag and Ag composites

6.1.3 Ni and Ni composites

6.2 Future Work

6.1 Summary

The objective of this thesis to understand the mechanism of the composite deposition in two DESs; 1:2 ChCl: ethylene glycol and 1:2 ChCl: urea. The systems have a number of variables; the metal matrix, the type and size of dispersed particles, the structure of the metal matrix crystallites and the loading of particulates. The physical parameters which were varied were the metal salt concentration, particulate loading, the particulate size and type, the type of ionic liquid, brighteners and reduction potentials. Clearly this study has not optimised all of these variables, but several general conclusions can be drawn.

6.1.1 Cu and Cu/ composites

Chapter 3 shows that ionic liquids based on eutectic mixtures of choline chloride and hydrogen bond donors can be used for the electrodeposition of copper with high current efficiency. The use of EQCM to study the deposition of copper composites was demonstrated for the first time using Al_2O_3 , SiC and PTFE as the dispersed phase. The high viscosity of the ionic liquids was shown to be a benefit in the preparation of composite materials. High composite loading was achieved without stirring or stabilisers and the addition of surfactants which is the normal way of stabilising colloidal dispersions, was actually found to be detrimental to the preparation of composites. The loading of particulates in the resulting electroplated films is strongly dependent on the concentration of particulate in solution but largely independent of the concentration of copper metal ion or time scale. Dragging of dispersed phase is the main mechanism for particulate inclusion into the electrolytic deposits. The inclusion of suspended particles in the liquid is found to have negligible effect upon the fluid viscosity and it is proposed that this is because of the tumbling motion of the particles acting as micro stirrers in the liquid.

6.1.2 Ag and Ag/ composites

From the ideal system studied in **Chapter 3** the metal matrix was changed to the softer silver system in **Chapter 4** for the practical application of producing wear resistant electrical contacts. In this study two types of ceramics were used; alumina and silicon carbide in two different sizes which differed by approximately 20 times. The morphology of silver with co deposited nano-

particles was relatively similar to the silver deposits without particulates *i.e.* it formed a microcrystalline matrix. When micro silicon carbide particles were included a significant difference was observed in the silver matrix which was nano-crystalline in structure.. It was found the mechanical properties such as hardness and wear resistance of silver deposited with particulate were improved and approximated those of bulk silver. The addition of LiF to the electrolyte solution significantly changes the surface texture of silver deposits with both nano and micro silicon carbide, and the hardness increases two folds in case of nanoparticles and three folds for micro-particles. This significantly affected the friction coefficient in both deposits.

The surface texture of silver deposits with and without particulate and as well as the worn surfaces have been examined by using digital holographic microscopy for the first time and it was found that there are no significant difference in surface roughness between the silver deposits with different composites particle sizes. This was explained in terms of the composite particles forming a barrier which stopped the matrix between the particles being worn.

6.1.3 Ni and Ni / Composites

Eutectic base ionic liquids ChCl:2EG and ChCl:2urea can be used for the electrodeposition of nickel. FAB-MS suggested that the major species present is NiCl_3^- . The deposition is less reversible than that for copper and silver and this is thought to be related to the geometry of the complex. The morphology of the nickel deposit can be changed by the ionic liquid and the addition of complexing agents such as en and acac and LiF as brighteners. These additives suppress the underpotential deposition of Ni and lead to smaller particulate deposits. The direct deposition of nickel on aluminium was observed for the first time. As discussed in Chapters 3 and 4 the incorporation of dispersed particles was related to the solution loading. In general more materials is incorporated from Reline because the suspensions are stabilized by the higher viscosity. The hardness and wear resistance are in line with those observed for silver and copper *i.e.* increased particle concentration increases hardness and decreases wear resistance. The incorporation of PTFE in the Ni films effectively lowers the friction coefficients. The hardness of Ni electrolytic deposits with both soft and hard composites was measured and the value reached up to 700 Hv for Ni when incorporated from Reline containing 20 % SiC, moreover the SEM images for cross section of the Ni coatings shows how the ceramics are evenly distributed

in the coatings. On the other hand the incorporation of soft materials like PTFE decreases the hardness.

6.2 Suggestions for Further Work

The results presented in this thesis show the incorporation of dispersed phases can be achieved using DESs. The main advantage of using these solvents arises from the circumvention of solution agitation and surfactant dispersants. The use of DESs also allows the deposition of metal composites directly onto water sensitive substrates. This thesis has qualitatively outlined the parameters for the deposition of composites and shown the effect of each of these on the properties of the materials. Clearly the first study that needs to be carried out is a more quantitative investigation of the particulate inclusion. Fransaer *et al.* in Leuven have offered to characterize the composites films more clearly and this will occur in the near future.

Chapter 5 has shown that there is some dispute about speciation and its effect upon redox potentials. EXAFS studies have recently been carried out by Frisch on NiCl_2 in Ethaline and Reline although interpretation of the data is complex. Analysis of this data will give a clearer picture of speciation and its effect upon redox potential.

It has been shown in all of the results that a finer metal crystallite component leads to a harder and more wear resistant coating. One aspect that still needs to be studied is the characterisation of particle size using XRD and the effect of ionic liquid, additive and reduction potential on crystallite size. To characterize this it would be important to understand the effect of LiF on the double layer properties. This can be achieved through capacitance studies and collaboration with Silva in Porto will investigate this in the near future. Previous studies have also shown that heat treatment of composites can remove internal stress and recrystallise the metal matrix.

Finally, deposition of composites onto useful soft substrates would be carried out. Previous studies have shown that zinc and zinc alloys can be deposited onto lightweight alloys such as Mg or Al alloys. These have poor wear resistance but the coating with chrome or nickel composites could lead to light, wear-resistant materials.

Appendix

- 1- A. P. Abbott, **K. El ttaib**, K. S. Ryder, E. L. Smith *Trans. Ins. Met. Finish.* **2008**, 86, 234.
- 2- A. P. Abbott, **K. El ttaib**, G. Frisch, K. J. McKenzie, K. S. Ryder *Phys. Chem. Chem. Phys.* **2009**, 11, 4269.